Habilitation à diriger des recherches

Sciences Physiques

Université de Lille

Chu-Chun FU

Défauts, diffusion et corrélations magnéto-chimiques dans les alliages de fer : études à partir des premiers principes

Date de soutenance: 21 février 2024

Rapporteurs :

Prof. Lionel Calmels : Université de Toulouse 3, CEMES

Prof. Pär Olsson : KTH Royal Institute of Technology, Suàde

Dr. Fabienne Ribeiro : Institut de Radio-protection et de Sûreté Nucléaire

Examinateurs :

Prof. Maria José Caturla (présidente) : Universidad de Alicante, Espagne

Prof. Robin Schäublin : ETH Zurich, Suisse

Dr. François Willaime : Université Paris-Saclay, CEA

Garante :

Prof. Charlotte Becquart : Université de Lille

Défauts, diffusion et corrélations magnéto-chimiques dans les alliages de fer : études à partir des premiers principes

Resumé

Mes recherches principales portent sur les propriétés des défauts dans les systèmes de métaux de transition (en particulier Fe) d'intérêt pour l'énergie nucléaire. L'objectif est de fournir des connaissances fondamentales sur les structures électroniques et les mécanismes à l'échelle atomique (diffusion, formation d'amas, ...) à l'origine du comportement macroscopique de ces matériaux métalliques : ségrégation, précipitation, comportement mécanique, etc. Les défauts considérés comprennent les défauts élémentaires de l'irradiation (lacunes et atomes auto-interstitiels), les impuretés et solutés, ainsi que les défauts étendus tels que les surfaces, les interfaces et les joints de grains. La plupart de mes études portant sur les alliages de Fe, une attention particulière est donc portée aux interactions magnéto-chimiques.

Les études sont basées sur la théorie de la fonctionnelle de la densité (DFT), mais sans s'y limiter. Dans de nombreux cas, des modèles et potentiels semi-empiriques paramétrés sur la DFT sont utilisés pour des simulations à plus grande échelle. En particulier, des modèles d'interaction sur réseau incluant explicitement des variables atomiques et de spin sont développés, afin de prédire l'évolution en température des propriétés thermodynamiques et cinétiques, notanment au voisinage de la transition ordre-désordre magnétique.

Ce rapport d'HDR résume certaines des parties les plus pertinentes de mes travaux de recherche effectués en SRMP. Il aborde les propriétés des défauts ponctuels structurels, ainsi que les solutés interstitiels et substitutionnels fréquents dans les systèmes à base de fer-α. Il décrit également mon approche récente en modélisation et ses résultats sur la stabilité de phase, la formation des lacunes et la diffusion atomique dans les alliages de Fe cubiques centrés et cubiques à face centrés, prenant en compte les effets d'ordre, d'excitation et de transition magnétique. Les résultats obtenus sont comparés, autant que possible, aux données expérimentales disponibles.

First-principles based studies for defects, diffusion and magneto-chemical interplay in Fe alloys

Abstract

My main research topic concerns properties of defects in transition-metal (particularly Fe) systems of interest for nuclear-energy industry. The aim is to provide fundamental knowledge on electronic structures and atomic-scale mechanisms (diffusion, clustering...) at the origin of macroscopic materials behaviour: segregation, phase ordering and precipitation, mechanical failure, etc. The defects considered include the elementary radiation defects (vacancies and self-interstitial atoms), impurities, solutes, and extended defects such as surfaces, interfaces and grain boundaries. Since most of my studies concern Fe alloys, a particular attention is paid to the magneto-chemical interplay.

The studies are based on density functional theory (DFT), but not limited to it. In many cases, DFT informed semi-empirical models and potentials are employed for larger scale simulations. In particular, on-lattice effective interaction models including explicitly both atomic and spin variables are developed, in order to predict temperature evolution of thermodynamic and kinetic properties across the magnetic order-disorder transition.

This HDR report summarizes some most relevant features of my research work performed at SRMP. It addresses properties of structural point defects, and common interstitial and substitutional solutes in α-Fe systems. It also describes my recent modelling approach and results on phase stability, vacancy formation and atomic diffusion in bcc and fcc Fe alloys, accounting for magnetic ordering, excitation and transition effects. The obtained results are compared, as much as possible, with available experimental data.

List of Abbreviations

1nn first-nearest-neighbor

2nn second-nearest-neighbor

AF anti-ferromagnetic

AFD anti-ferromagnetic double-layered

DFT density functional theory

DLM disordered local moment

EIM effective interaction model

EP empirical inter-atomic potential

FM ferromagnetic

GB grain boundary

GBs grain boundaries

GGA generalized gradient approximation

He$_{int}$ interstitial He

He$_{sub}$ substitutional He

kMC kinetic Monte Carlo

MC Monte Carlo

MCE magnetic cluster expansion

MD molecular dynamics

MGS magnetic ground state

NM non-magnetic

PAW projector augmented-wave

PM paramagnetic

SDWs spin density waves

SIA self-interstitial atom

SRO short-range order

SQS special quasi-random structure

$\mathbf{T}_c$ Curie temperature

Contents

Chapter 1

Introduction

Iron alloys such as ferritic and austenitic steels are widely used in numerous technological areas including the nuclear-energy industry. Although their macroscopic behavior such as phase stability and mechanical properties are extensively investigated over decades, there are still several open questions concerning the electronic- and atomic-scale origin of the observed materials behavior, especially properties driven by magnetism and those related to the kinetic and out-of-equilibrium processes. They are often not directly accessible via experiments. First-principles DFT based studies are powerful tools to provide useful information, contributing to interpret and complement experimental results.

This HDR report gives a brief summary of three relevant chapters of my research work in this field, since my arrival at SRMP, CEA Saclay in late 2002. I choose to focus it on our DFT based predictions of magneto-chemical phase stability and transition, as well as diffusion and clustering properties of point-defects and solutes in bcc and fcc Fe systems. The objective of these studies is to contribute to a more accurate theoretical description of thermodynamic and kinetic properties of the ferritic and austenitic alloys in thermal equilibrium and under irradiation. This report is certainly not exhaustive. In particular, one of my recent topic concerning properties of carbides in Fe based alloys is not mentioned in this document.

Chapter 2 deals with elementary structural point defects in α-iron, that is, vacancies, self-interstitial atoms and their small clusters. In fact, when I joined SRMP, there was relatively little DFT-level knowledge on properties of the points defects in Fe based systems. For instance, even the diffusion mechanism of a single self-interstitial atom (SIA) in pure α-Fe was not fully established. There were also some long-lasting debates, based on various complementary experiments, related to the activation energies of mono-vacancy and vacancy clusters. Our DFT based studies contributed to solve such open questions.

Chapter 3 addresses diffusion and clustering of interstitial and substitutional solutes in bcc Fe systems. These properties play a key role to control the kinetics of microstructural evolution in materials. I show here a systematic comparison of

properties of carbon, nitrogen and oxygen, the most common interstitial solutes in Fe systems, emphasizing the impact of their clustering with vacancies on their diffusion. Among the substitutional solutes, I focus on the oversized solutes and the specificity of their diffusion. Then, a detail description is devoted to He and H elements in Fe, due to their production under high-energy neutron irradiation.

In chapters 2 and 3, the defects and solutes properties are investigated in bcc Fe systems by adopting a ferromagnetic (FM) order for the underlying Fe lattice. Chapter 4 is dedicated to the exploration of the impact of magneto-chemical interplay on thermodynamic, vacancy formation and atomic diffusion properties in bcc and fcc Fe alloys. On one hand, we address low-temperature effects such as magnetic frustration and local environment dependence of solute magnetism, via DFT beyond the usual collinear approximation. On the other hand, we improve the finite-temperature description of Fe alloys through the consideration of thermal magnetic excitations and magnetic transitions. To this end, an efficient DFT based spin-atomic Monte Carlo approach has been developed. An appropriate treatment of the finite temperature magnetism is particularly important for addressing properties in austenitic Fe alloys, since they are usually in a paramagnetic (PM) state at temperatures of technological interest.

At the end of each chapter, I mention and acknowledge the collaborations involved in the studies. Also, the most representative publications (with their abstract) are listed.

Finally conclusions are given in Chapter 5 together with some perspectives.

I also have to mention that, I am definitely not exhaustive when citing literature references. This is because I mainly pretend to provide a summary of our own studies in this HDR report. However, there is always an extensive quoting of references in our published papers linked to the reported results.

Chapter 2

Structural point-defects in α-Fe

Microstructural evolution of structural materials in nuclear reactors is largely dictated by properties of the most elementary defects created by irradiation, that is, vacancy (V), SIA and their clusters. Key properties of these defects include: the low energy configurations, their migration mechanisms, and the way they form clusters. It is worth mentioning that generally such atomic-scale information cannot be directly obtained by experiments. Thus, accurate modeling and simulation come to be essential.

Among various possible theoretical approaches, electronic-structure based first principles study is clearly the most powerful one for the study of defects in iron-base systems, particularly because the FM order is indispensable to stabilize the bcc structure of Fe, and it also affects significantly properties of defects in iron systems [1, 2]. In addition, electronic-structure analysis can evidence the change of the nature of inter-atomic interactions *e.g.* in the presence of impurities such as carbon and nitrogen [3]. Even though the application of first principles studies in the topic of irradiation defects is considered as routinary nowadays. it was still rare before the 21st century. Below, I summarize our first studies on point lattice defects in FM bcc iron. All the results shown here are obtained from collinear spin polarized DFT-generalized gradient approximation (GGA) calculations using the SIESTA [4] code.

2.1 Self-interstitial atoms in α-Fe

An example illustrating the relevance of DFT to predict defects properties in metals concerns the energetics and mobility of single SIAs in α-iron.

Extensive studies prior to 2003 applying empirical embedded-atom potentials predicted that the <110> and <111> dumbbell configurations of SIAs in Fe are very close in energy, and that SIAs migrate via very fast one-dimensional motion of the <111> dumbbell, combined with occasional thermally activated reorientations [5]. This is indeed true for most of bcc metals, where the SIA migration en-

ergies given by experiments are quite small, around 0.1 eV. This widely accepted energetic landscape has however been questioned by early DFT calculations for the case of bcc Fe [6]. They showed an unexpectedly large energy difference between the ground state <110> and the <111> dumbbells, namely 0.7 eV This large value makes a migration via the <111> dumbbell incompatible with the experimental value (0.30 eV) of the SIA migration energy [7] (Fig. 2.1). We have therefore investigated via DFT various migration mechanisms and determined that the most favorable mechanism corresponds to the first-nearest-neighbor (1nn) translation- rotation jump , with a migration energy, of 0.34 eV (Fig. 2.1) in excellent agreement with the experimental value. This mechanism, implies a fully three-dimensional migration of SIAs. Curiously, it has been also suggested in an early study via empirical inter-atomic potential (EP) based on elastic properties [8]. It is worth mentioning that such a particular SIA migration behavior in bcc Fe (due to the large energy difference between <110> and <111> dumbbells) seems to be closely connected to magnetism [9], that is, the <111> dumbbell, located along the densest direction of a bcc crystal, induces a more important decrease of local magnetic moments on the SIA, which contributes to increase its energy. At variance, there is a local anti-ferromagnetism around the <110> dumbbell but with a significantly larger moment magnitude [10]. Indeed, a non-magnetic (NM) structure has a much larger energy than an anti-ferromagnetic (AF) structure in bcc Fe [11].

Like in most bcc metals, it is energetically favorable that vacancies and SIAs form clusters, respectively. What is again particular in Fe is that small SIA clusters made of parallel <110> dumbbells have lower formation energies than those made of <111> SIAs, up to a size of around 4 SIAs [12]. These very small <110> interstitials show rather high mobility. For instance, both di- and tri-interstitials have almost the same migration energies (around 0.42 eV) via the same translation-rotation jump like the mono-interstitial. These migration barriers are also in quantitative agreement with experimental evidences [7]. It is worth mentioning that, besides these highly mobile configurations, more recent atomistic simulation results have also proposed another family of small SIA clusters with a ring structure [13], which may be similar or even slightly lower in energy than the current parallel- <110> clusters, but exhibiting a low mobility.

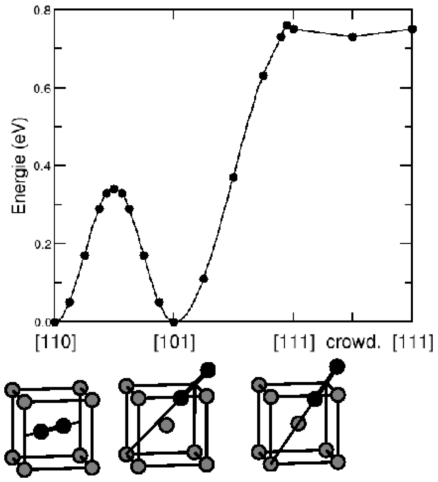

Figure 2.1: Calculated energy barrier for the translation-rotation mechanism of the <110> dumbbell in α-Fe, its rotation to a <111> direction, and the one-dimensional migration, between thr <111> dumbbell and the <111> crowdion configurations.

2.2 Vacancy and small vacancy clusters

The lowest-energy configuration of vacancy clusters in α-Fe shows rather a three-dimensional compact structure. We have shown that the small vacancy clusters migrate by successive nearest-neighbor mono-vacancy jumps [14]. Their mobility is in principle expected to decrease with their size. However, the smallest clusters may behave differently. Indeed, we have obtained low migration energies for the V_2, V_3 and V_4 clusters (respectively 0.62, 0.35 and 0.48 eV), which are even lower than the calculated barrier for a mono-vacancy (0.67 eV) [14]. Fig. 2.2 shows the mechanism for the V_3 migration, where this cluster can migrate while keeping its ground-state configuration. Its low energy barrier can be, at least partially, explained by this geometrical reason. As will be described in Chap. 3, the fast migration of the $V3$ cluster can also play a relevant role in dragging impurities towards sinks. Interestingly, a very recent experimental study measuring the growth rate of SIA loops in α-iron [15] derived an effective vacancy formation energy of around 0.52 eV, which is fully compatible with our calculated average migration energy of V to V_4 clusters, being 0.53 eV.

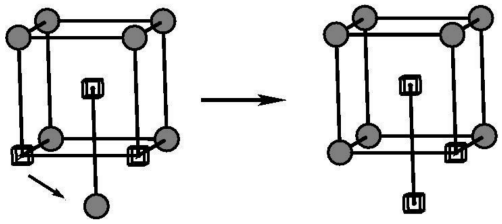

Figure 2.2: Schematic representation of the lowest energy migration mechanism of a tri-vacancy cluster in α-Fe. The empty cubes symbolize the vacancies.

2.3 Comparison with experimental data

It is always challenging to directly compare atomistic modeling results with experimental observations. As described above, several DFT results appear to be in good agreement with experimentally derived values. In order to go one step farther in the comparison, we tried to simulate a specific experiment with the whole set of our DFT data (thanks to a collaboration with various SRMP colleagues). The experiment chosen consists in electrical resistivity recovery measurements in ultra-high purity and carbon doped bcc iron [7]. After low temperature electron irradiation and along the isochronal annealing, various thermally activated processes come into play, inducing abrupt decrease of the electrical resistivity, producing the so called "recovery stages".

The whole set of defects interaction and migration energies from DFT was used as input data of an event-based kinetic Monte Carlo model for a real-time simulation [14, 16]. As a result, all the experimental recovery stages have been successfully reproduced. Moreover, the mechanisms responsible for those stages have been clearly identified. Concerning the self-interstitial type defects, we confirmed the migration of mono-interstitials (stage I) via the translation-rotation mechanism of the <110> dumbbells, as predicted by DFT. We have also shown that both di- and tri-interstitials contribute to the stage of the SIA cluster migration (namely stage II). Another key result from the simulation is to provide strong evidence that the very controversial stage III is due to the migration of vacancy and small vacancy-type clusters. As mentioned above, V_2 to V_4 clusters exhibit migration energies even lower than that of a mono-vacancy, they are therefore immediately mobile when formed as a result of vacancy migration at stage III. These small V_n clusters can perfectly play the role of the anisotropic defects detected by Magnetic After Effect (MAE) experiments at the stage III [17]. It is important to stress that, the resistivity recovery and the MAE experimental data could not be compatible if only the mono-vacancy but not the small V clusters contribute to the Stage III.

In addition to the pure iron case, an excellent experimental-modelling agreement in C-doped Fe [16] gives further confidence on the DFT predictions to explain the physical mechanisms at the origin of the recovery stages. For instance,

the suppression of the stage I confirms the attractive interaction between C and the SIA. Also, successful simulation of the high temperature stages, that is, suppression of the stage III and the emergence of the even higher temperature stages, support quantitatively the DFT predictions on the decrease of effective mobility of vacancy and small vacancy clusters due to carbon (see details in Sec. 3.1).

It is worth mentioning that even though the resistivity recovery experiments allow to access to activation energies for point defects, their interpretation is not trivial. One example to illustrate this concerns the nitrogen doped α-Fe after proton irradiation. Very recently, a joint experiment and DFT-informed rate-theory simulations confirmed the DFT predicted strong nitrogen-vacancy binding) [18], and refuted previously proposed about 10 times smaller N-vacancy binding, the latter being derived only from experimental recovery measurements [19].

2.4 Associated collaborations and publications

Please find below the two publications (P2.1 and P2.2) the most representative of the studies described in this chapter. These studies were the first ones I carried out at SRMP, and thanks to a very nice collaboration I had with all the co-authors of these papers. I want to acknowledge particularly to F. Willaime (advisor of my postdoctoral stay at SRMP) and J. Dalla Torre. More recently, there were also interesting collaborations with T. Jourdan and G. Apostolopoulos (Greece) on the simulation and interpretation of resistivity recovery stages in C and N doped Fe.

- **P2.1: Stability and mobility of mono-and di-interstitials in α-Fe**

  CC Fu, F Willaime, P Ordejón, Phys. Rev. Lett. **92** , 175503 (2004),

  https://doi.org/10.1103/PhysRevLett.92.175503.

  Abstract: We report a detailed ab initio study of the stability and migration of self-interstitial atoms (SIAs) and di-interstitials (di-SIAs) in α-Fe. The $\langle 110 \rangle$ dumbbell is confirmed to be the most stable SIA configuration, 0.7 eV below the $\langle 111 \rangle$ dumbbell. The lowest-energy migration path corresponds to a nearest-neighbor translation-rotation jump with a barrier of 0.34 eV. The most stable configuration for di-SIAs consists of $\langle 110 \rangle$ parallel dumbbells. Their migration mechanism is similar to that for SIAs, with an activation energy of 0.42 eV. These results are at variance with predictions from existing empirical potentials and allow one to reconcile theory with experiments.

- **P2.2: Multiscale modelling of defect kinetics in irradiated iron**

  CC Fu, J Dalla Torre, F Willaime, JL Bocquet, A Barbu Nature materials **4**, 68 (2005),

  https://doi.org/10.1038/nmat1286.

Abstract: Changes in microstructure and mechanical properties of nuclear materials are governed by the kinetics of defects produced by irradiation. The population of vacancies, interstitials and their clusters can however be followed only indirectly, for example by macroscopic resistivity measurements. The information on the mobility, recombination, clustering or dissociation of defects provided by such experiments is both extremely rich and difficult to interpret. By combining ab initio and kinetic Monte Carlo methods, we successfully reproduce the abrupt resistivity changes—so-called recovery stages—observed upon annealing at increasing temperatures after electron irradiation in α-iron. New features in the mechanisms responsible for these stages are revealed. We show that di-vacancies and tri-interstitials contribute to the stages attributed to mono-vacancy and di-interstitial migration respectively. We also predict the effect of the unexpected low migration barriers found for tri- and quadri-vacancies, and discuss the challenging questions raised by the mobility of larger defect clusters.

Chapter 3

Diffusion and clustering of solutes in Fe systems

After addressing the lattice defects in pure Fe, I summarize in this Chapter our most relevant studies on impurities and solutes in FM bcc Fe. I mainly focus on: diffusion and clustering with vacancies of common interstitial elements (C, N, O) in Fe (Sec. 3.1), vacancy mediated diffusion of standard and oversized substitutional solutes (Sec. 3.2), and the behavior of He and H atoms in Fe bulk and grain boundaries (GBs) (Sec. 3.3).

All the studies were DFT based. In various cases, a combination with empirical models and potentials for larger-scale molecular dynamics (MD), Monte Carlo (MC) or Rate Theory type simulations were applied. The DFT calculations were performed using mainly the SIESTA [4] code within the GGA and the collinear magnetism approximation. The bcc Fe matrix was assumed to be fully ferromagnetic.

3.1 Interstitial solutes in α-iron

First, we have performed a systematic DFT study on the behavior of interstitial solutes X (X = C, N or O) in α-Fe [3]. We have shown that the decreasing strength of the X–Fe interactions, from C to O, is mainly dictated by the respective electronic configuration around the solutes rather than by their known atomic radius. It can be seen from Fig. 3.1 a covalent interaction between Fe and C, a very localized charge around the O atom reflecting an ionic interaction, and an intermediate behavior for the Fe-N interaction. The Voronoi volume of the solutes in bcc Fe, controlled by the X-Fe interaction strength, is indeed a relevant parameter characterizing for instance the vacancy-solute interaction: the larger the solute Voronoi volume, the stronger the V-X binding.

Next to vacancies, the competition between available free volume effects and X-Fe interaction results in the preference of the solutes to occupy off-centered

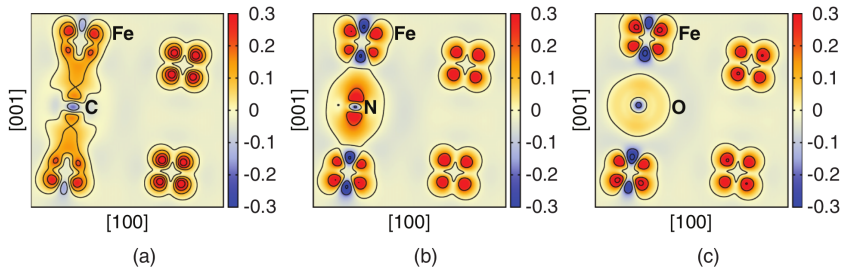

Figure 3.1: Differential electronic density distributions (in $eV/\text{Å}^3$) at the (010) plane) for (a) C, (b) N, and (c) O at the lowest-energy octahedral solution site. We show the distribution around the solutes and their 1nn Fe atoms.

sites, decorating the mono-vacancy and vacancy clusters. But, solutes forming V_nX_m clusters (with n vacancies and m solutes) behave differently depending on their electronic configurations, in particular, the formation of C dimers is highly energetically favorable due to the strong covalent bond between the two C atoms. Such a configuration is not seen with neither N nor O (Fig. 3.2).

It is interesting to go into some details about the energetics of clusters with an increasing number of C solutes around a vacancy (VC_m). Fig. 3.3a shows the lowest-energy configuration for small VC_m clusters (m = 1 to 4), and the energy balance for the VC_{m-1} + C $\rightarrow$ VC_m reaction is represented in Fig. 3.3b. The binding energy (E^b) associated to the reaction can be better understood by splitting it into two contributions, namely "Mechanical" and "Chemical" [20], where the "Mechanical"′ contribution accounts for the energy variation associated to the lattice distortion (or atomic relaxation) when moving a C from its bulk octahedral site to the near-vacancy site. This energy, dictated by the available free volume around the vacancy for C, decreases linearly with increasing number of C around the vacancy. The "Chemical" contribution represents the variation of system energy related to the removal of C from its initial bulk site and the insertion to its final near-vacancy site keeping all Fe atoms frozen. This energy has the same variation shape as the E^b, showing a maximum due to the C dimer formation in VC_2. Some electronic configuration analysis reveals a decrease of covalency in C-C bonds with more than two C atoms, while there is an increase of charge accumulation between C and Fe atoms. This behavior explains the decrease of the "Chemical" energy from VC_2 to VC_4.

Fig. 3.4 shows the binding energy associated to the formation of small V_nX_m clusters. Due to a much stronger V-O binding and significant O-O attraction, the $V_nO_{m-1} + O \rightarrow V_nO_m$ binding energies are generally around 1 eV higher than the corresponding values for C and N. Because of the formation of C dimers, the binding energy for V_nC_m clusters exhibits systematically a maximum if the cluster contains an even number of C atoms.

Based on the DFT calculated set of small V_nX_m cluster binding energies, we

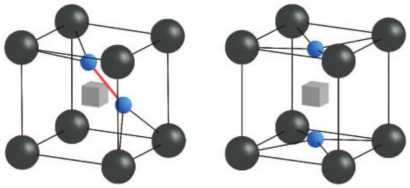

(a) (b)

Figure 3.2: Schematic representation of the lowest energy configurations obtained for: (a) VC_2 and (b) VO_2 (and VN_2) clusters in α-Fe.

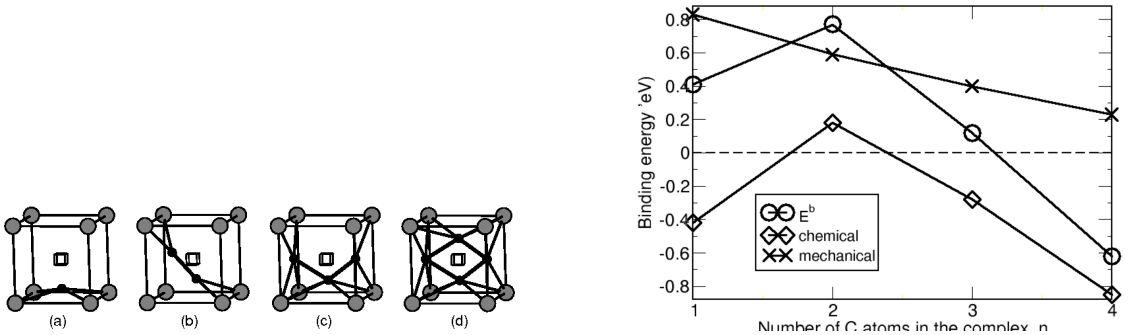

(a) (b)

Figure 3.3: (a) Schematic representation of the lowest energy configurations for VC_m complexes (m = 1 to 4), where cubes, gray and black spheres denote vacancies, Fe and C atoms respectively. (b) "Chemical" and "Mechanical" contributions and the resulting binding energy (E^b) for a VC_m complexes. The considered reaction is VC_{m-1} + C $\rightarrow$ VC_m, with m = 1 to 4. Positive binding energy means exothermic reaction.

have parameterized an interaction model considering vacancies and solute atoms in a bcc Fe lattice, including 2-, 3- and 4-body interaction terms [3]. Thanks to a collaboration with T. Schuler and M. Nastar and via the interaction model, we have extended the DFT results by generating an extensive set of V_nX_m cluster configurations and estimated their energy. Then, by applying statistical mechanics calculations using these clusters data, we have evidenced that a very small amount (probably undetected experimentally) of O and N impurities in α-Fe can be responsible for drastic changes of vacancy concentrations, inducing large deviations from an Arrhenius behavior even at low temperature. This finding is fully compatible with existing experiments, and changes the common vision that C has the dominant effect among the common interstitial impurities [21].

The high energetic stability of the small V_nX_m clusters (Fig. 3.4) motivated

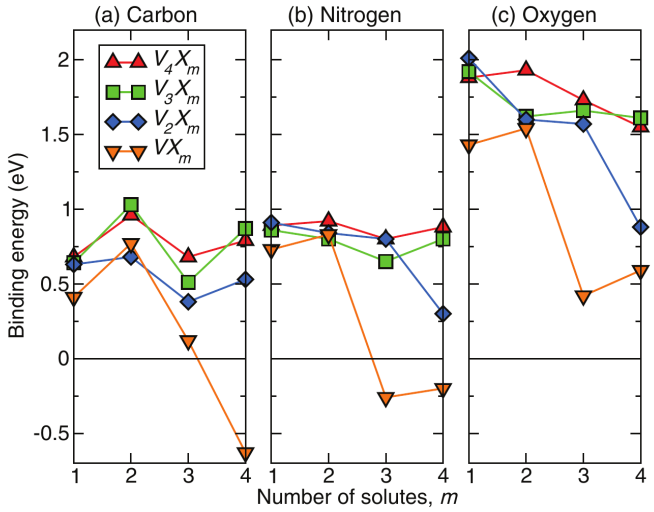

Figure 3.4: Calculated binding energies for the vacancy-X clustering reactions V_nX_{m1} + X $\rightarrow$ V_nX_m for X = C, N, and O and for n, m = 1 to 4. Positive values indicate exothermic reactions.

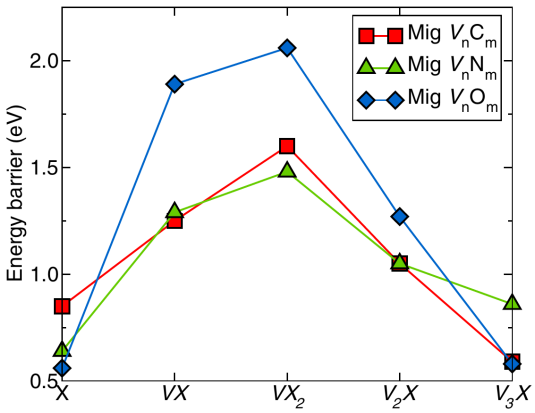

Figure 3.5: Calculated effective migration energies of small vacancy-X clusters (X = C, N, O): V_nC_m (squares), V_nN_m (triangles), and V_nO_m (diamonds).

us to investigate migration mechanisms and barriers for these clusters without dissociation via DFT [22]. Clusters containing any of the three solutes (C, N, O) exhibit similar diffusion characteristics, that is, VX and VX_2, which are the dominant clusters at thermal equilibrium, show a quite low mobility (Fig. 3.5). Therefore, the solute monomers are essentially the only species responsible for the mobility of the solutes in equilibrium conditions. On the other side, V_2X and V_3X clusters are found to be overall more mobile. In particular, by comparing the effective migration energies, V_3X is systematically the most mobile cluster for X = C, N, and O (Fig. 3.5) as well as for X = H [23]. The interstitial solutes follow the migration of the tri-vacancy through successive jumps while staying bound to at least one of the vacancies. This high mobility of V_3X relies on the high stability and mobility of the compact tri-vacancy V_3 in a bcc lattice. This is indeed the case of bcc Fe [14] and bcc Nb [22].

In the present case of iron, we find that, very interestingly, V_3O may be as mobile as the octahedral oxygen, and V_3C may be even more mobile than an isolated C atom. Therefore, at variance with common beliefs, trapping of interstitial solutes by vacancies does not necessarily reduce their mobility.

In order to illustrate the impact of the attraction between vacancies and the interstitial solutes, we have applied a simple thermodynamic model to evaluate the effective vacancy diffusivity in bcc Fe systems containing the equilibrium concentration of free vacancies and a significantly larger amount of C atoms. In the simple model, we considered the presence of VC and VC$_2$ clusters in addition to C solutes and mono-vacancies. Based on our DFT results, the two types of clusters were assumed immobile [20]. The resulting effective vacancy diffusion coefficients (Fig. 3.6) show a non-Arrhenius behaviour even with only 1.2 appm of C. These results reveal the relevant role of small vacancy-carbon clusters, in particular the VC$_2$, to decrease vacancy mobility in α-Fe at relatively low temperatures. In principle, the highly stable small vacancy-N and vacancy-O clusters can also have the same effect reducing vacancy diffusivity. Additional simulations could be performed to confirm this.

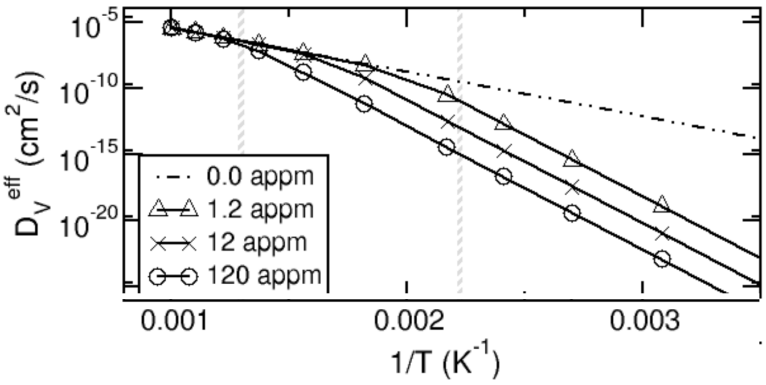

Figure 3.6: Predicted effective vacancy diffusion coefficients versus reciprocal of temperature in α-Fe with four distinct C concentrations, from 0 to 120 appm.

3.2 Substitutional solutes and alloying elements

The so-called vacancy mechanism is generally the dominant diffusion mechanism for the host atoms, and the substitutional solutes and alloying elements in transition-metal systems. This is the case for bcc Fe based systems without irradiation. The standard vacancy mediated diffusion consists in successive exchanges of 1nn atom-vacancy pairs.

It is well known that, for a pure or an extremely dilute system, the tracer self and solute diffusion coefficients can be determined via simple expressions (Eqs. 3.1 and 3.2). In particular the solute correlation factor (f_B) can be well approximated by an analytical function of distinct (limited) vacancy-atom exchange frequencies around the solute, based on the Le Claire model [24–26].

The tracer diffusion coefficient of A atoms in the A matrix (D^* for self-diffusion) can be written as [27, 28] :

$$D_A^{A*} = a^2 f_0 x_v \Gamma_A \tag{3.1}$$

where a is the lattice constant, f_0 is the self-diffusion correlation factor (0.727 for a bcc lattice [25]), x_v is the vacancy concentration. Γ_A is the 1nn vacancy-atom exchange frequency, equal to $\nu_A \exp(\frac{-E^m}{k_B T})$, with ν_A the attempt frequency, E^m the energy barrier for the exchange, and k_B and T are respectively the Boltzmann factor and the absolute temperature.

Similarly, the solute (B) tracer diffusion coefficient in an "A-element" matrix in the dilute limit can be expressed as [27, 28]:

$$D_A^{B*} = a^2 x_v \exp(\frac{G^b}{k_B T}) f_B \Gamma_B \tag{3.2}$$

where G^b is the solute-vacancy binding free energy at a 1nn distance, f_B is the

solute correlation factor, and Γ_B is the 1nn solute-vacancy exchange frequency.

We have considered solutes such as Cu, Al, Ti, Cr in FM bcc Fe [29–33]. The atom-vacancy exchange frequencies were determined via DFT-GGA calculations. When considering alloys beyond the dilute limit, the diffusion coefficients and other diffusion driven properties (*e.g.* kinetic of phase decomposition) were calculated via DFT parameterized on-lattice kinetic Monte Carlo (kMC) simulations. As an example, the DFT-kMC study, in close collaboration with F. Soisson, revealed the importance of highly mobile Cu nano-clusters on the kinetics of Cu precipitation in bcc Fe [29]. A similar approach also pointed out the relevance of including magnetic transition for a correct prediction of the $\alpha - \alpha'$ decomposition kinetics in Fe-Cr [31, 34].

Besides the standard vacancy mechanism, some DFT calculations predicted an atypical behaviour for oversized solute atoms (OSAs) in bcc and fcc iron. These OSAs include the transition metal elements at the beginning of the series (Sc, Y, Lu, Zr and Hf), due to their big atomic size compared with the host atoms [35–37]. Also, the noble-gas elements can behave as OSAs in a transition-metal lattice, because of the strong repulsion with the host atoms which creates a large effective solute volume. This is *e. g.* the case of helium in bcc Fe [38]. At variance with standard substitutional solutes in a cubic lattice, due to an expected very strong attraction with vacancies, an oversized solute atom next to a vacancy tends to form a tightly bound complex (Fig. 3.7 middle), in which the solute sits in the middle of the two 1nn vacancies..

It is clear that the diffusion of the OSAs cannot be carried out via the standard vacancy mechanism. In close collaboration with J.-L. Bocquet, we proposed a new approach [37] that includes a new mechanism for a quantitative determination of diffusion properties of the OSAs in bcc and fcc lattices. The main idea is to split the OSA trajectory into macrojumps (Fig. 3.7), providing a simple way to define the quadratic displacement and the macrojump frequency.

Some oversized solutes can act as important alloying elements in advanced steels, which is the case of yttrium in ODS (oxide dispersion strengthened) steels. We applied our developed approach to the case of yttrium diffusion in bcc and fcc iron, based on low-energy configurations and migration barriers from DFT data [37].

Under thermal vacancy conditions, yttrium is found to diffuse a few orders of magnitude faster than iron in the two structures (Fig. 3.8). To the best of our knowledge, there is no tracer diffusion experimental data available for Y in pure iron. Our prediction is opposite to previously reported Y diffusion coefficients, indirectly deduced from experimental data in ODS-FeCr alloys based on the kinetics of the nano-particle precipitation [39]. A plausible explanation of the apparent discrepancy can be stated as follows: the fabrication process of the ODS steels incorporates a large supersaturation of dislocations, grain-boundaries, vacancies and oxygen atoms. A significant amount of vacancies and oxygen atoms remains in the solid solution during the precipitation, and they strongly bind to

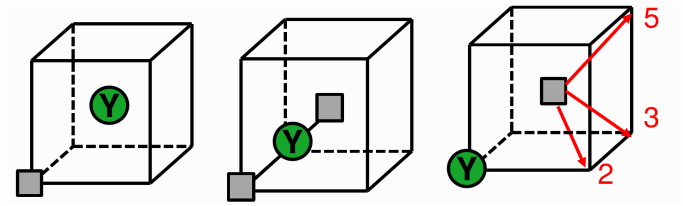

Figure 3.7: OSA diffusion mechanism (a macrojump) in a bcc lattice (represented by yttrium in iron). The left panel shows a vacancy arriving at a 1nn site of the OSA. Then, the OSA spontaneously relaxes to the mid-point between two vacancies forming a stable complex (middle panel). Finally, a vacancy dissociates from the complex (three possible jumps are indicated by arrows), while the OSA moves to a new lattice site (right panel). Circle and square denote respectively the OSA and the vacancy. The numbers in the right panel indicate the neighbor shell of the OSA.

Y leading to the formation of Y-vacancy and Y-O-vacancy clusters. These clusters generally present very low mobility because the Y atoms (like He in Fe [38]) tend to stay at the center of a vacancy cluster. The presence of such clusters decreases significantly the effective diffusion coefficients of yttrium.

Besides the example of yttrium in iron, our proposed modelling method is directly transferable to other OSAs in cubic lattices.

In addition to the diffusion coefficients, activation energies for the macrojumps can be derived. These energies can be then used to parameterize kMC simulations with a twofold advantage: the simulations will not need to explicitly account for the intermediate sites in the on-lattice model, and will be able to skip the trapping-detrapping jumps included in a macrojump [37].

In addition to vacancy mechanisms, it is also important to consider SIA mediated diffusion under irradiation, for example via the diffusion of mixed dumbbells. Properties such as irradiation induced segregation can depend on the interplay between vacancy and interstitials fluxes dragging solutes towards (or away from) dislocations, GBs and other sinks. Several studies on this topic exist in literature. I do not enter into details here, because only very few of my works concern this topic [32, 40].

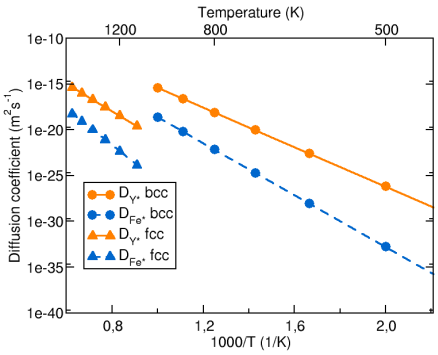

Figure 3.8: Calculated tracer diffusion coefficients of yttrium and iron in FM bcc and NM fcc Fe. Here the magnetic excitation and transition are not considered.

3.3 Helium in α-iron

In addition to intrinsic defects, *i.e.* vacancies (V) and SIAs, a large amount of He and H are also produced by nuclear transmutation under high energy neutron irradiation. Structural materials of future fusion devices may suffer from swelling, intra- and inter-granular embrittlement due to the accumulation of He. As a first and indispensable step to understand these macroscopic properties, the energetics and diffusion of He atoms in α-Fe, as well as their interaction with structural defects must be accurately addressed.

3.3.1 Bulk diffusion and clustering

Even though He is a close-shell element, many relevant questions are still worth investigating using electronic-structure based methods, for instance, what is the dominant nature of He-He and Fe-He interactions in a metal matrix such as bcc Fe ? and, what is the atomic-scale mechanism dictating the nucleation of bubbles observed experimentally ? To address these issues, some early DFT calculations on this topic, ,including our own studies [38, 41, 42] were focused on the stability of He in substitutional and various interstitial sites, on the migration energies of He, and on the interaction of He with vacancies and SIAs in α-Fe. All the DFT studies predicted that the most favorable solution site for helium is the substitutional site, followed by the tetrahedral and then the octahedral sites. The energy difference between the substitutional and the tetrahedral site is rather small (around 0.2 eV). These results are at variance with those from previous EPs, proposing the octahedral site to be more stable than the tetrahedral one. More importantly, a much larger difference between the substitutional and the preferential interstitial site was predicted., that is, 2.1 eV instead of 0.2 eV by DFT. As described below, the discrepancy on such elementary energetic properties has a significant impact on the diffusion properties of He in iron. Thanks to the DFT results, new empirical potentials were developed for an improved description of Fe-He interactions.

It is woth mentioning that a simple repulsive pairwise Fe- He potential revealed capable to capture the main features of He energetics in Fe as predicted by DFT [43].

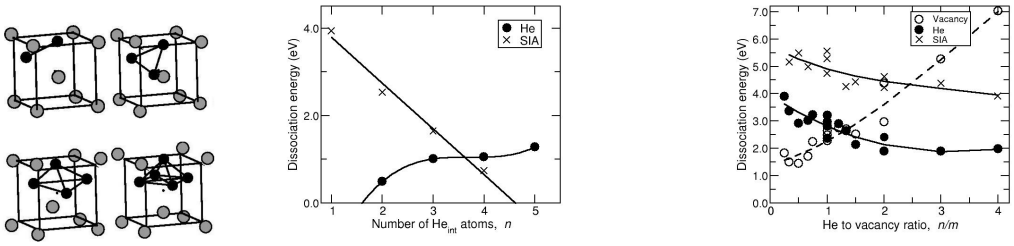

(a) (b) (c)

Figure 3.9: (a) Schematic representation of the lowest-energy interstitial He_n clusters with n = 2, 3, 4 and 5, where the atoms are on their optimized positions, (b) dissociation energy of an interstitial He (He_{int}) or a SIA from the He_n clusters, and (c) dissociation energy of a He_{int}, a SIA or a vacancy from He_nV_m clusters versus He to vacancy ratio, n/m. Here n = 0 to 4, and m = 1 to 4.

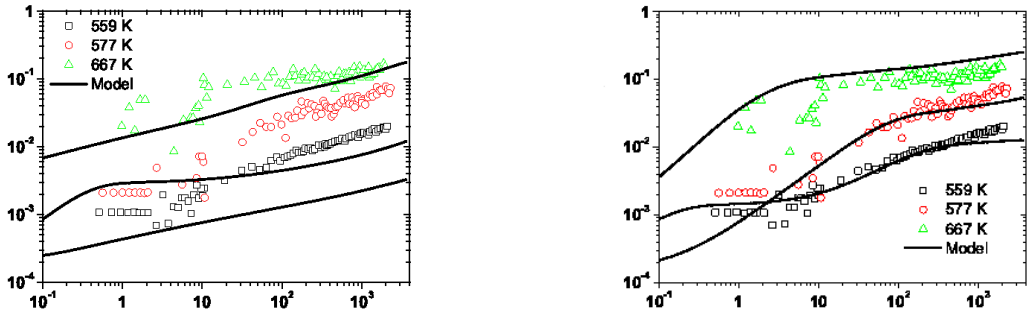

(a) (b)

Figure 3.10: Fraction of desorbed He (y-axis) as a function of isothermal annealing time (x-axis, in seconds). Comparison between experimental data from [44] (symbols) and two sets of thoretical results (lines) by considering either (a) He in pure bcc iron, or (b) He in iron containing C impurities in the modelling.

The strong repulsion between Fe and He atoms is fully consistent with the negligible solubility of He in iron. As a consequence, interstitial He atoms tend to bind to each other although in the absence of vacancies or any other structural defects. Indeed, the driving force of such He clustering is due to the Fe-He repulsion rather than He-He attraction. The lowest-energy state of such small He_n

clusters (Fig. 3.9a shows rather a compact structure. As expected, the He clustering induces a significant local lattice distortion. Interestingly, according to the dissociation energies shown in Fig. 3.9b, the emission of a SIA creating a vacancy is energetically more favourable than the emission of an interstitial He from a He_n cluster with $n \geq 4$. This self-trapping of He atoms followed by the emission of a SIA may constitute the initial stage towards the nucleation of He bubbles. For instance, this mechanism is fully compatible with He bubbles observed at low temperatures where vacancies in Fe are still immobile.

Another consequence of Fe-He repulsion, much more expected, is the tendency of He clustering with vacancies. The lowest-energy structure and the stability of small He_nV_m clusters were determined by DFT studies [38]. It is interesting to note that the strength of binding between a defect (He_{int}, SIA or V) and a cluster are shown to depend mainly on the He density, thta is, the n/m ratio [38, 42], rather than the absolute He content of the He_nV_m cluster. At finite temperatures, these clusters may change their n/m ratio by *e.g.* emitting He atoms, SIAs or vacancies according to their respective dissociation energies. There are also clear trends for the He (SIA, vacancy) dissociation energies from He_nV_m, as a function of n/m (Fig. 3.9c). In particular, at variance with the He_n clisters, the emission of a SIA from clusters containing at least one vacancy always requires higher activation energies than the emission of interstitial He atoms. The over-pressurized He_nV_m clusters are therefore expected to emit He atoms while the under-pressurized clusters emit vacancies, in order to attempt an optimal He/V ratio, which is predicted to be about 1.3 based on DFT studies on the small clusters. In practice, the situation would be of course much more complex. He content in bubbles would be strongly governed by the precise irradiation conditions and the local microstructures, etc.

In order to understand the long range diffusion of He, the elementary mechanisms of He migration must be known. He can migrate almost athermally from one interstitial site to another, requiring an energy barrier of only 0.06 eV [38]. In addition, other possible mechanisms – the vacancy, dissociative, replacement (kick-out), and the exchange mechanism – have been proposed for decades and described by Trinkaus et al. [45].

We have revisited with DFT the vacancy, the dissociative, and the kick-out mechanisms for a substitutional He [38]. The fist mechanism requires an incoming vacancy. Then, the He jumps to an interstitial position between the both vacancies forming a HeV_2 complex. Diffusion of the He atom by vacancy mechanism can be governed by the HeV_2 migration without a total dissociation[38], which is a specific case of the macrojumps as described in Sec. 3.2. The corresponding activation energy was estimated to be 1.1 eV. It is true that, in principle, migration of larger HeV_m clusters may also contribute to the vacancy mechanism, being the HeV_3 a promissing candidate.

A substitutional He (He_{sub}) may also migrate via a dissociative mechanism. The simplest picture can be drawn as follows: when a substitutional He dissoci-

ates from its vacancy, it migrates between interstitial sites until being trapped by another vacancy. The two important quantities for the dissociative mechanism are therefore the interstitial He migration energy, and the energy difference between the He_{sub} and the He_{int}. The former value is given by the tetrahedral He migration energy (0.06 eV). Concerning the latter, DFT predicted a significantly lower value than the one from previous EPs, which makes the dissociative mechanism much more probable to occur [38].

Besides these two mechanisms, a third one comes into play under irradiation, that is, the kick-out mechanism, which may even become the dominant process in the presence of abundant free-migrating SIAs. When a self-interstitial atom approaches a substitutional He, a spontaneous recombination-replacement (kick-out) reaction is expected to occur. We confirmed that the He_{sub} + SIA = He_{int} reaction implies a large energy decrease, namely 3.6 eV. In other words, the energy decreased by recombining a Frenkel pair (5.9 eV) largely overcomes the energy increase by moving a helium atom from a substitutional to a tetrahedral site leaving an empty vacancy behind.

It is generally not trivial to make direct comparison between modeling and experimental data. However, it is absolutely essential, on one side, to check the validity of the numerous assumptions and approximations in the models and theories. On the other side, the modeling results are useful to complement the experiments by providing the detailed physical driving forces and mechanisms behind the observed phenomena.

To better understand the behavior of He in iron, we have chosen to simulate the thermal He desorption measurements during isothermal anneallings after He implantation [44]. We have adopted a multi-scale modeling procedure, that is, a Cluster Dynamics model has been parameterized using all the energetic and mobility data obtained by our DFT study [46]. In this way, a real-time simulation of the experiment were carried out. The results of such a simulation is indeed an interesting example to illustrate how the modeling of an extremely simplified system may or may not capture some of the main features of a real material under a given experimental condition.

As a first attempt, the modelling only accounts for the He properties in pure bcc iron. As a result, significant underestimations of the desorbed He fraction along the isothermal anneallings are observed (Fig. 3.10a). The disagreement strongly suggests that Some relevant physical ingredients are missing in the model.

A very likely possibility concerns the presence of impurities. Indeed, no real materials can be absolutely pure. In the particular case of Fe, it always contains interstitial impurities such as C and N, from some tens to a few hundreds atoms per million (appm). We have then performed a more realistic modeling by considering He in an iron matrix containing C impurities. [46]. Very interestingly, the modeling-experiment agreement becomes significantly better as shown in Fig. 3.10b.

In fact, it is now widely accepted that C atoms trap vacancies in iron. Exper-

imental data, on one side, indicated that a few amount of C may be sufficient to decrease the effective vacancy mobility [7]. On the other side, DFT results also proposed the formation of very stable carbon-vacancy complexes, for example VC, and VC_2, with a dissociation of around 1 eV or higher [3, 47]. Therefore, vacancies are largely trapped by C atoms. The population of the smallest He-vacancy clusters, and particularly the HeV (or He_{sub}) tends to dominate over the larger complexes in the presence of carbon. In this specific experiment, the dissociative mechanism ($He_{int} + V \leftrightarrow He_{sub}$) for He diffusion was proposed to be the dominant one [44], due to a rather high He/V ratio in the samples. The presence of C appears to be able to enhance the effective mobility of He, and therefore, the kinetics of He desorption [46].

3.3.2 Comparison helium-hydrogen

Hydrogen is often present in structural materials used for a wide variety of applications. The occurrence of hydrogen-assisted materials failure via embrittlement and corrosion is well known. Also, as mentioned above, high energy neutron irradiation (as occurring in fusion reactors) produces H in addition to He in the Fe-based structural materials. Both of them interact with the lattice defects, particularly with vacancies. Our atomistic studies, which employ DFT and EP simulations, provide insight into key elementary behavior of H in α-Fe [23, 48]. Below, I summarize the main results and compare them with properties of He in iron.

Before addressing the physical properties, just a few words about the simulation methods. In order to reach low-energy configuration and migration mechanism of hydrogen-vacancy clusters, we first applied MC simulations using EPs for a systematic and efficient exploration. Then, the lowest-energy configurations and paths found were used as inputs for DFT-SIESTA [4] calculations. All details can be found in Ref. [23]. Please note that zero point energy corrections are important for calculations involving hydrogen. This is particularly true when calculating solution energies and H migration barriers, and less so when calculating binding energies because of compensation effects in the involved terms.

Concerning the dissolution of H in bcc iron, the most energetically favorable site far from any lattice defect is the tetrahedral interstitial site. When trapped at vacancies, at variance with He, H atoms do not move to the center of vacancies but rather stay at a nearly octahedral site, decorating the vacancies.

In the bulk, H atoms migrate between tetrahedral sites with very low energy barriers, at about 0.04 eV, giving diffusion coefficients that are in good agreement with experimental data [23, 49]. Similar to the He case, the mobility of hydrogen is generally largely decreased due to the binding with vacancies. Further diffusion of trapped H is expected to occur mainly by dissociation. However, the H-tri-vacancy cluster is an exception (different from the He-tri-vacancy cluster). This is due to the very low diffusion barrier of the tri-vacancy (V_3) cluster in bcc Fe [14] and the off-centered position of H in the V_3 cluster. The fast diffusion of

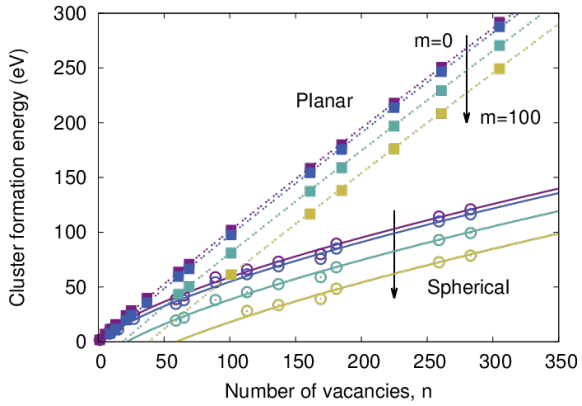

Figure 3.11: Formation energy of H_mV_n clusters as a function of number of vacancies n in the undersaturated region. The curves are calculated from a deduced empirical law as described in Eq. 8 of [23], while data points are from atomistic simulations using an empirical potential. Planar-cluster curves are indicated by dotted lines with filled square data points, while spherical-cluster curves are solid with hollow circle data points. The formation energy is also a function of the nummber of H atoms, m (curves shown for m = 0,10,50,100).

HV_3 without dissociation suggests the relevant role of vacancies to drag H atoms towards sinks such as dislocations and grain boundaries.

We have proposed two regimes of interest for hydrogen clusters/bubbles. In the undersaturated regime, with low H-to-vacancy ratio, almost non-interacting H atoms decorate the surface of a nano-cavity. They maintain a minimum H-H distance of about 1.9 Å. In this regime, we have determined that the compact or spherical shapes of H_mV_n clusters are lower energy structures than planar and linear configurations (Fig. 3.11). This behavior is similar to that of He_mV_n clusters even though the arrangement of He and H atoms in the clusters is different.

On the other side, the oversaturated regime emerges once the surface sites are all occupied by H atoms, and the H_2 molecule formation can occur in the center of clusters as illustrated in Fig. 3.12. We have proposed a rather simple model, with which we outlined a strategy for determining the saturation state [48]. Although this model is built for H in bcc iron, the same concept should be possible to generalize to other systems of interest.

3.3.3 Grain-boundary diffusion, clustering and embrittling effect of helium

Due to the very strong repulsion between Fe and He atoms in α-iron, it is expected that He tends to segregate to GBs where there is generally significant free volume. Several properties of He in GBs, such as diffusion, clustering and their impact on grain boundary (GB) decohesion are not fully understood. Below, I

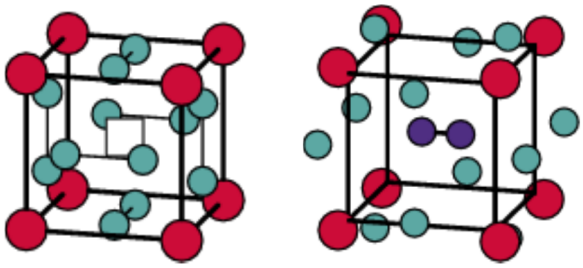

Figure 3.12: Schematic representation of a $H_1 2V$ cluster before (left) and after (right) structural optimization. The small square denotes the vacancy. A H_2 molecule is formed in the center of the vacancy upon the structural optimization. This example illustrates the behavior of over-saturated H-vacancy clusters.

briefly summarize our findings and conclusions based on a combination of DFT and EP calculations [50, 51]. Because the energetic landscape in GBs is much more complex than in the volume, with several inequivalent sites, our strategy consists in: (i) application of EP-MD simulations for an exploration of possible low-energy sites and diffusion paths for He, and (ii) verification of the obtained results using DFT structural optimization and determination of energy barriers. We have considered three symmetric tilt α-Fe grain boundaries: $\Sigma 5(310)/[001]$, $\Sigma 9(114)/[110]$, and $\Sigma 3(111)/[110]$.

Before the calculations involving He, we have shown that structural relaxations, including simulated annealing and atom removal, are crucial for finding the stable GB structure at a given temperature. For instance, a negative formation energy of a vacancy near a GB is a signature of an unstable GB structure, so the non-desired atom should be removed [50].

Concerning He formation energy at distinct substitutional and interstitial sites around the GBs, as expected, the obtained values are much smaller than in the bulk. This confirms the strong He segregation tendency. At variance with the bulk Fe case, the formation energy of an interstitial He is either lower than or similar to that of a substitutional He in the GBs, due to the preence of free volume.

Regarding He diffusion in the vicinity of GBs, even though the diffusion details and precise paths and barriers are GB dependent, some common features are found in the studied GBs: (i) all the barriers found for He diffusion along the GBs are much lower than the He-GB dissociation energy. Consistently, our MD simulations showed that while diffusing, the He atom remains confined in the GB region up to 900 K; (ii) fast one-dimensional paths are found for the GBs, making the He diffusion highly anisotropic along the GBs. In general, we do expect an anisotropic diffusion along GBs presenting ordered structures; (iii) all the diffusion barriers obtained in the GBs are higher than the interstitial He diffusion barrier in the bulk. However, this result does not necessarily imply that the He diffusion along GBs is slower than in the bcc bulk. since the interstitial He in

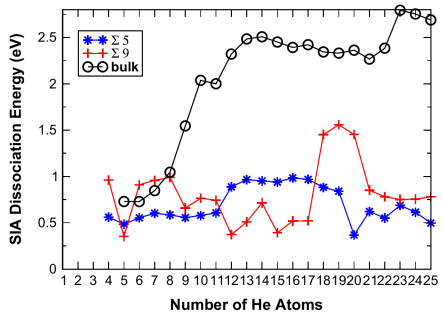

Figure 3.13: Dissociation energy (in eV) of the outer-shell SIA of a He cluster from it, in the $\Sigma5(310)$ and the $\Sigma9(114)$ GBs and in bcc-Fe bulk,

the GB may still diffuse faster than the dominant He species in the bulk, *i.e.*, the substitutional He. Please see Ref. [50] for more details.

For He clustering behavior, we have also performed MD annealings combined with MC Metropolis sampling steps, using EPs, for an efficient searching of the lowest energy configurations of He clusters at two distinct GBs in α-Fe: the $\Sigma5(310)$ and the $\Sigma9(114)$, and compared to the bulk case, for various He concentrations. Complementary DFT calculations were also performed on some of the relevant configurations in order to validate the EP results [51]. Some common features of He clustering in the three environments are found as follows: He atoms strongly prefer to aggregate into clusters rather than distribute homogeneously; when the number of He atoms in the cluster is large enough (typically 4 or 5), the strong local pressure promotes creation of vacancies inside the clusters and emission of SIAs. We proposed this loop punching mechanism to be a crucial elementary mechanism for the cluster growth, particularly in the GBs when a large amount of higly mobile interstitial He atoms migrate from the volume to the GBs.

Certain properties of He clustering found in the considered GBs are visibly different from the bcc bulk. For instance, the formation energy of He clusters in the GBs is much lower than that in the bulk, confirming the strong segregation tendency of He clusters in the GBs. As expected, the He clusters in the GBs are elongated in the directions parallel to the GB plane, while they are isotropic in the bulk. In addition, the loop punching in the GBs is expected to occur more easily than in the bulk, due to a significantly lower Frenkel pair formation energy. The He density in the clusters at the GBs is therefore systematically lower than in the bcc bulk due to a lower He-to-vacancy ratio. Regarding the emitted SIAs, they can more easily dissociate from the clusters in the GBs than in the bulk (lower dissociation energy as in Fig. 3.13, leading to relatively lower local pressures around the clusters in the GBs. This behaviour may contribute to promote a larger cluster and bubble formation in GBs.

Finally, we found that He segregation indeed decreases GB cohesion. Accord-

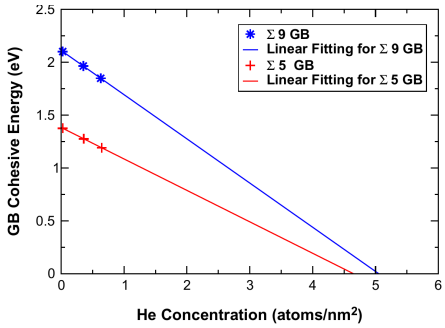

Figure 3.14: GB cohesive energy versus He concentration with He atoms uniformly distributed in the $\Sigma5(310)$ and the $\Sigma9(114)$ GB region. The critical He concentration at each GBs is obtained via a linear extrapolation to the zero cohesive energy. It corresponds to a nomical He concentration of 4467 appm and 4679 appm respectively for the $\Sigma5(310)$ and the $\Sigma9(114)$.

ing to the Rice-Wang thermodynamic criterion [52], He is clearly a GB embrittler. As expected, the embrittling effect of He increases with its concentration (Fig. 3.14). However, having the same He concentration, this effect decreases with He clustering, due to a more localized structural perturbation of GB by the He cluster. Although a direct comparison is not possible, our finding is nevertheless compatible with existing experimental evidence suggesting a stronger GB embrittlement at relatively low temperatures ($\leq 250^o$C) than at higher temperatures when large He bubbles are formed [53, 54]. We have estimated that, even for the extreme case of a uniform distribution of He in the GBs, a very high He concentration of about 5000 appm may be required for a complete decohesion of the considered GBs, which is consistent with some experimental observations [53, 55].

3.4 Associated collaborations and publications

The works related to this Chapter were carried out thanks to fruitful collaborations with several colleagues:

- C. Barouh (former Ph.D student), M.-F. Barthe, T. Schuler, M. Nastar and A. Barbu, concerning the interstitial solutes (Sec. 3.1).
- F. Soisson, E. Martinez (former postdoc), J.-L. Bocquet and C. Barouh about the substitutional solutes (Sec. 3.2).
- M.J. Caturla (Spain), C. Ortiz (Spain), F. Willaime, L. Zhang (former Ph.D student), E. Hayward (former postdoc) on the study of He and H properties in α-Fe (Sec. 3.3. These studies were also performed in the framework of Eurofusion Materials Modelling programme (IREMEV) and the frenco-chinese ANR "HSynThEx" project.

You may find below a set of publications the most representative of the studies described in this chapter: papers P3.1 and P3.2 for Sec. 3.1, P3.3 and P3.4 for Sec. 3.2, and P3.4 to P3.9 for Sec. 3.3.

- **P3.1: Interaction between vacancies and interstitial solutes (C, N, and O) in α-Fe: From electronic structure to thermodynamics**

  C Barouh, T Schuler, CC Fu, M Nastar Phys. Rev. B **90**, 054112 (2014),

  https://doi.org/10.1103/PhysRevB.90.054112.

  Abstract: The interplay between vacancies (V) and interstitial solutes X (X=C, N, and O) and its impact on thermodynamic properties of αFe solid solutions are studied, starting from first principles calculations. A systematic comparison between the three solutes is performed, investigating X–Fe, X–X, and V–X interactions. In the Fe lattice, the strength of X–Fe interactions is found to govern the dissolution properties. Next to vacancies, the competition between solute volume effects and X–Fe interactions results in the preference of all the solutes to occupy off-centered sites. Low-energy configurations of small VnXm clusters are calculated for n and m up to 4. They are used to parametrize lattice interaction models at the atomic scale. A detailed analysis of the cluster properties suggests the relevance of many-body terms in these models. The accuracy of the resulting models is verified through their satisfactory prediction of vacancy-solute cluster properties beyond the fitting database. From these models, an entire set of VnXm clusters is generated with a new configurational space exploration method. Statistical treatment of the solid solution including these clusters is then achieved by means of low-temperature expansions, checked against Monte Carlo simulations in some specific conditions. Based on the calculation of equilibrium cluster distributions, it is shown that the solubility limit of oxygen in Fe, hardly measurable experimentally, is largely affected by the presence of small VnOm clusters.

- **P3.2: Predicting vacancy-mediated diffusion of interstitial solutes in α-Fe**

  C Barouh, T Schuler, CC Fu, T Jourdan, Phys. Rev. B **92**, 104102 (2015),

  https://doi.org/10.1103/PhysRevB.92.104102.

  Abstract: Based on a systematic first-principles study, the lowest-energy migration mechanisms and barriers for small vacancy-solute clusters (VnXm) are determined in α-Fe for carbon, nitrogen, and oxygen, which are the most frequent interstitial solutes in several transition metals. We show that the dominant clusters present at thermal equilibrium (VX and VX2) have very reduced mobility compared to isolated solutes, while clusters composed of a solute bound to a small vacancy cluster may be significantly more mobile. In particular, V3X is found to be the fastest cluster for all three solutes. This

result relies on the large diffusivity of the most compact trivacancy in a bcc lattice. Therefore, it may also be expected for interstitial solutes in other bcc metals. In the case of iron, we find that V3X may be as fast as or even more mobile than an interstitial solute. At variance with common assumptions, the trapping of interstitial solutes by vacancies does not necessarily decrease the mobility of the solute. Additionally, cluster dynamics simulations are performed considering a simple iron system with supersaturation of vacancies, in order to investigate the impacts of small mobile vacancy-solute clusters on properties such as the transport of solute and the cluster size distributions.

- **P3.3: Decomposition kinetics of Fe-Cr solid solutions during thermal aging**

  E Martínez, O Senninger, CC Fu, F Soisson Phys. Rev. B **86** , 224109 (2012),

  https://doi.org/10.1103/PhysRevB.86.224109.

  Abstract: The decomposition of Fe-Cr solid solutions during thermal aging is modeled by atomistic kinetic Monte Carlo simulations, using a rigid lattice approximation with pair interactions that depend on the local composition and temperature. The pair interactions are fitted on ab initio calculations of mixing energies and vacancy migration barriers at 0 K. The entropic contributions to the mixing of Fe-Cr alloys and to the vacancy formation and migration free energies are taken into account. The model reproduces the change in sign of the mixing energy with the alloy composition and gives realistic thermodynamic and kinetic properties, including an asymmetrical miscibility gap at low temperature and diffusion coefficients in good agreement with available experimental data. Simulations of short-range ordering and α-α' decomposition are performed at 773 and 813 K for Cr concentrations between 10% and 50%. They are compared with experimental kinetics based on three-dimensional atom probe and neutron scattering measurements. The possible effect of magnetic properties on diffusion in the α and α' phases, and therefore on the decomposition kinetics, is emphasized.

- **P3.4: Migration mechanism for oversized solutes in cubic lattices: The case of yttrium in iron**

  JL Bocquet, C Barouh, CC Fu, Phys. Rev. B **95**, 214108 (2017),

  https://doi.org/10.1103/PhysRevB.95.214108.

  Abstract: Substitutional solutes in metals generally diffuse by successive exchanges with vacancies, that is, via the so called vacancy mechanism. However, recent density functional theory (DFT) calculations predicted an atypical behavior for the oversized solute atoms (OSAs) in bcc and fcc iron. These solutes exhibit a very strong attraction with a nearby vacancy (V) at a

first neighbor (1nn) distance. The attraction is so large that the 1nn OSA-V pair is no longer stable and relaxes spontaneously towards a new configuration where the OSA sits in the middle of the two half-vacancies (V/2). As a consequence, the diffusion of OSAs cannot be described by the standard vacancy mechanism. A new migration mechanism with a new formulation of correlation effects is required. The present study rests on a revised expression of the diffusion coefficient of the OSAs in bcc and fcc lattices, which introduces the concept of macrojumps. The formalism is applied presently to the case of yttrium (Y: a principal alloying element of advanced steels) in iron, using DFT data. But it is directly transferable to other OSAs in cubic metal lattices. At variance with the standard substitutional solutes, the Y atom is found to diffuse more rapidly than iron at all temperatures by orders of magnitude in the two cubic-Fe structures. This finding is opposite to the recent common belief that yttrium is a slow diffusing species in Fe alloys, based on experimental evidences. Several suggestions are proposed to solve this apparent inconsistency.

- **P3.5: Ab initio study of helium in α-Fe: Dissolution, migration, and clustering with vacancies**

  CC Fu, F Willaime, Phys. Rev. B **72**, 064117 (2005),

  https://doi.org/10.1103/PhysRevB.72.064117.

  Abstract: Density functional theory calculations have been performed to study the dissolution and migration of helium in α-iron, and the stability of small helium-vacancy clusters HenVm (n,m=0 to 4). Substitutional and interstitial configurations of helium are found to have similar stabilities. The tetrahedral configuration is more stable than the octahedral by 0.2 eV. Interstitial helium atoms are predicted to have attractive interactions and a very low migration energy (0.06 eV), suggesting that He bubbles can form at low temperatures in initially vacancy-free lattices. The migration of substitutional helium by the vacancy mechanism is governed by the migration of the HeV2 complex, with an energy barrier of 1.1 eV. The activation energies for helium diffusion by the dissociation and vacancy mechanisms are estimated for the limiting cases of thermal-vacancy regime and of high supersaturation of vacancies. The trends of the binding energies of vacancy and helium to helium-vacancy clusters are discussed in terms of providing additional knowledge on the behavior of He in irradiated iron, necessary for the interpretation of complex experimental data such as thermal He desorption spectra.

- **P3.6: Influence of carbon on the kinetics of He migration and clustering in α-Fe from first principles**

  CJ Ortiz, MJ Caturla, CC Fu, F Willaime, Phys. Rev. B **80**, 134109 (2009),

https://doi.org/10.1103/PhysRevB.80.134109

Abstract: Density functional theory (DFT) calculations have been performed to study the interaction of carbon with He-vacancy complexes in α-Fe. Using the DFT predictions, a rate theory model that accounts for the evolution of carbon, helium, and defects created during irradiation has been developed to explore the influence of carbon on the kinetics of He diffusion and clustering after implantation in α-Fe. This DFT-based rate theory model predicts that carbon not only influences vacancy (V) migration but also He desorption, enhancing He mobility in particular for low V/C ratios. The reason for this behavior is mainly the formation of VC and VC2 complexes, which significantly reduces the mobility of vacancies with respect to pure Fe, inhibiting the formation of higher order clusters, i.e., HenVm, and increasing thus the number of He at substitutional positions at room temperature. Assuming reasonable values of carbon concentration, we successfully reproduce and interpret existing desorption experimental results, where all the energetic parameters for the relevant reactions were obtained from first-principles calculations. In addition, our study provides a detailed explanation of the various He migration mechanisms that prevail under the considered experimental conditions.

- **P3.7: Interplay between hydrogen and vacancies in α-Fe**

  E Hayward, CC Fu Phys. Rev. B **87**, 174103 (2013),

  https://doi.org/10.1103/PhysRevB.87.174103.

  Abstract: We present an atomistic study of the behavior and interactions of hydrogen and vacancies in body centered cubic (bcc) iron, using both ab initio and classical molecular dynamics methods. Hydrogen causes damage to materials through embrittlement, hardening, and swelling; we investigate the role of vacancies in these processes. Hydrogen, which normally diffuses with a very small barrier, is strongly trapped at monovacancies and vacancy clusters, resulting in changes to its electronic structure. Following saturation of the surface of a vacancy cluster, the formation of H2 molecules is possible, at variance with the situation in the bulk. High local concentrations of hydrogen increase the likelihood of vacancy formation and stabilize vacancy clusters. Small hydrogen-vacancy clusters generally tend to diffuse by dissociation, but the trivacancy is shown to be capable of dragging hydrogen while migrating. We describe the structure of clusters of vacancies with varying hydrogen concentrations, finding that compact or spherical bubbles are generally lower energy than planar or linear configurations. Comparison with other bcc metals and with experiment is provided. For systems involving light elements such as hydrogen, corrections for zero-point energy are very important; we include these in our calculations and discuss their importance for different properties.

- **P3.8: Energetic landscape and diffusion of He in α-Fe grain boundaries from first principles**

  L Zhang, CC Fu, GH Lu, Phys. Rev. B **87**, 134107 (2013),

  https://doi.org/10.1103/PhysRevB.87.134107.

  Abstract: Combined density functional theory and empirical-potential calculations are performed to investigate the lowest-energy sites and migration mechanisms of He in various α-Fe grain boundaries (GBs). Before the defect calculations, we show that structural optimizations, including simulated annealing and atom removal, are crucial for locating the stable GB structure in a given temperature regime. Then, the He formation energies for all the substitutional and interstitial sites in two different GBs are evaluated, showing a strong He segregation tendency. At variance with the bulk Fe case, the formation energy of an interstitial He is either lower than or similar to that of a substitutional He in the GBs. Finally, both static and dynamic barriers for interstitial He diffusion in the GBs are determined. Although the diffusion details and precise paths are GB dependent, some common features are identified: (1) The He atom always remains confined to the GB region while diffusing; (2) the He diffusion is highly anisotropic along the GBs; (3) the GB diffusion of an interstitial He atom is found to be always slower than its bulk diffusion, but it can still be faster than the bulk diffusion of a substitutional He.

- **P3.9: Properties of He clustering in α-Fe grain boundaries**

  L Zhang, CC Fu, E Hayward, GH Lu, J. Nucl. Mater. **459**, 247 (2015),

  https://doi.org/10.1016/j.jnucmat.2015.01.008.

  Abstract: Classical molecular dynamics and density functional theory calculations are performed to study the impact of two distinct Fe grain boundaries (GBs) on the clustering properties of helium (He) and the possible He effect on GB decohesion. Several He concentrations are considered. Common properties of He clustering are found for the both GBs, which are visibly different from the bcc bulk. In particular, He clusters in the GBs are always elongated in the directions parallel to the interface and contracted in the direction normal to the GB plane, while they are isotropic in the bcc bulk. When the He number in the clusters is sufficiently large, the strong local pressure promotes the occurrence of loop punching, which is easier to trigger in the GBs than in the bulk, resulting in a lower He-to-vacancy ratio in the GB clusters. The emitted self-interstitial atoms (SIAs) can more easily dissociate from the clusters in the GBs than in the bulk, leading to relatively lower local pressures around the clusters in the GBs, and facilitating the clusters growth. He is found to decrease GB cohesion, and the embrittling effect of He increases with its concentration. But interestingly,

this effect decreases with He clustering. The present findings are fully compatible with existing experimental evidence, for instance, for a stronger GB embrittlement due to He at rather low temperatures than at higher temperatures.

Chapter 4

Impact of magneto-chemical interplay on thermodynamic, defect and diffusion properties

In the two previous chapters, we have addressed various properties in bcc Fe systems by assuming a perfect FM state, that is, neglecting possible effects of *e.g.* non-collinear magnetism, magnetic excitation and magnetic order-disorder transition. For a more accurate and realistic prediction of properties in Fe systems (and in any other magnetic alloy), an appropriate description of the magnetic effects and their interplay with other degrees of freedom (chemical, vibrational, elastic...) is essential. At low temperatures, when the system is well below the magnetic transition temperature, magnetic frustrations often occur because distinct magnetic-interaction tendencies cannot be simultaneously satisfied. Moreover, magnetic excitations and transitions emerge with increasing temperature. The inclusion of these finite-temperature magnetic effects in atomic-scale studies for a prediction of bulk Fe-alloys properties (especially kinetics) is not trivial. An efficient and sufficiently accurate approach is required.

In this chapter, I first give a description of our study methodology, especially of an efficient DFT-based spin-atomic MC approach that we developed for the prediction of thermodynamic and kinetic properties of magnetic metal alloys, as a function of temperature (Sec. 4.1). Then, I discuss the issue of low-temperature magnetic frustration and local-environment dependency in Sec. 4.2. In Secs. 4.3, 4.4 and 4.5, I show our results on respectively thermodynamic, vacancy and atomic-diffusion properties as functions of temperature and alloy composition in various bcc and fcc Fe alloys. Finally, a first attempt to link magnetic and microstructural evolution is summarized in Sec. 4.6.

4.1 Methodology

Effects of magnetism can be addressed via first principles electronic-structure calculations in magnetically ordered configurations, which are now routinely performed using DFT. In Sec. 4.2 we employ DFT as implemented in VASP [56–58], SIESTA [4] and PWSCF [59] codes within GGA. At variance with most existing DFT works on Fe bulk systems, we go beyond the collinear-spin approximations, which is indispensable when addressing effects of magnetic frustration. When necessary, we also apply local-spin constraint on selected atoms via our own modifications in the above-mentioned DFT codes.

Considering finite–temperature effects, it remains a challenging task to model magnetic excitations, transitions, and paramagnetism [60] even in the case of defec-free alloys. Available first principles approaches dealing with finite temperature magnetism in alloys include, for instance, the disordered local moment (DLM) [33, 61–65] and the spin-wave [64, 66] methods. However, these approaches generally provide direct results only at the perfectly ordered magnetic ground state (MGS) and the totally disordered ideal PM state. Furthermore, these methodologies are too computationally expensive for a systematic exploration of properties dependent on local spin-chemical configurations, in non-dilute magnetic alloys. On the other side, DFT-informed atomistic approaches such as spin-lattice dynamics [67–70] and spin-atom MC simulations [1, 71–76] provide an efficient way to investigate finite temperature magneto - chemical correlations. However, as expected, the accuracy of their outcome strongly depends on the quality of the parameterized potentials and models.

As the simplest structural defect in metals and alloys, vacancy plays a dominant role in *e.g.* atomic diffusion. For magnetic metal systems, theoretical studies addressing finite-temperature magnetic effects on vacancy formation properties have been dominantly focused on pure and extremely dilute Fe alloys [2, 65, 66, 68, 75, 77–80], using either the DLM or the spin-wave method for vacancy formation energy in the perfect FM and PM states [33, 65, 66, 77–80], or via spin-lattice dynamics [68], or in our works, predicting the full temperature-evolution of vacancy properties [2, 75] It is worth mentioning that, the DLM and the spin-wave methods usually adopt the semi-empirical Ruch model (Eq. 4.1 for the determination of the temperature-evolution of the vacancy formation energy. The Ruch model [81] proposes:

$$E_f(T) = E_f^{PM}(1 + \alpha S^2) \tag{4.1}$$

where E_f^{PM} is the vacancy formation energy in the perfect PM state, with zero magnetic short-range order (SRO). S is the magnetic order parameter (the reduced magnetization) and α is a scalar. Note that to apply the Ruch model, the temperature dependence of S, and either E_f^{PM} or α should be known, in addition to E_f^{FM}.

At variance with the dilute systems, most available theoretical studies addressing vacancies in concentrated alloys only computed their formation energy in the ordered magnetic ground states [82–88]. Only a few studies computed the value in the ideal PM state [63]. Also, theoretical investigations of the alloying effects on vacancy formation are mainly restricted to either nearly-perfect ordered phases [89–94] or fully random solid solutions [82–88, 95–97]. A continuous and consistent modelling of vacancy (and any other point defect) properties as a function of temperature and hence of chemical and magnetic orders is still rare [76, 98]

Considering kinetic processes, and more predisely atomic-diffusion properties, again, some DFT-based DLM studies [33, 77, 78], computed the diffusion activation energies (Q) at both the fully ordered MGS and the ideal PM state. and obtained the temperature-dependent $Q(T)$ using the Ruch model (Eq. 4.1 replacing E_f by Q).

Another approach used to determine the temperature evolution of the diffusion properties is the spin-lattice dynamics [67, 68], employing empirical potentials with Heisenberg-interaction terms for the magnetism. A major advantage of such an approach consists in the natural inclusion of the combined phonon-magnon effects. However, in practice an accurate potential is not obvious to parameterize, especially for magnetic alloys. Furthermore, such spin-lattice dynamics simulations can hardly reach very long time scales and large simulation systems (typically around a few tens of nanoseconds and 16000 atoms as in Ref. [68]).

As briefly mentioned above, our modelling strategy to investigate finite temperature magnetic effects on thermodynamic, defect and diffusion properties in Fe alloys is to apply on-lattice spin-atomic MC and kMC simulations using the effective interaction models (effective interaction model (EIM)s). The on-lattice kMC approach is particularly powerful for the simulation of kinetics processes (*e.g.* precipitation, phase ordering) driven by thermal activated events such as atomic diffusion [29, 32, 99, 100]. In our approach, the EIM contains explicitely both chemical and magnetic variables, it allows therefore to gain insights into the effects of magneto-chemical interplay behind the physical properties. I want to stress that our EIMs are only parameterized on DFT results on several chemical and magnetic configurations. Neither experimental nor CALPHAD data are included in the fitting data-base.

It is worth mentioning that some previous studies have already proposed EIMs with both magnetic and chemical variables [66, 71, 72, 101–103], but without considering lattice defects and, therefore, not able to study diffusion. On the other hand, more conventional EIMs have been developed to study thermodynamic and kinetic properties without explicitly including spin variables [29, 31, 34, 104, 105].

In our studies, we employ the following Hamiltonian for the EIMs (Eq. 4.2, where magnetic interactions are described via a generalized Heisenberg approach

(similar to Refs. [72, 102, 106]), enabling both longitudinal and transversal spin fluctuations. In addition, a pairwise "chemical" (or nonmagnetic) interaction term is included. Please note that when applying these EIMs in Monte Carlo simulations, we evolve both the atomic and the magnetic configurations. For the latter, a quantum-statistic treatment of spin is necessary for a correct prediction of the magnetic entropy at low temperatures. We therefore adopted the Bose-Einstein statistics in our spin-MC simulations [2] up to the magnetic transition temperature, following the quasi-harmonic approach of Ref. [107].

$$H = \sum_{i}^{N} A_i^{(S)} M_i^2 + B_i^{(S)} M_i^4 + \sum_{i}^{N} \sum_{n}^{P} \sum_{j}^{Z_n} J_{ij}^{(n)} \mathbf{M}_i \cdot \mathbf{M}_j + \sum_{i}^{N} \sum_{n}^{P} \sum_{j}^{Z_n} V_{ij}^{(n)} \sigma_i \cdot \sigma_j \tag{4.2}$$

Here N is the total number of atoms, P is the maximum range of interactions in terms of neighbor shells, Z_n is the coordination number of the n-shell, $\mathbf{M}_i$ represents the magnetic moment of the i-th atom, and M_i is its magnitude. $V_{ij}^{(n)}$ and $J_{ij}^{(n)}$ represent respectively the chemical pair-interaction and the magnetic exchange-coupling parameters between sites i and j, as n-shell neighbors. These interaction parameters ($V_{ij}^{(n)}$ and $J_{ij}^{(n)}$) depends on the chemical species of the i-th and the j-th atoms. σ_i is the occupation variable of the i-th site. It is 1 if there is an atom on the site, and 0 if there is a vacancy. $A_i^{(S)}$ and $B_i^{(S)}$ are the magnetic on-site parameters of the i-th atom, where "S" indicates the distance between the site and a vacancy. These onsite parameters for at least the first and second nearest neighbors of a vacancy differ from the values for a bulk atom [75]. In some cases, the on-site and the pair-wise interaction parameters are also functions of the local chemical composition. A temperature-dependent term can be also included in the chemical interaction term ($V_{ij}^{(n)}$) in order to account for the vibrational-entropy effects based on DFT calculations [76].

So far, we have parameterized such model Hamiltonians for bcc Fe, Fe-Cu, Fe-Mn, Fe-Co, and fcc Fe-Ni alloys. For each system, sets of parameters are determined to describe atoms in a defect-free environment, close to a vacancy, and in the saddle-point position of vacancy-atom exchange. The latter is required for the prediction of vacancy-mediated diffusion. All the corresponding parameter values, as well as a description of the fitting procedure are given in Refs. [2, 33, 73, 75, 76, 108].

Regarding our MC set-up using the EIMs, all details can be found in Refs. [2, 76, 108]. Among them, it is worth mentioning that the magnetic free energy for vacancy formation (including magnetic but not vibrational excitation) at any temperature and composition is computed via a kind of Widom substitution method

[76, 85, 88, 109], as explained in detail in Ref. [76]. The same method can also be applied to the case of other point defects such as SIAs in alloys.

Then, in order to compute tracer diffusion coefficients, we determine the two constituents of the Einstein's formula [110–112] with kMC, where $< r^2 >$ and t in Eq. 4.3 are respectively the mean square displacement of the tracers and the corresponding physical time:

$$D^* = \frac{< r^2 >}{6t} \tag{4.3}$$

For the self-diffusion case, the tracer diffusion coefficients of A atom in a pure or infinitely dilute A system (D^*) can also be written in terms of the vacancy concentration and the migration barrier at a given T as [27, 28]:

$$D_A^{A*} = a^2 f_0 x_v \nu_A \exp(\frac{-G_{mag}^m}{k_B T}) \tag{4.4}$$

where a is the lattice constant, f_0 is the self-diffusion correlation factor (0.727 for a bcc lattice [25]), x_v is the vacancy concentration, ν_A is the attempt frequency, G_{mag}^m is the magnetic free energy barrier for the exchange between the vacancy and the host atom (A), and k_B and T are respectively the Boltzmann factor and the absolute temperature. If at thermal equilibrium, $x_v = exp(\frac{-G^f}{k_B T})$, with G^f being the vacancy formation free energy. Both magnetic and vibrational entropies are considered in this study, and the latter is calculated just via DFT at the MGS.

Similarly, the solute (B) tracer diffusion coefficient in an "A-element" matrix at the dilute limit can be written as [27, 28]:

$$D_A^{B*} = a^2 x_v^{1nn} f_B \nu_B \exp(\frac{-G_{mag}^{m,B}}{k_B T}) \tag{4.5}$$

where x_v^{1nn} is the vacancy concentration at a 1nn site of the solute, ν_B is the vacancy-B exchange attempt frequency, f_B is the solute diffusion correlation factor and $G_{mag}^{m,B}$ is the magnetic free energy barrier for the vacancy-solute exchange.

It is worth noting that the expressions 4.4 and 4.5 differ slightly from respectively the equations 3.1 and 3.2 because here we include the magnetic excitation and transition effects in the distinct terms, for example in the vacancy-atom exchange barriers. As shown in Sec. 4.5, we have also proposed a generalization of Eqs. 4.4 and 4.5 to systems beyond the dilute limit.

Please note that the time t for Eq. 4.3 obtained from the kMC has to be rescaled in order to get the physical time for a real system containing the equilibrium vacancy concentration instead of the vacancy concentration of the simulation box (concretely the diffusion coefficient is multiplied by the factor C_v/C_{MC}). [2, 29, 31]

During these kMC simulations, at each temperature, we start performing spin Metropolis MC steps to reach the equilibrium magnetic state, then we start mov-

ing atoms. Some spin steps are also performed after each atomic move (a 1nn atom-vacancy exchange) based on a time residence algorithm. For simplicity, we assume the typical time spent for one atom-vacancy exchange is sufficiently short, so that all the atomic spins are kept frozen while going from the initial to the saddle-point state. However, we have determined that considering another assumption has a negligible effect on the results. Indeed, similar simulations were performed assuming the opposite, being that the spin-variation time is much shorter than the lifetime of both the initial and the saddle-point states, and very close migration barrier were obtained [2]. This verification suggests that these properties are not sensitive to the detailed way of implementing the characteristic time of spin variations, and contribute to support the validity of our results [2].

4.2 Low-temperature Magnetic effects

4.2.1 Magnetic frustrations in bcc Fe-Cr

In this Sec. 4.2.1, we consider the bcc Fe-Cr systems (in particular, Fe/Cr interfaces and Fe or Cr nano-clusters) in order to investigate effects of magnetic frustrations. We have performed DFT-GGA calculations to determine magnetism and energetics at low temperatures (without thermal excitations), and checked the temperature dependency of these properties via spin-MC simulations using a magnetic cluster expansion (MCE) model [1, 113, 114]. The simulations adopt a bi-crystal setup representing infinite interfaces. Please note that this MCE for Fe-Cr (developed by Lavrentiev *et al.* [115]) is essentially the same type of models as our EIMs for various Fe alloys, but mostly devoted to magnetic properties.

Cr magnetic order	AF	NM	NColl
(100)	0.11 (0.14^a)	0.14 (0.16^a)	0.17 (0.17^b)
(110)	0.19 (0.26^a)	0.09 (0.14^a)	0.17 (0.15^b)
(111)	0.13 (0.19^a)	0.12 (0.16^a)	0.20 (0.19^b)

Table 4.1: DFT calculated interface formation energies (in J/m^2) between bcc Cr with various magnetic structures (AF, NM or non-collinear (NColl)) and FM bcc Fe. The SIESTA [4] values are compared with the plane-wave-DFT (^{a}PWSCF [59] or ^{b}VASP [56–58]) results, which are given in parentheses.

First, we have determined the formation energy of three low-index ((100), (110) and (111)) interfaces between FM bcc Fe and bcc Cr with various magnetic configurations. Results from three different DFT implementations are shown in Table 4.1.

If considering NM-Cr, the densest (110) interface has the lowest formation energy, just as expected for an interface between two bcc metals exhibiting phase separation tendency. However, the (110) interface shows the highest energy among the three interfaces if Cr has a collinear AF structure. This is a direct consequence of magnetic frustration resulting from competing bulk FM-Fe and AF-Cr magnetic ordering, and AF Fe-Cr 1nn and second-nearest-neighbor (2nn) coupling tendency at the interface. Once the collinear constraint is removed, the energy of the (110) interface decreases due to partial relaxation of magnetic frustration. On the other hand, the non-collinear structures are found to be overall higher in energy than the respective collinear configuration for the (100) and (111) interfaces. This comes from a subtle balance between two competing interactions. On one hand, the Fe-Cr 1nn anti-parallel coupling at the interface is best satisfied in a collinear structure. On the other hand, in a non-collinear structure, magnetic frustration associated with the parallel orientation of moments for the 2nn Fe-Cr pairs is partially relaxed, but at the same time this destroys the perfect antiparallel coupling between the 1nn Fe-Cr moments.

When checking in detail the magnetic structure of both collinear and non-collinear low-energy states, we notice that the reduction of magnitudes of local moments near the interface represents a visible signature of magnetic frustration. We also note that the lowest-energy magnetic configuration of the (110) interface consists in the local moments of bulk Fe and Cr atoms being orthogonal to each other, in excellent agreement with available experimental neutron diffraction measurements [116, 117].

Otherwise, keeping in mind that the magnetic ground state of bcc Cr actually consists in collinear spin density waves (SDWs) ([118] and references therein), we also suggest another possibility to relax partially the magnetic frustration, for instance on the (110) interface. The development of in-plane SDWs (having the wave vector parallel to the interface) with the nodes located at the interface plane induces the formation of periodic low-moment sites at Fe/Cr(110), which helps to relax the magnetic frustrations and lower the interfacial energy. Based on our results, we may expect that, as a combination of the two alternatives, non-collinear-SDWs may also occur near the Fe/Cr(110) interface, contributing to further lower its formation energy [113].

The temperature variation of magnetic structures near the interfaces has been investigated using the MCE model and large-scale Monte Carlo simulations. Non-collinear configurations found at low temperatures (the same as by DFT) remain stable up to the Néel temperature pf bcc Cr. The interfacial energy exhibits significant variation near the magnetic phase transition temperatures. Magnetization of interfacial layers of Cr remains nonzero at temperatures well above the Néel temperature, due to exchange interactions between Cr and Fe moments (Fig. 4.1). At temperatures close to the Curie point the (110) interface becomes the one showing the lowest energy, in agreement with DFT results for the FM-Fe/NM-Cr interface [1].

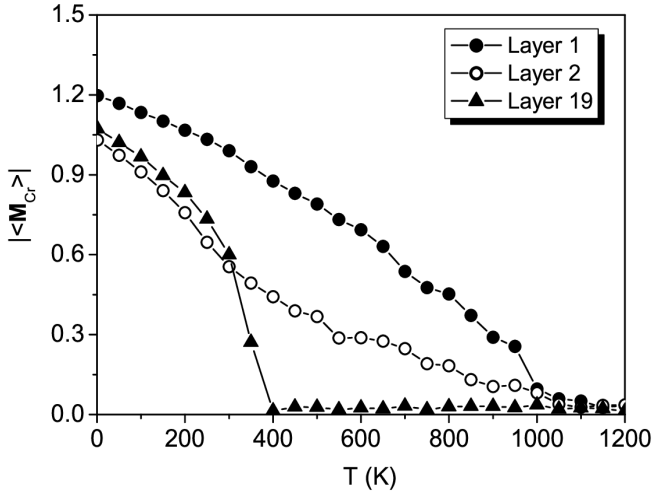

Figure 4.1: Temperature dependence of the average Cr magnetic moment from MCE near the Fe/Cr(100) interface and in the Cr bulk.

The infinite interfaces are rather good representation of interface between the matrix and big precipitates, Going to the opposite side, we have also investigated magnetic and energetic properties of very small clusters (from dimer to nano-sized clusters), employing the same methodology [114]. More precisely, we carried out calculations to find the lowest-energy magnetic configurations and explore finite temperature magnetic properties of Cr clusters in FM bcc-Fe and Fe clusters in AF bcc-Cr. In particular, we studied either very small clusters or clusters with (100) and/or (110) interfaces.

Our DFT study shows that the magnetic frustration caused by the competing Fe-Fe, Fe-Cr and Cr-Cr magnetic-coupling tendencies, determines the low-energy magnetic configurations of the clusters, inducing either small local magnetic moments or non-collinear structures, which partially release magnetic frustration. Small local atomic moments are often found in collinear ground states of Cr clusters in Fe. Non-collinear configurations are unstable for most of the studied Cr clusters, except for the clusters where interfacial Cr atoms dominate the structure, with either four or six Cr 1nns, in which case non-collinear states are found as local minima. A particularly interesting feature is the non-zero cluster magnetization caused by the dominance of Fe-Cr over Cr-Cr AF interaction in the small and medium-size Cr clusters [114].

At variance with the case of Cr clusters in Fe, non-collinear configurations often occur in Fe clusters in Cr matrix, as a way of relaxing magnetic frustration. In particular, non-collinear ground states are observed if the cluster size is sufficiently small ($N_{Fe} \leq 5$) so that Fe-Cr AF coupling competes with, or even dominates over, Fe-Fe FM interactions. For larger clusters, all the Fe local moments remain parallel to each other. The energies of various collinear and non-collinear

are generally not very dissimilar [114].

The spin-MC simulations, validated on low-temperature results by DFT, enable extending these predictions to much larger clusters and finite temperature effects. In particular, we find that the temperature dependence of magnetic properties of Cr clusters is strongly influenced by the Fe matrix. Strong Fe-Cr interaction results in the total magnetization of clusters remaining nonzero even at fairly high temperatures, close to the Curie temperature of pure Fe for larger clusters. Cr-Cr magnetic SROs persist until high temperatures due to magnetic coupling of interfacial Cr atoms with the Fe matrix. The latter is fully consistent with the significant high-temperature average Cr moments at the infinite interfaces (Fig. 4.1).

Besides the relevance of the cluster and interface properties for the understanding of microstructure in Fe-Cr systems, these features also offer a way to determine the relative strength of various competting Fe-Fe, Fe-Cr and Cr-Cr magnetic interactions.

4.2.2 Environment-sensitive Mn magnetism in bcc Fe-Mn

From an application point of view, manganese is a common alloying element in *e.g.* austenitic steels, because of its ability to trap sulfur and its desoxidization properties. Also, ferritic/martensitic steels containing manganese are especially interesting as structural materials in nuclear applications due to their reduced activation properties.

Considering an isolated 3*d*-metal solute in FM bcc-Fe system, it is known that for an element on the lefy-hand of Fe in the Periodic Table, its spin is generally anti-parallel to the Fe spin. Meanwhile, the righ-hand elements exhibits a FM interaction with Fe. However, Mn with a half-filled 3*d* band presents a rather atypical magnetic behavior. It was shown from previous DFT calculations that the Mn spin in bcc Fe can be very sensitive to the various DFT approximations such as the parametrization of the GGA exchange-correlation functional and the different types of pseudo-potentials [119]. The discrepancy in predicted Mn spin may also arise from the presence of more than one collinear energy minima for a Mn solute in bcc Fe, showing a moment either parallel or anti-parallel to the lattice Fe moments, as suggested in an early theoretical work [120].

We have applied DFT calculations in order to further investigate magnetic and energetic properties of Mn in bcc Fe-Mn alloys, as functions of the alloy composition and local chemical environment [121]. Some most relevant results are summarized as follows.

For the simplest case of an isolated Mn in FM bcc Fe, we confirm the presence of two collinear energy minima, with the Mn magnetic moment either parallel or anti-parallel to the Fe moments, named respectively the FM-Mn and the AF-Mn state. The latter being the ground state (Fig. 4.2a). Generally, the preference of the Fe-Mn magnetic interaction is highly sensitive to even minor changes of the

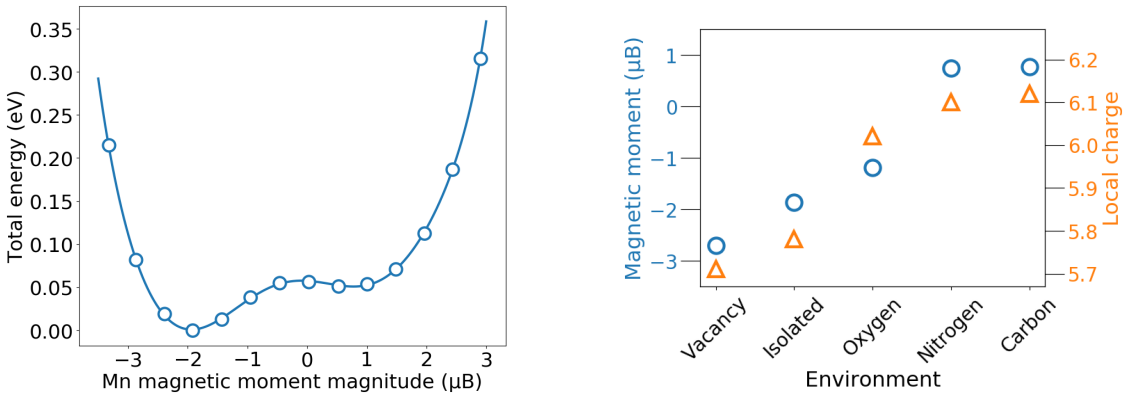

(a) (b)

Figure 4.2: (a) Total system energy as a function of the magnetic moment magnitude of an isolated Mn atom in bcc Fe. (b) Correlation between local magnetic moment (triangles) on a Mn atom and its local electronic charge (circles) for various local chemical environments: isolated in Fe, 1nn of a vacancy, and 1nn of a X interstitial atom (X = C, N, O).

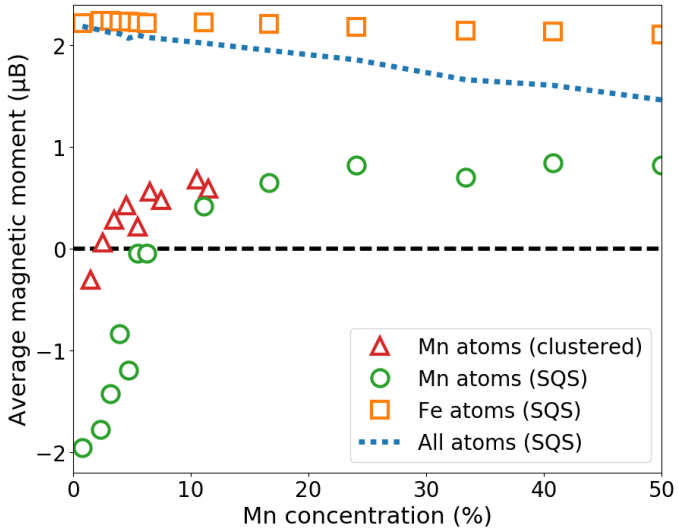

Figure 4.3: Average magnetic moment of Fe atoms, of Mn atoms and of all the atoms in bcc Fe-Mn alloys either with a special quasi-random structure (SQS) or containing Mn clusters, as a function of Mn concentration.

Mn local environment, due to the presence of a high Mn majority-spin electronic density around the Fermi level [121].

A direct correlation is identified between the local electronic charge and the local magnetic moment on a Mn solute, being isolated (Fig. 4.2b) or forming a small Mn cluster. For instance, the presence of a vacancy near the Mn atom,

inducing a local charge depletion, tends to favor the AF Fe-Mn interaction. Also, common interstitial impurities (C, N, and O) present an attraction with a Mn atom if located at its 1nn site. C and N show a strong electronic hybridization with Mn and stabilize the FM-Mn state. At variance, an oxygen atom, with a rather ionic Mn-O interaction and therefore a very localized charge distribution, does not modify the magnetic ground state of an isolated Mn.

Clustering of Mn atoms is found to be energetically favorable, consistently with the unmixing tendency found for the bcc Fe-Mn alloys. Various collinear and non-collinear magnetic minima are found for the Mn dimer, which are rather close in energy. It is relevant to point out that our results suggest a dominance of Mn-Mn magnetic interactions over the Fe-Mn interactions, both exhibiting an AF tendency, especially for the 1nn and 2nn distances. This behavior is opposite to the Fe-Cr alloy case (Sec. 4.2.1, where Fe-Cr AF interactions prevail over the Cr-Cr anti-ferromagnetism.

Locally random (SQS) Fe-Mn solid solutions have been systematically investigated for a large range of Mn concentrations. Consistently with experimental findings, the average magnetic moment of the alloys decreases linearly with increasing Mn content. In addition, the average Mn moment tends to be antiparallel (resp. parallel) to lattice Fe moments for Mn concentrations smaller (resp. larger) than approximately 6 at.% Mn. The same trend is observed experimentally, but the deduced transition concentration is around 2 at.%. (Table IV of Ref. [121] for details). Various possible reasons can be at the origin of this experimental-theoretical discrepancy. In particular, the calculated transition concentration is lowered if considering Mn clustering (Fig. 4.3). Indeed Mn clusters may be present in the experimental Fe-Mn samples, depending on the applied heat treatment.

4.3 Impact of Magneto-chemical interplay on thermodynamic properties

In this section, I want to evidence the role of magnetism and magneto-chemical coupling on key thermodynamic properties such as mixing enthalpy and magneto-chemical phase diagram. Some binary Fe alloys (bcc Fe-Cr, Fe-Mn, Fe-Co, and fcc Fe-Ni) are considered to ilustrate the magnetic effects and to attest the accuracy of our EIM + MC approach.

4.3.1 0 K and temperature evolution of mixing enthalpy: bcc Fe-Cr, Fe-Mn and Fe-Co

We first discuss systematically the mixing enthalpy and magnetism of bcc Fe-X alloys, being X = Cr, Mn and Co (neighboring 3*d* magnetic elements). Their 0 K

values are determined via DFT, and used to parameterize our EIMs. Then, spin-MC simulations employing the EIMs are applied to investigate the temperature dependence of the mixing behavior.

Mixing enthalpies of bcc Fe-Cr, Fe-Mn and Fe-Co systems at 0 K were determined in various DFT calculations [62, 73, 104, 121–127]. They provide information on the mixing (or unmixing) tendency of the alloys, and about the relative stability of ordered phases and solid solutions. The mixing enthalpy of an Fe-X system is defined with the following expression:

$$H^{mix}(\text{Fe-X}) = \frac{H(n\text{Fe} + p\text{X}) - nH(\text{Fe}) - pH(\text{X})}{n+p}, \tag{4.6}$$

where $H(n\text{Fe} + p\text{X})$ is the enthalpy of the Fe-X system with nn Fe atoms and p X atoms, $H(\text{Fe})$ is the enthalpy per atom of pure Fe in its magnetic ground state (the FM state) and $H(\text{X})$ is the enthalpy per atom of the pure X system (here we consider the AF state, the anti-ferromagnetic double-layered (AFD), and the FM state for X = Cr, Mn and Co, respectively). In addition to some most relevant ordered structures, SQSs [128], with negligible chemical SROs, are adopted to mimic random solid solutions. Our obtained values are shown in Fig. 4.4. The 0 K mixing enthalpy and the composition dependence of the system magnetism are briefly summarized as follows:

Bcc Fe-Cr

Fe-Cr alloys exhibit an unmixing tendency (positive mixing enthalpy) for most compositions, except at very low Cr concentrations (below approximately 10%-Cr) where they show slightly negative mixing enthalpies. The latter can be explained by a stabilization of isolated Cr solutes in a FM-Fe lattice [11, 123, 129] due to a strong Fe-Cr anti-ferromagnetism with an induced moment on Cr. The magnitude of the Cr magnetic moment in bcc Fe is around 1 μ_B larger than its value in pure bcc Cr. For a SQS system with a higher Cr concentration, it is unavoidable that some Cr atoms get close to each other. Therefore, the ferromagnetism between Fe atoms, the anti-ferromagnetism between Cr atoms, and the tendency of Fe and Cr moments to be antiparallel (especially for the 1nn and 2nn Fe-Cr pairs) cannot be simultaneously satisfied. Such a magnetic frustration promotes the mixing to unmixing transition. Note that in the very dilute Fe region, the magnetic frustration (see Sec. 4.2) also contributes to a clustering tendency of Fe atoms in the AF-Cr matrix [114].

Bcc Fe-Mn

Regarding Fe-Mn alloys, it is well known that the bcc phase is thermodynamically stable only up to a few percent of Mn, while for most compositions there is

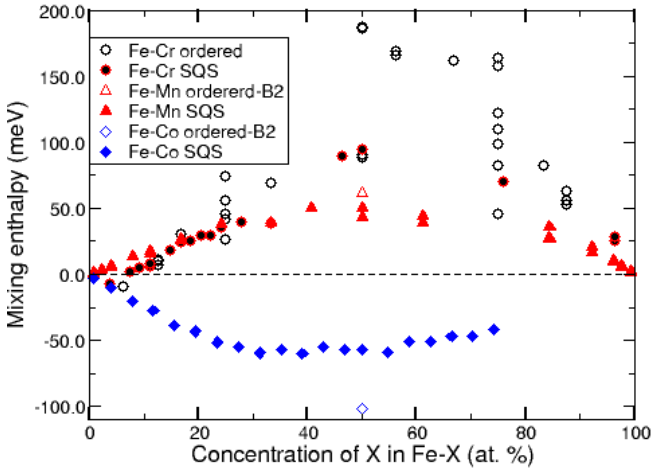

Figure 4.4: Mixing enthalpy for bcc Fe-Cr, Fe-Mn and Fe-Co alloys from 0 K DFT calculations.

an α+γ two-phase domain. However, in order to have a thorough understanding of the compositional dependence of energetic and magnetic behaviors of bcc Fe-Mn alloys, it is relevant to perform a systematic study for all concentrations. As can be seen in Fig. 4.4 , the obtained mixing enthalpies are positive for all the concentrations (although smaller than the Fe-Cr values in the concentrated region), which reveals an unmixing tendency. Moreover, the shape follows well the regular solution model (described with $H^{mix} = A \cdot x_{\mathrm{Fe}} \cdot x_{\mathrm{Mn}}$) with A = 192 meV (18.5 kJ/mol). This is in good agreement with previous theoretical and experimental results, as detailed in [121] and references therein.

Concerning the magnetic properties, we look especially at bcc Fe-Mn alloys in the Fe-rich domain, up to 50% of Mn. The magnetization in the SQS solid solutions shows a linear decrease with increasing Mn concentration, in very good agreement with the Slater-Pauling curve [121]. This behaviour is also consistent with available experimental studies, showing a linear decrease up to 11 % of Mn before a bcc-fcc phase transition [130]. This can be overall explained by a magnetic-dilution scenario. On one hand, as expected, the Fe moment remains close to 2.2 μ_B in any configuration of any composition, showing a very small perturbation of the α-Fe moment due to the presence of Mn atoms. On the other hand, the Mn moment shows smaller magnitudes.

As mentioned in Sec. 4.2.2, depending on the local configuration, the magnetic moment of Mn atom can be either antiparallel (AF-Mn) or parallel (FM-Mn) to the Fe moments. Having a closer look to the compositional dependence of the Mn magnetism (Fig. 4.3), the average Mn moment is antiparallel to Fe moments at the lowest concentrations, followed by a rapid decrease of the moment magnitude with increasing Mn concentration. This finally leads to a transition from

AF to FM Fe-Mn interaction tendency at approximately 6% Mn (in SQS systems). After that, the average Mn magnetic moment converges to a value around 0.8 μ_B, parallel to Fe moments. This constant value of 0.8 μ_B results from the presence of an approximately constant fraction of 75% FM-Mn and 25% AF-Mn atoms in each SQS configuration, where both types of Mn present an average moment magnitude of around 1.6 μ_B (that is, 1.6*0.75-1.6*0.25=0.8) [121].

Bcc Fe-Co

At variance with the Fe-Cr and Fe-Mn alloys, the alloying of Fe with Co (having a higher 3*d*-band occupation than Fe) in a bcc lattice shows a mixing tendency for the whole range of compositions (see Fig. 4.4). In both ordered and disordered structures, the Fe and Co magnetic moments tend to be parallel to each other. The moment magnitude of Co only varies slightly with the change of Co content, which is consistent with experimental observations. On the other hand and different from the Fe-Cr and Fe-Mn systems, the moment of Fe is strongly affected by the presence of Co solutes. In the SQSs, the average moment of Fe atoms increases rapidly from around 2.2 μ_B to 2.5 μ_B in the range from 0 to 20%-Co content, then it increases slowly up to a saturated value of 2.6 μ_B and remains almost constant above 50%-Co. In the ordered B2 phase, the magnetic moment of Fe increases with Co concentration and reaches a maximum at 50%-Co before decreasing. It is worth noting that this stoichiometrical FeCo B2 phase, showing the highest magnetization, is also the most stable chemical phase of bcc Fe-Co at low temperatures [131].

Mixing energy as a function of temperature

The main advantage of the EIM + MC approach is able to extend the DFT calculations of the mixing energies to finite-temperature studies. We have determined mixing energies of bcc Fe-Cr, Fe-Mn and Fe-Co random alloys via spin-MC simulations using the DFT parameterized EIMs. We have adopted chemical SQSs to represent the random solutions (results in Figs. 4.5a, 4.5b and 4.5c). For each composition and temperature, we performed spin-MC simulations with fixed atomic configurations. Since on-lattice MC is adopted, we talk about mixing energies instead of enthalpies when referring to these results. The obtained lowest-temperature values are in good agreement with the 0 K DFT results (Fig.4.4 [73–75]).

Fig. 4.5a shows the Fe-Cr mixing energies at 10 K and 2000 K. At 10 K, the system is found at the ordered magnetic ground state and it is paramagnetic at 2000 K, for all compositions. The low-temperature curve is asymmetric due to the magnetic-driven anomaly at the low-Cr limit, as described above. As expected, this anomaly disappears at the PM state, making the high-temperature curve symmetric. Interestingly, the height of the both mixing-energy curves appears to be very similar [74]. When comparing this result with literature data, the

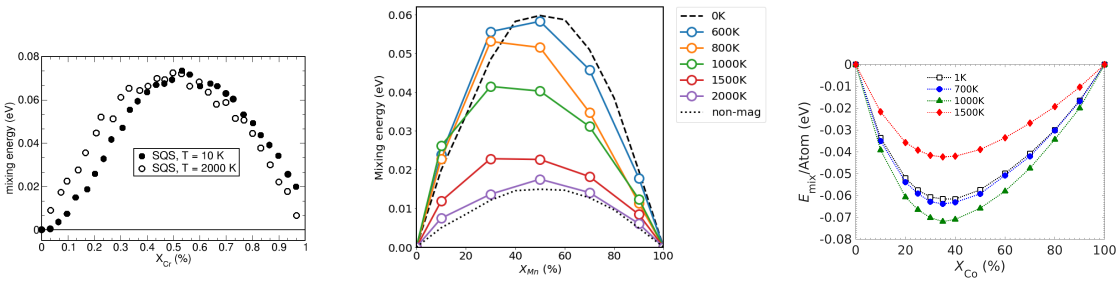

(a) Fe-Cr (b) Fe-Mn (c) Fe-Co

Figure 4.5: Mixing energies of bcc (a) Fe-Cr, (b) Fe-Mn and (c) Fe-Co alloys, for various temperatures, as predicted by EIM + spin-MC simulations.

recent CALPHAD study by Xiong *et al.* concludes that the maximum of mixing enthalpies H^{mix} near 50% Cr decreases by only 0.015 eV from 0 to 1529 K [132], while this difference is approximately 0.03 eV between the perfectly FM and PM states according to a DFT-DLM study [133].

Regarding bcc Fe-Mn, the temperature evolution of the bcc Fe-Mn mixing energy is closely related to the magnetization of the system (see Fig. 4.5b). Indeed, for any given composition, two regimes can be clearly identified: below the magnetic transition temperature (see Fig. 4.6), the mixing-energy curve remains quite similar to the 0 K curve, while beyond the magnetic transition temperature, it converges to its high-temperature PM limit. It can also be noticed that at both high and low temperature limits, that is, as soon as for all the concentrations the temperature is located either below or above the magnetic transition temperatures, the mixing-energy curve is symmetric. However, for the intermediate temperatures an asymmetry appears between the Mn-rich and the Fe-rich domains. Also, the Mn-rich mixing energies decrease faster with increasing temperature than the Fe-rich values. This asymmetry is consistent with the just-mentioned two-regime behavior, considering the difference between the Fe-rich and the Mn-rich magnetic transition temperatures. Indeed, we predict the magnetic transition temperature to decrease with Mn concentration, in agreement with experimental data (see Sec.c. 4.3.2 and Fig. 4.6) [75].

Also, we notice that the paramagnetic limit (2000 K) of the mixing energy curve is very similar to the non-magnetic contribution (in the Fe-Mn EIM) to the 0 K mixing energy [75], indicating that the mixing between Fe and Mn atoms has a negligible impact on the average magnitude of their respective magnetic moments. Overall, the present results suggest that the spin disorder favors the mixing of Fe and Mn, while spin ordering favors the phase separation tendency. Our results are in qualitative agreement with a recent CALPHAD prediction [134], in which the thermodynamic parameters lead to a fully positive mixing energy of bcc Fe-Mn alloys, and it decreases with increasing temperature.

In Fig. 4.5c, the mixing energies of disordered bcc Fe-Co alloys are presented

for various temperatures: namely low (1 K), intermediate (700 K) and high (1000 K, 1500 K) temperatures. For all the studied temperatures, the mixing energies remain negative. The mixing energy curve presents a minimum around 40% Co at 1 K and this minimum slightly shifts to a lower concentration of Co when temperature increases. The temperature-evolution of the mixing energies is not monotonous. They decrease slightly when temperature increases from 1 K to 700 K. At higher temperatures, the variation is more visible as the mixing energies drop rather fast from 700 K to 1000 K. Interestingly, the trend is reversed at higher temperatures as the mixing energies increase from 1000 K to 1500 K, in the paramagnetic regime.

These variations can be rationalized in terms of distinct Curie temperatures for systems of different compositions. As an example, we consider the 50%-Co system. We can look at the change of total energy of the systems involved in the mixing energy expression (pure Fe, pure Co, and Fe-50% Co A2-phase) at a given temperature with respect to their respective 1 K values [73]. At low temperatures, the change of energy in all the three systems is almost the same, it leads to the almost unchanged mixing energy. In the range of 700 K - 1100 K, the change in the total energies of pure Fe and pure Co is faster than that in the Fe-Co system, due to the strong magnetic disordering near the magnetic phase transition in the pure systems (1065 K for Fe and 1077 K for Co from the Fe-Co EIM). As a result, the mixing energy decreases. Above 1100 K, the total energies of the pure Fe and Co systems tend to saturate, while the one of the Fe-Co alloy increases more rapidly as this system goes close to its Curie point and thus the mixing energy increases.

4.3.2 Magnetic and chemical phase stability

Spin-atomic MC simulations using the EIMs also allow us to predict the composition-evolution of magnetic transition temperature, the stability of chemical phases, and their interplay. In this section, I present a few examples of such studies and compare our predictions with experimental data. These examples concern: the concentration-dependent Curie temperature in bcc Fe-Mn [75], and the magneto-chemical phase diagram of bcc Fe-Co and fcc Fe-Ni alloys. [73, 76]. As shown below, the bcc Fe-Co and the fcc Fe-Ni alloys exhibit some distinct characteristics in terms of the relative importance of magnetic and vibrational excitations on chemical phase transitions. Finally, I describe the strong sensitivity of chemical phase boundary to magnetism in bcc Fe-Cr alloys [74].

Curie temperature of bcc Fe-Mn

Concerning the Curie temperature (T_c) evolution of bcc Fe-Mn alloys in the Fe-rich region, the obtained values up to 20 at. % Mn are shown in Fig. 4.6. As can be seen, $\mathbf{T_C!}$ ($\mathbf{T_C!}$) decreases with Mn concentration with a slope of around 10 K

per Mn at.%, in excellent agreement with most literature data. Indeed, various experimental works have shown that the T_c tends to decrease in the dilute limit linearly with Mn content, at a rate of approximately 10 K per Mn at.% [135–138], as shown in Fig. 4.6.

For larger Mn concentrations up to 20 at.% of Mn, some discrepancy in experimental data appears. While there is still a decrease of 10 K per Mn at.% in the case of Paduani *et al.* [135], Yamauchi *et al.* [130] found a much larger decreasing slope of around 43K per Mn at.%. One possible explanation for the deviation of Yamauchi's result is that their magnetic measurements are biased by the use of cold-rolling on the samples in order to stabilize the body-centered cubic phase [130, 139], which is not the case in the other experimental studies. A recent CALPHAD assessment [134] also proposed such a decrease of $\mathbf{T}_C$**!** with Mn content of approximately 10 K per Mn at.%, as shown in Fig. 4.6.

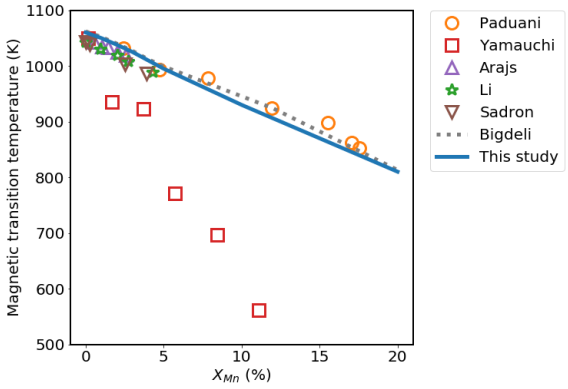

Figure 4.6: Curie temperature versus Mn concentration of Fe-Mn random solutions: a comparison between EIM + MC simulation results and various experimental data [135–138].

Magneto-chemical phase diagram of bcc Fe-Co

In the Fe-Co case, Curie temperatures were determined to be 1316 K and 1461 K for respectively the 50 %-Co A2 and ordered B2 structures. Systematic calculations were also performed for other Co concentrations. The results allow us to predict the magnetic phase diagram of bcc Fe-Co alloys (Fig. 4.7). The experimental data from Refs. [140–142] were also added for a comparison. However, please note that some of these experimental Curie temperatures may not always come from direct measurements, but obtained by data extrapolations [142]. They roughly coincide with the bcc–fcc transition temperatures for a large range of Co concentrations. As can be seen, the Curie points obtained by our model via MC simulations are in good agreement with the experimental data, with the highest discrepancy not exceeding 100 K, which is within a reasonable margin of error.

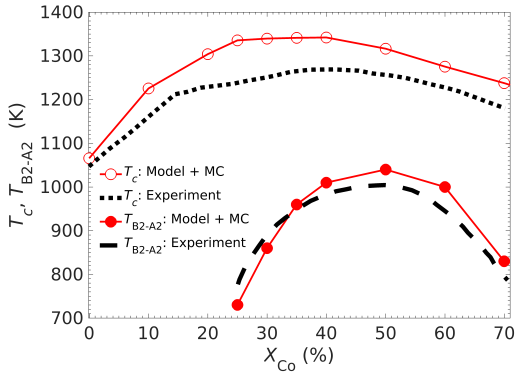

Figure 4.7: Curie temperature and chemical B2-A2 transition temperature in bcc Fe-Co alloys: a comparison between EIM + MC simulation results and various experimental data [140–143].

The obtained result is also compatible with the equilibrium phase diagram, in which the both B2 and A2 bcc phases present a FM state while the fcc phase presents a PM state. Our predicted Curie temperature is found to increase significantly (from around 1060 K to above 1220 K) in the range from 0 to 20% Co, then it reaches the maximum value of about 1340 K at 40% Co before decreasing to about 1200 K for 70% Co.

According to the equilibrium phase diagram, the ordered B2 and the disordered A2 phases are separated by a second-order transition [143]. We have then determined the phase boundary between these two phases, via a determination of the temperature-dependence of the chemical long-range-order at each Co concentration [73]. To this end, coupled spin-atom Monte Carlo simulations were performed.

It is worth mentioning that the present model, like most on-lattice EIMs, does not include naturally the contribution of lattice vibrations. Nevertheless, even without the vibrational entropy, our model still provides a satisfactory prediction of the B2-A2 transition temperature (Fig. 4.7). This is because in the bcc Fe-Co systems, the vibrational entropies of the B2 and the A2 structures are found to be very similar. For instance, 3.25 k_B, per atom for the B2 and 3.31 k_B for the A2 phase, at 50 % Co from DFT. Indeed, for this phase transition, we found that effect of the lattice vibrations is negligible compared to that of magnetic excitation although both A2 and B2 are FM phases [73].

Phase diagram of fcc Fe-Ni

Fig. 4.8 shows the fcc Fe-Ni phase diagram predicted by the EIM, compared with those from our pure DFT study [144] and a recent CALPHAD [145] assessment. As expected, there is an absence of the fcc PM (γ_{PM}) solid solutions from DFT considering only FM configurations. Besides, there is an overall good agreement

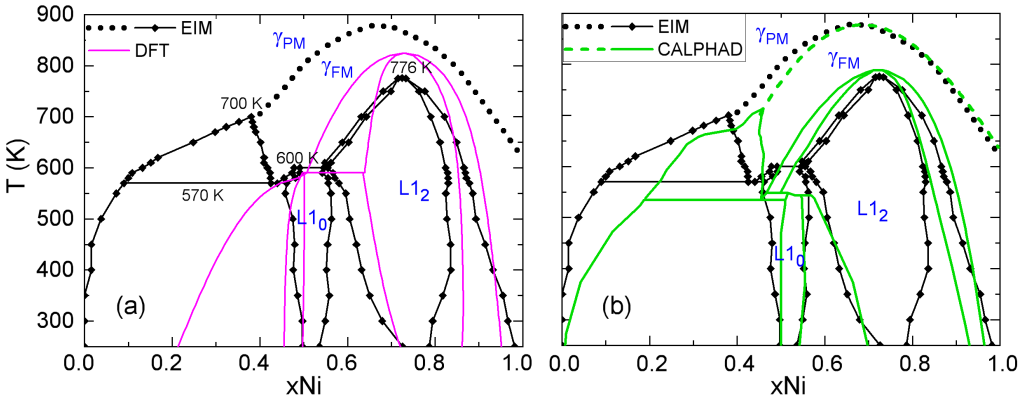

Figure 4.8: Fcc Fe-Ni phase diagram predicted by the present EIM simulations, compared to the ones from (a) our DFT study [144] and (b) the CALPHAD prediction by Ohnuma *et al.* [145].

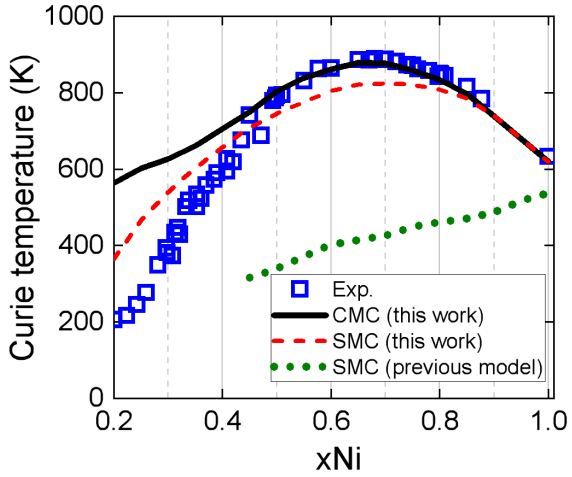

Figure 4.9: Curie temperature of fcc Fe-Ni solid solutions from experiments [146–148], from our developed EIM and from a previous MCE model Ref. [71]. SMS and CMC denote respectively spin MC and spin-atom MC equilibrations.

between data from the three methods although some differences on chemical order-disorder transition temperatures (T_{chem}) can be observed,

Before going into details of the chemical phase transitions, we first look at the composition evolution of Curie temperature. According to our EIM, the fcc random solid solutions with more than 20% Ni present a collinear FM ground state [76]. Fig. 4.9 shows the predicted and experimental Curie temperatures. The experimental data were measured in samples quenched from 923-1273 K [147, 148] with non-zero atomic SRO. The "SMC" (spin-MC) results are obtained by equilibrating the magnetic configuration but keeping atoms frozen to a fully random structure with zero atomic SRO. The "CMC" results are obtained with the equilibrium spin-atom structures which show stronger atomic SRO than the experimental samples. The predicted Curie temperatures of the experimental samples should therefore lie between the CMC and SMC curves.

In alloys with $x_{\mathrm{Ni}} > 0.45$, the CMC results of Curie points are in very good agreement with the experimental data (Fig. 4.9), while the SMC results are slightly lower. This indicates that the experimental atomic SRO is closer to that of the equilibrium structures obtained in CMC simulations than the zero value of the random alloys. However, the CMC results show a large deviation from the experimental data in alloys with $x_{\mathrm{Ni}} <0.4$. Indeed, the predicted equilibrium structures around 10-40% Ni at 570-700 K consists of two different disordered phases, as shown in the Fe-Ni phase diagram (Fig. 4.8). Therefore, the structures from CMC simulations do not correspond to the experimental homogeneous disordered samples. Meanwhile, the difference between the SMC results and experimental T_cs in alloys with $x_{\mathrm{Ni}} <0.3$ may be due to the non-zero atomic SROin the measured samples.

The ordered structures $L1_0$-FeNi and $L1_2$-$FeNi_3$ have a FM ground state, with the experimental T_c higher than those in the disordered alloys of the same compositions. This feature is well reproduced by our EIM predictions, which compare favourably with the experimental results

Turning to the chemical order-disorder transitions, as summarized in Table 4.2, we find that the transition temperature (T_{chem}) at 50% and 75% Ni are increased by respectively 332 K and 154 K, if the vibrational entropy term is switched off in the EIM. This confirms the strong vibrational effects on the chemical transitions in fcc Fe-Ni alloys as suggested in our previous DFT study [144]. As shown in Table 4.2, that DFT study showed that considering only the ideal configurational entropy leads to largely overestimated values of T_{chem}, whereas a reasonable estimation of T_{chem} can be obtained if vibrational entropies of mixing are included. The effects of magnetic excitations, which are neglected in the DFT study [144] but included in the EIM, are found to have a relevant but smaller impact than the vibrational contribution on these chemical transitions occurring in the FM state.

Interestingly, the calculated phase diagrams from both EIM and CALPHAD predict a triangle-shape miscibility gap between the ferromagnetic and paramag-

netic random alloys. This gap is consistent with observations in the Invar alloys, in which the Ni-rich and Fe-rich local regions are suggested to be ferromagnetic and paramagnetic respectively [149, 150]. Further details on the phase diagram can be found in Ref. [76].

Table 4.2: Chemical order-disorder transition temperatures (in K) in the Fe-Ni alloys with 50% and 75% Ni. The excitations (configurational (conf), vibrational (vib) and magnetic (mag)) considered in the calculations are indicated in parenthesis.

	50% Ni	75% Ni
DFT [144] (conf)	920	1030
DFT [144] (conf+vib)	640	830
EIM, this work (conf+mag)	930	920
EIM, this work (conf+vib+mag)	598	766
Exp. [151–154]	593	770-790

Magnetization is known to have an impact on the chemical order-disorder transition temperature. To study how different magnetic states influence the chemical transitions, we control the magnetic state with a temperature T_{spin} different from the temperature controlling the chemical evolution. Here we consider two extreme cases with the fixed spin temperature, namely the 1 K MGS and the ideal PM state (T_{spin}=1500 K).

Table 4.3 shows the chemical transition temperatures in the alloys with 50% and 75% Ni with different magnetic states. In the alloy with 75% Ni, the predicted transition temperature ranges from 715 K to 885 K depending on the magnetic state of the system. A strong FM order as in the MGS tends to further stabilize the ordered alloy over the disordered one, while the paramagnetism reduces the phase stability of $L1_2$-$FeNi_3$. On the other hand, the trend is reversed in the alloy with 50% Ni. The influence of the magnetic state on the $L1_0$-disorder transition temperature is less important than on the $L1_2$-disorder transition temperature.

Table 4.3: Chemical order-disorder transition temperatures (in K) in fcc Fe-Ni alloys with 75% and 50% Ni, obtained with various magnetic states. EQ: equilibrium magnetic state at considered temperatures. MGS: perfectly ordered magnetic ground state (T_{spin}=1 K), and ideal PM: state (T_{spin}=1500 K).

Composition	EQ	MGS	PM
75% Ni	766	885	715
50% Ni	598	555	610

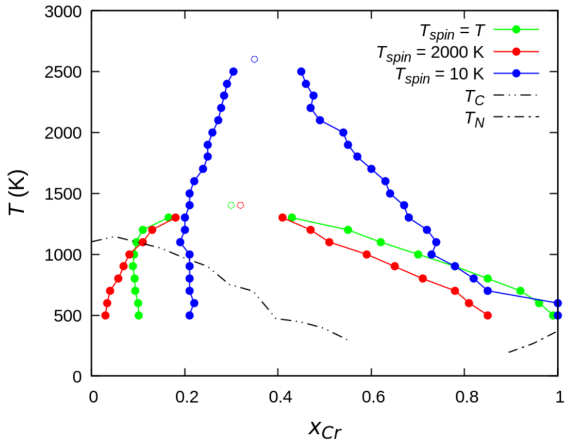

Figure 4.10: Fully equilibrated bcc Fe-Cr phase diagrams (blue solid symbols): compared with the ones obtained with imposing a spin temperature (T_{spin} different from the system's temperature : T_{spin} = 10 K (green), and T_{spin} = 2000 K (red). Curie and Néel temperatures are shown with dashed lines for information. The open symbols indicate the presence of stable solid solutions fo the distinct cases.

Phase diagram of bcc Fe-Cr

It is also relevant to illustrate the sensitivity of the chemical phase boundary to the magnetic state via the chemical phase diagram of bcc Fe-Cr [74]. To this end, we have determined the phase boundary (or the solubility limit in this case) by imposing a spin temperature (T_{spin} for the spin MC steps) different from the one (system's T) for the atomic MC steps. The comparison of these results with the equilibrium phase diagram is shown in Fig. 4.10. We considered two extreme cases with T_{spin}= 10 K and T_{spin} = 2000 K, corresponding to respectively a maximum and a zero magnetic long-range order imposed for the Fe-Cr alloys at any Cr concentration. In the former case, the magnetic entropy is practically zero.

Note that all the considered system temperatures are above the Néel temperature curve. With T_{spin} = 10 K, the system is constrained to be at the magnetic ground state of any atomic configuration, for example, overall FM in an Fe-rich α region and mainly AF in a Cr-rich α' region. In the former, the spin of Cr solutes are anti-parallel to the Fe spins, while in the latter, Fe spins are generally non-collinear to the Cr spins due to the presence of magnetic frustration [114, 123]. It is therefore not surprising to notice a clear increase of Cr solubility limit in the Fe-rich phase at rather low system temperatures (below 800 K), compared with the T_{spin}=T case (Fig. 4.10). It is fully consistent with the stabilization of Cr solution in FM, due to the anti-ferromagnetism between Cr and the surrounding Fe atoms. On the other side, there is only minor changes in the Fe solubility in the Cr-rich limit below 1000 K. Another specificity of this low T_{spin} phase diagram is that the alloy remains decomposed at least up to 1500 K, for 30–50 at. % Cr.

At variance, beyond 1000 K and 20 at. % Cr, the real Fe-Cr system exhibits a PM state based on our magnetic phase diagram, and the system is already out of the miscibility gap. As already mentioned, in a concentrated Fe-Cr solid solution, the FM Fe-Fe, AF Fe-Cr and AF Cr-Cr magnetic interaction tendencies present in the magnetic ground state induce strong frustrations [123]. They destabilize the solid solution leading to the α-α' phase separation.

By setting T_{spin} = 2000 K, the system is constrained to be PM for the whole concentration range. By comparing results with the real phase boundary, we notice, as expected, a decrease of Cr solubility in Fe at low temperatures Concerning the Fe solubility in the Cr-rich limit, there is a significant increase up to around 1000 K. The resulting more symmetric phase diagram (compared to the real one) is fully consistent with the more symmetric shape of the mixing energy curve (Fig. 4.5a).

4.4 Magnetic effects on vacancy formation

4.4.1 Vacancy formation in bcc Fe, fcc Fe, and fcc Ni

As mentioned in Sec. 4.1, most studies on temperature-evolution of vacancy formation in literature are devoted to bcc iron. Via spin-atomic MC simulations using DFT informed EIMs, we have systematically compared the temperature behavior of vacancy formation magnetic free energy in fcc Ni, and in bcc and fcc Fe [155]. In this study, we pay a special attention to distinct effects of orientational and magnitude fluctuations of the considered atomic spin, namely respectively transversal and longitudinal spin fluctuations.

Before checking the vacancy properties, we first looked at the magnetic properties of the defect-free systems. The spin-MC results reveal that the longitudinal spin fluctuations are more significant in fcc Fe and Ni than in bcc Fe. In particular for fcc Ni, neglecting the temperature evolution of spin magnitudes leads to an overestimation by 220 K of the Curie point. Then, we determined the vacancy formation energy, magnetic entropy and magnetic free energy as functions of temperature for the three systems. Results are shown in Fig. 4.11.

The overall impact of the magnetic transition on the vacancy formation properties are found to be more significant in bcc Fe than in fcc Fe and Ni. The substantial decrease of the vacancy formation energy from the FM to the PM state in bcc Fe is mainly due to the transversal rather than the longitudinal spin excitations. This is coherent with the strong dependence of the formation energy on the spin-orientation ordering in bcc Fe as predicted by DFT calculations [155]. Consistently, a weaker dependence of the vacancy formation energy on the spin ordering in fcc Fe and Ni leads to a smaller variation of the vacancy properties below and above the magnetic transition.

Otherwise, We noted a significant effect of longitudinal spin excitations on

the magnetic free energy of vacancy formation in fcc Fe, resulting in its steady decrease above the Néel point. Below its Néel point, such effect is comparable but opposite to that of the transversal excitations. These features are also consistent with our DFT results in fcc Fe, which demonstrated a stronger dependence of vacancy formation energy on the spin magnitude rather than the spin ordering [155]. Interestingly, it is noted that the predicted vacancy formation energy in the PM fcc Fe is close to the AFD-state value, but it is significantly (0.52 eV) lower than the formation energy obtained with NM fcc Fe. Although the latter has been largely adopted in some recent publications studying diffusion properties in fcc Fe, our results suggest that the PM fcc Fe is better represented by the AFD rather than the NM state.

Regarding the vacancy formation in fcc Ni, the transversal spin excitation just below the Curie temperature leads to a sudden increase of the vacancy formation magnetic free energy, while the longitudinal spin fluctuation above the Curie temperature leads to a steady increase of this quantity.

The cases of fcc Fe and Ni reveal a relevant role of longitudinal spin excitation on the vacancy formation properties (not seen in bcc Fe), which can not be well captured by a classical Heisenberg model. At variance with the bcc-Fe case, the widely used Ruch [81] model (Eq. 4.1) cannot be applied in these systems to predict the temperature evolution of energetics of vacancy formation.

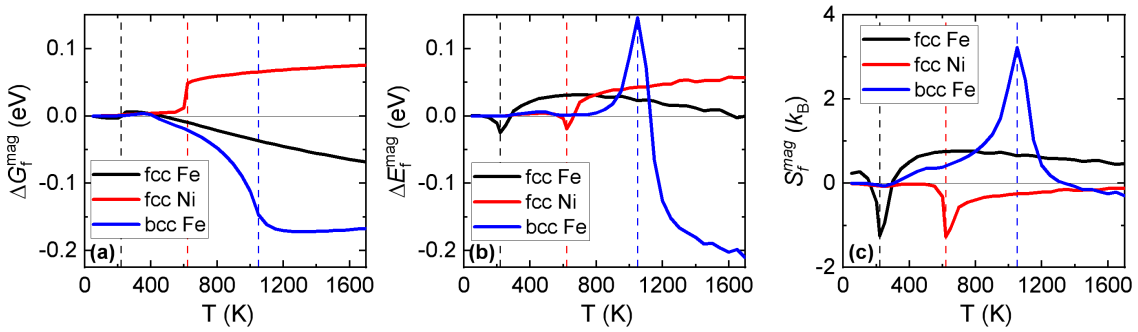

Figure 4.11: Vacancy formation properties (free energy, energy and entropy, including the magnetic contributions) in the three systems calculated from the EIM approach. G_f^{mag} and E_f^{mag} are given with respect to the 0 K MGS values (1.43 eV for FM fcc Ni, 1.83 eV for AFD fcc Fe and 2.20 eV for FM bcc Fe). The vertical lines denotes the EIM-predicted magnetic transition temperatures.

Of course, for a prediction of equilibrium vacancy concentration, we also need to include the vibrational entropy. Since the focus of this study is the magnetic effects, we just estimated the vibrational entropies via DFT for the collinear MGS of each system, and assumed them to remain the same as a function of temperature. This approximation naturally neglects the magnon-phonon coupling and the anharmonic vibrational effects at high temperatures. Within the present approximation, the predicted vacancy formation energies and equilibrium vacancy

concentrations are overall in good agreement with experimental data, which are available only at high temperatures (see [155] and references therein). We confirm that the vibrational entropy of vacancy formation has a stronger contribution than the magnetic one for all the three systems. But the latter is clearly nonnegligible in bcc Fe, as neglecting this contribution leads to an underestimation of the equilibrium vacancy concentration by a factor of 5.

4.4.2 Vacancy-solute binding across the magnetic transition

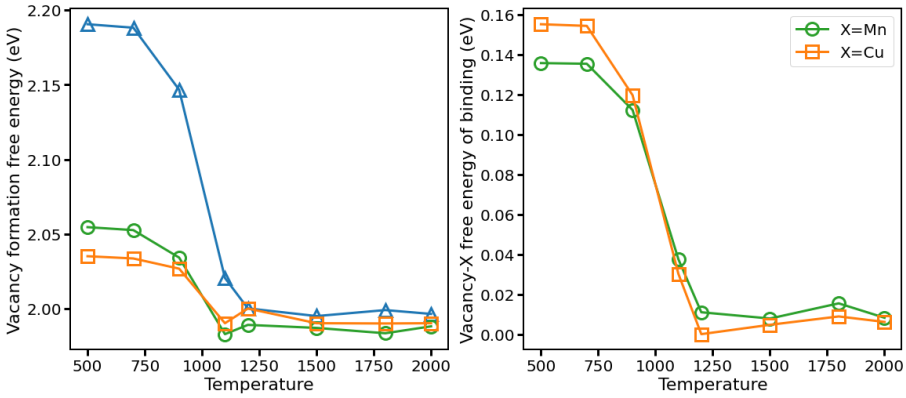

Figure 4.12: Magnetic free energy versus temperature (in K) of : vacancy formation in pure Fe (triangles), at a 1nn site of a Cu or a Mn solute (left), and binding between a solute and a 1nn-vacancy (right), as predicted by EIM + MC simulations.

Temperature evolution of vacancy-solute interaction properties, such as the magnetic free energy of binding (accounting for the magnetic entropy), can also be determined via MC simulations coupled with EIMs. The vacancy-solute binding energy at a 1nn distance dictates the vacancy concentration next to a solute atom, which is especially important for the determination of solute diffusion coefficients via a vacancy mechanism. [25, 27]

Using the spin-atomic MC approach, we have determined the binding energy for the very dilute limit via the difference of the magnetic free energy of formation of a vacancy at a 1nn site of a solute and in a pure bcc Fe system. The vacancy formation energies are determined by evaluating the corresponding equilibrium vacancy concentrations as a function of temperature. A detailed description of the numerical method employed can be found in Refs. [2, 75].

The left panel of Fig. 4.12 shows the vacancy formation magnetic free energy in pure Fe and at 1nn sites of a solute (Cu or Mn) in bcc Fe, as functions of temperature. Concerning the pure Fe case, the vacancy formation magnetic free energy obtained in the low and high temperature limits (respectively 2.20 and 1.99 eV in FM and PM states) is in agreement with previous experimental and DFT data

from literature, ranging from 2.00 to 2.24 eV in the FM state and from 1.54 to 1.98 eV in the ideal PM state [68, 77–79, 156]. The vacancy formation magnetic free energy in the PM state shows very scattered results in the literature. The values are extremely sensitive to the computational details, while the various studies are very consistent concerning the 0 K FM state [33, 68, 77–79, 156]. As can be noticed, at low temperatures, the formation free energy at the 1nn sites of a Mn (resp. Cu) solute is approximately 0.14 eV (resp. 0.16 eV) lower than the value in pure Fe, which is overall consistent with the FM binding energies obtained via DFT calculations: between 0.15 eV and 0.17 eV for vacancy-Mn [33, 75, 157], and 0.24 eV for a vacancy-Cu pair [2].

Interestingly, as the temperature increases, the formation energy difference or the binding energies decrease towards approximately zero in the fully PM regime, for both Mn and Cu cases (right panel of Fig. 4.12). This solute-vacancy binding behaviour indicates that the magnetic disorder is able to erase the chemical-interaction effects in the very dilute Fe alloys. Since we have observed an identical behavior in the case of two solutes that exhibit quite different electronic and magnetic properties, it appears to be a rather general behaviour in bcc Fe systems, independent of the chemical nature of the solute. This dominance of magnetic-disorder over chemical effects is fully coherent with a significant increase of the solute kinetic correlation factor (indicating the approach to a random walk) from the FM to the PM state, as discussed below, in Sec. 4.5.

4.4.3 Vacancy formation as a function of alloy composition

The prediction of the vacancy formation energy in alloys beyond the extremely dilute limit is a more difficult task, since the thermal magnetic effects and the magneto-chemical coupling can be strongly dependent of the alloy composition. Also, it involves some technical complexities when applying the Widom substitution techniques. I describe such a composition dependence in the case of fcc Fe-Ni alloys for the whole composition range via spin-atomic MC simulations [76].

Vacancy formation magnetic free energy G_f^{mag} in fcc Fe-Ni alloys was calculated as a function of temperature and composition using the Widom-like substitution method [76, 85, 88, 109]. Interestingly, the results show that magnetic disorder leads to an increase of G_f^{mag} while chemical disorder has the opposite effect.

In the Fe-Ni solid solutions (from 700 K to 1500 K), G_f^{mag} tends to decrease with increasing Ni concentration. They are in reasonably good agreement with available experimental data, considering the dispersion of the latter (Fig. 4.13a). Our results reveal that the effects of magnetic excitations and magnetic disorder on vacancy formation properties are much more significant in concentrated Fe-Ni alloys than in pure Fe or Ni, due to a stronger magnetic interaction in the concen-

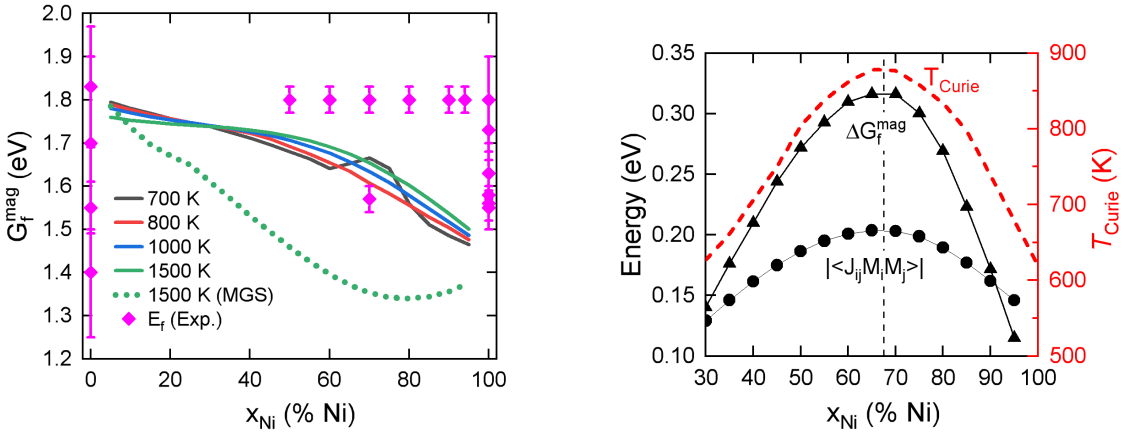

Figure 4.13: (a) Predicted vacancy formation magnetic free energy, G_f^{mag} as a function of Ni concentration in fcc Fe-Ni at several temperatures, compared to the experimental vacancy formation energies (fcc Fe [158–161], fcc Ni [162–166], fcc Fe-Ni alloys [167, 168]). The solid lines denote the results obtained in the equilibrium spin-atom structures, whereas the dotted line denotes the results obtained in the chemically disordered structures in the MGSs, which are FM above 25% Ni and non-collinear below 25% N. (b) Difference between G_f^{mag} in the disordered chemical configurations at 1500 K with the equilibrium magnetic states and with the 1 K MGS, the average magnetic exchange interaction energies $| < J_{ij}M_iM_j > |$, and the Curie temperatures in the disordered structures are shown.

trated alloys as reflected in the concentration dependence of Curie temperatures (Fig. 4.13b). Such a behaviour suggests that the MGS is not a good representation of the PM state for the modelling and determination of vacancy formation properties in no-dilute fcc Fe-Ni (and probably also in fcc Fe-Ni-Cr) alloys.

It is also worth noting that the temperature evolution of G_f^{mag} in the magnetic alloys cannot be described by the Ruch model [81] or the Girifalco model [169] due to the simultaneous evolution of magnetic and chemical degrees of freedom.

4.5 Impact of magnetic excitation and transition on atomic diffusion

4.5.1 Self and solute diffusion in α-Fe across the Curie point

We have determined atomic diffusion properties in Fe-based systems based on the DFT-parameterized EIM coupled with on-lattice kMC simulations. As outlined in Sec. 4.1, we have constructed EIMs to describe the magnetism and the energetics of atoms in the bulk, near a vacancy, and at a saddle-point site for an

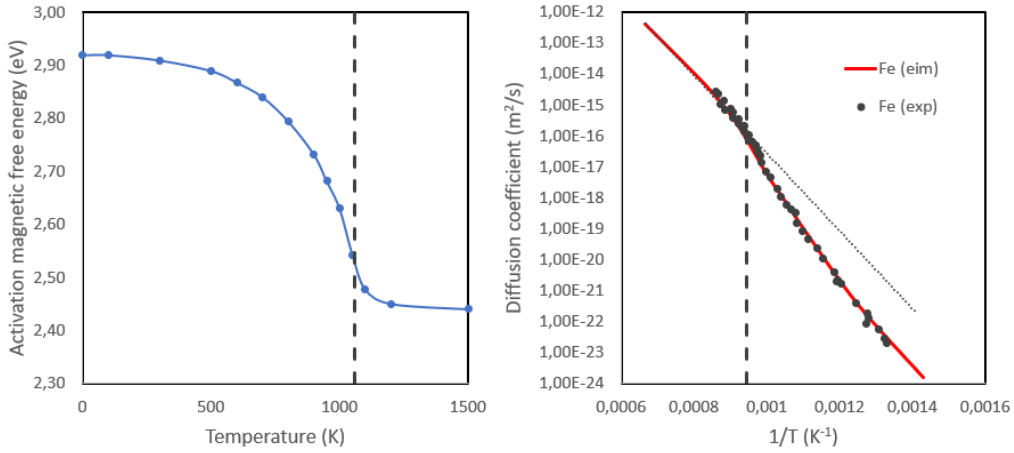

Figure 4.14: Activation magnetic free energy (left) and tracer diffusion coefficients (right) for self-diffusion in bcc iron, from EIM + MC simulations. The predicted Curie temperature (1050 K) is indicated by a vertical dashed line. The various experimental diffusion coefficients come from Refs. [170–181].

vacancy-atom exchange. Details of the model parameters and of the kMC setup can be found in Ref. [2, 33]. Please note that as mentioned in Refs. [68, 107, 182], a quantum treatment of spins is necessary for a correct prediction of the magnetic entropy at low temperatures. The self-diffusion coefficients are obtained by directly simulating the tracer diffusion experiments with the kMC simulations [2]. We compute the mean square displacement of the tracers and we determine the physical time at each temperature using Eq. 4.3 [2]. Note that the lattice-vibration effects (in the vacancy formation entropy and the attempt frequency) are not intrinsically accounted for in the present EIM-kMC setup but calculated separately by DFT in the FM state. The magnon-phonon effects are therefore not considered.

Via the same kMC simulations, we also determined the magnetic free energy of vacancy migration. Adding the latter to the magnetic free energy of vacancy formation, as described previously, we obtained the activation free energy for tracer self-diffusion in α-Fe. The values are shown in Fig. 4.14. Regarding the activation free energies, the EIM reproduces closely the DFT value at the low-temperature limit (2.90 eV). The asymptotic PM value is evaluated at 2000 K (2.46 eV). These energies are in good agreement with previous DFT and available experiments data (2.63 – 3.10 eV and 2.48 – 2.92 eV for ideal FM and PM states, respectively [78, 156]).

As shown in Fig. 4.14, our approach predicts the self-diffusion coefficients versus temperature in excellent agreement with experimental data [170–181]. Especially, the sudden deviation from Arrhenius law (namely the "kink") near the Curie temperature is predicted without any additional assumption. The difference of slope (activation energy) between the FM and the PM regimes is also successfully predicted. It is worth mentioning that if we adopt the Boltzmann

(instead of the Bose-Einstein) distribution in the spin-MC, the "kink" around the Curie point will be significantly underestimated, due to a delocalization of magnetic-excitation effects over a large region of temperatures below T_{Curie} [2].

At variance with the DFT based DLM approach [33, 78], where an additional interpolation model (often the Ruch model[81]) is required to access the diffusion properties at intermediate temperatures, the current approach provides an equal description for all temperatures regardless of the magnetic state. The crucial point is, of course, an accurate parametrization of the EIMs. On the other hand, our approach allows to reach time scales of several orders of magnitudes longer than the spin-lattice dynamics simulations [68]. Therefore, it is also promising to address more complex kinetic processes than the atomic diffusion, such as segregation, phase ordering or precipitation.

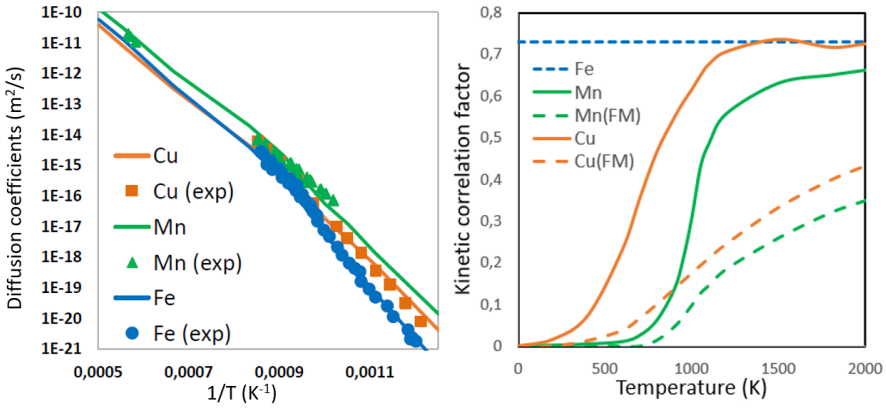

Figure 4.15: Tracer diffusion coefficients for Fe, Mn and Cu in iron from EIM + MC and experiments (left), and the corresponding kinetic correlation factors (right). For the latter, the values are also determined with constraining the system to a FM state, for a comparison. The experimental results of Iijima et al. [176] and Lübbenhusen & Mehrer [183] (Fe), Hegde et al. [33] (Mn) and Salje et al. [181] (Cu) are shown.

In order to investigate solute diffusion in bcc iron, we applied the same methodology as for the self-diffusion [2, 75]. Fig. 4.15 provides a comparison of the tracer diffusion coefficients for Fe, Cu and Mn in α-iron, as resulted from the current EIM approach [2, 33]. The simulation results are compared with the experimental data of Iijima et al. [176] and Lübbenhusen & Mehrer [183] (Fe), Hegde et al. [33] (Mn) and Salje et al. [181] (Cu).

From the obtained results (Fig. 4.15), we note a kink of a different size at the Curie point in the Arrhenius plot of the different elements, which is proportional to the respective ΔQ (difference of activation energy between the FM and the PM regimes). The ΔQ is the largest for Fe (0.46 eV), followed by Cu (0.22 eV), and the smallest being for Mn (0.11 eV). This hierarchy is in fully agreement with

available experimental data [33]. In addition, it is interesting to note that the difference of activation energy between the different solutes is significantly larger in the FM state (up to 0.48 eV) than in the PM state (up to 0.13 eV).

Fig. 4.15 also shows that the kinetic correlation factor f_{solute} for Cu and Mn diffusion increases with temperature up to an asymptotic limit of 0.73, which is the f_{Fe} value in pure bcc Fe. To clarify the role of magnetic disorder on the f_{solute}, we have performed similar kMC simulations for Cu and Mn diffusion, but imposing a perfect FM order for all atomic-kMC temperatures. The results show that the kinetic correlation factor of a solute diffusion increases much more slowly when magnetic order is imposed. This observation, together with the smaller difference between the activation free energies of Fe and distinct solutes in α-Fe at the PM than at the FM state (as shown in Fig. 4.16), suggest a dominance of the magnetic-disorder over the chemical-interaction effect in the extremely dilute Fe-X systems. Indeed, the magnetic free energy of binding between a vacancy and a solute atom (both Mn and Cu) practically vanishes at the high-temperature limit as shown in Fig. 4.12 [2, 75].

4.5.2 The "magnetic kink": the diffusion of $3d$-elements in α-Fe

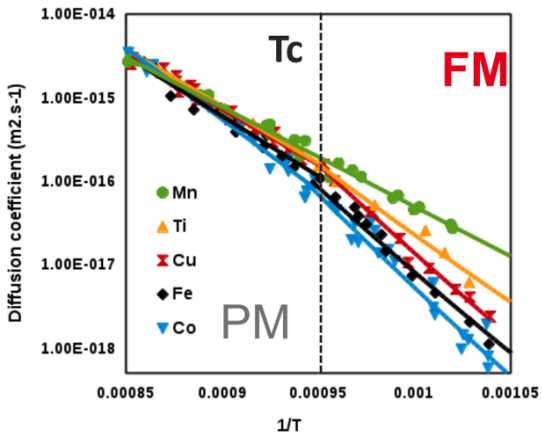

Figure 4.16: Experimental tracer diffusion coefficients for Fe and some other 3d solutes in bcc-iron, normalized with a high-temperature value in order to better compare the slopes. The data come from Refs. [174, 176, 181, 183–185].

As observed experimentally (Fig. 4.16), Fe and any 3d-solute in bcc-iron present a rather similar activation energy (Q) in the PM regime, while their Q in the FM state can be significantly different. Therefore, the size of the kink and the difference between the FM and PM activation energies (ΔQ) of the distinct solutes are mainly dictated by the Q in the FM state. To better understand this, we have determined, by means of DFT calculations, the 1nn solute-vacancy binding en-

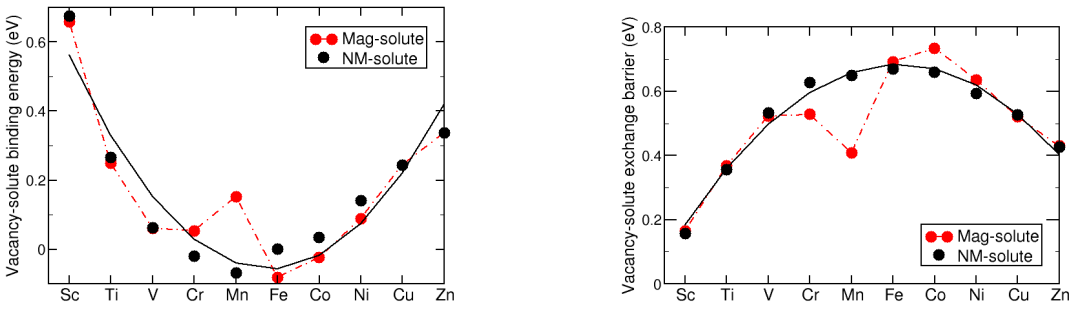

(a) (b)

Figure 4.17: Solute-vacancy (a) binding energy and (b) exchange barrier from DFT. We show the values with fully relaxed magnetic moments and with the solute moment constrained to zero (NM solute).

ergy and the solute-vacancy exchange barrier (two important components of the activation energy) in α-Fe for all the 3d solutes [33].

It is well known that, several properties of the magnetic 3d elements (Cr, Mn, Fe, Co, Ni) show a deviation from the expected parabolic behaviour as a function of the d-band filling [186]. We have therefore computed the binding energy (Fig. 4.17a) and the exchange energy barrier (Fig. 4.17b) under two different conditions: either (i) imposing the solute magnetic moment to zero while relaxing the moment of all other atoms, or (ii) relaxing the magnetic moment of all the atoms. In the former case, we observe the expected nearly-parabolic behaviour, while we note in the latter case some deviation from the overall trend for certain magnetic elements, especially for Mn and Co. For Mn, the very strong deviation leads to an increase of vacancy-Mn binding energy and a decrease of vacancy-Mn exchange barrier, both of around 0.2 eV. This results to a decrease of the activation energy of around 0.4 eV in the FM state, making it closer to the Q value in the PM state. Therefore, the resulting "kink" in the diffusion coefficients is significantly reduced for Mn in α-iron, as shown both experimentally and by DFT-based simulations [33]. For Co, the deviation leads to an opposite effect, that is, an increase of the Q in the FM regime, and therefore a larger kink at the Curie point. These predictions are fully consistent with experimental data shown in Fig. 4.16.

The above mentioned deviations can be rationalized by comparing the total system energy difference (ΔE) between the system with and without imposing the solute moment to zero, for three distinct solute local environments involved in the calculation of the binding energy and the exchange barrier. We see from Fig. 4.18a that, at the saddle-point position, the ΔE curve follows the solute moment magnitude curve (Fig. 4.18b), while deviations from the solute moment curve are observed for Mn and Co ΔE, with the solute either in the defect-free bulk

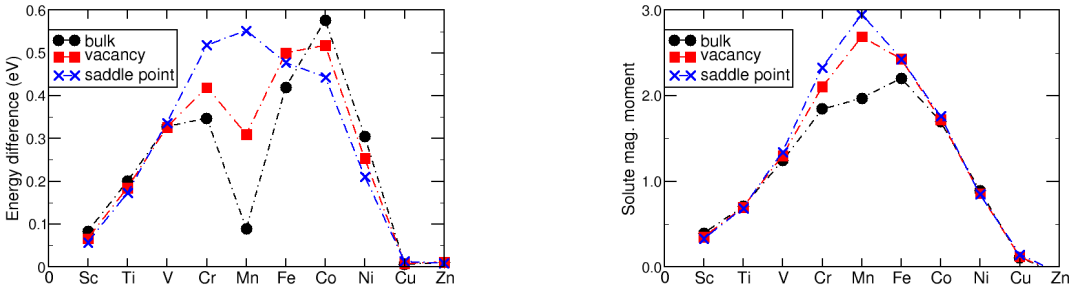

(a) (b)

Figure 4.18: (a) Total system energy difference (ΔE) between the cases with the solute-moment relaxed and constrained to zero. (b) Relaxed magnetic moment magnitude of the solute (in μ_B). Data are shown for the solute in the defect-free FM Fe, next to a vacancy, or in the saddle-point position.

environment or next to the vacancy.

For Mn, these deviations are due to the very strong local-environment dependence of the energy differences shown in Fig. 4.18a, with the smallest ΔE for a Mn solute in the bulk, then next to the vacancy, and then at the saddle point. Please note that the relaxed Mn spin is anti-parallel to Fe spin in the three local environments. In fact, a specificity of Mn, DFT calculations predicted the presence of two energy minima for a single Mn solute in bcc iron (Sec. 4.2.2) [121]: the AF-Mn with a large Mn moment anti-parallel to the Fe moments, and the FM-Mn state showing a small Mn moment parallel to the Fe moments. We note that the ΔEs for Mn shown in Fig. 4.18a closely follow the trend of the energy difference between the AF-Mn and the FM-Mn states. In the bulk, there is only 0.07 eV of energy difference between these two states. The FM-Mn configuration is energetically less favorable next to a vacancy (with an energy difference of 0.28 eV) , and such energy difference is even larger for a Mn at the saddle-point position (0.53 eV).

4.5.3 Composition-dependence of atomic diffusion properties

The magneto-chemical effects on atomic diffusion in concentrated alloys cannot be easily extrapolated from the knowledge in the dilute limits, because these effects can be strongly sensitive to the alloy composition. The impact of magnetic transition may also be composition dependent. From a technical point of view, dealing with concentrated alloys requires a proper statistical sampling of both chemical and magnetic configurations, which is practically impossible employing only DFT calculations.

In order to illustrate the composition-dependence of diffusion properties, I

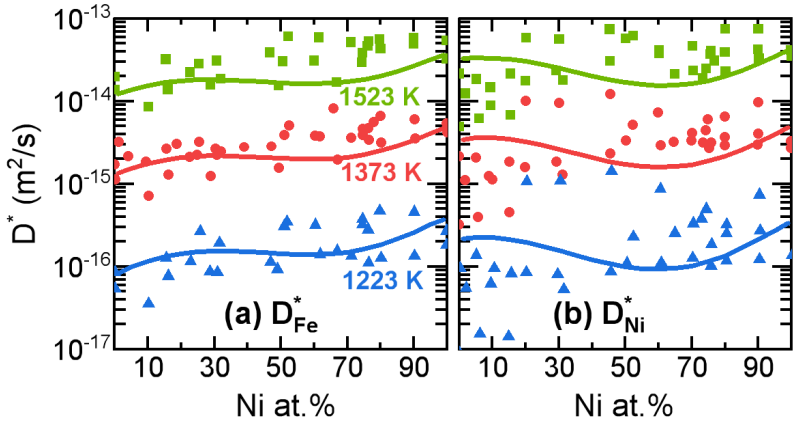

Figure 4.19: Tracer diffusion coefficients in PM fcc Fe-Ni alloys under equilibrium conditions. Lines represent the predictions from our work. Symbols are the experimental data compiled in Ref. [187], including ten different studies in non-dilute alloys (only two of them measured simultaneously D^*_{Fe} and D^*_{Ni}).

discuss, in this section, the tracer diffusion in fcc Fe-Ni alloys and in bcc Fe-Mn alloys. In the Fe-Ni system, we predict the composition-evolution of the tracer diffusion coefficients, in good agreement with experimental data in the PM solid solutions. In the Fe-Mn case, we analize the composition-dependence of the Curie-point impoact on Mn diffusion, via a concerted modelling-experimental study.

Diffusion in fcc Fe-Ni

We computed Fe and Ni tracer diffusion coefficients in PM Fe-Ni solid solutions at temperatures above 1200K [108] in the whole composition range, via the DFT-informed EIM-kMC simulations. Fully consistent with previous experimental data [187], we predicted a rather weak composition dependence of the diffusion coefficients (Fig. 4.19).

We rationalized this weak composition dependence as a compensation of distinct contributions of the main constituents of the diffusion coefficients, namely the equilibrium vacancy concentration and the effective jump frequency. For this purpose, we proposed a way to express the tracer diffusion coefficient in concentrated alloys in terms of its components, using the same formal expression as in the dilute limit [108].

First of all, I remind that in an infinitely dilute alloy containing B-solute atoms, the solute-diffusion coefficient is known to have the following expression (the same as Eq. 4.5) [24, 26, 28]:

$$D^*_B = a^2 f_B x_V \exp(G_b^{V\text{-}B}/k_B T)\Gamma_B \tag{4.7}$$

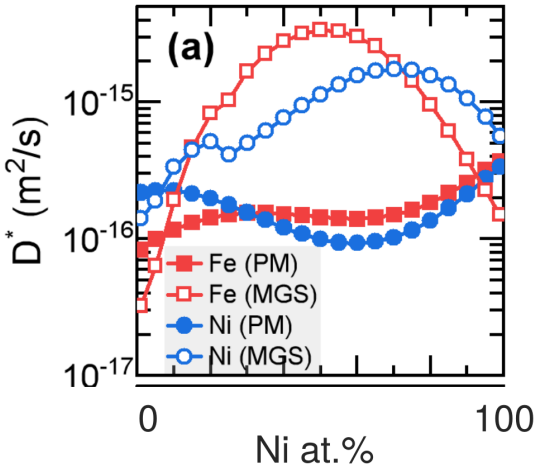

Figure 4.20: Comparison of tracer diffusion coefficients in fcc Fe-Ni structures at 1223 K, between results with the equilibrium PM state and imposing the 1 K MGS.

where a is the lattice constant, f_B is the correlation factor for the solute atom, x_V is the vacancy concentration of the corresponding system without the solutes, $G_b^{\text{V-B}}$ the solute-vacancy binding free energy, and Γ_B is the jump frequency of the B-solute atoms. Note that this expression is totally equivalent to the Eq. 4.5.

For non-dilute alloys of a given composition, we propose that the diffusion coefficients of the B element can be formally written as:

$$D_B^* = a^2 f_B x_V (1 - [ASRO]_{\text{V-B}}^{\text{1nn}}) \Gamma_B \tag{4.8}$$

where x_V in this equation denotes the vacancy concentration in the alloy, $[ASRO]_{\text{V-B}}^{\text{1nn}}$ is the Cowley-Warren short-range order parameter of 1nn vacancy-B pairs [188, 189], and Γ_B represents an effective jump frequency of the B atoms. Pleasee note that 1-$[\text{ASRO}]_{\text{V-B}}^{\text{1NN}}$ becomes $\exp(G_b^{\text{V-B}}/k_B T)$ in Eq. 4.7 in an infinitely dilute alloy. The derivation of Eq. 4.8 is detailed in Ref. [108].

In order to better understand the impact of magnetic disorder, we compare the obtained diffusion coefficients in the PM state wiut the ones obtained with the same high-temperature solid solutions but by imposing the 0-K ordered magnetic state corresponding to each composition. Interestingly, a much stronger composition dependence of the diffusion properties is predicted if the 0-K magnetic configurations are adopted instead of the PM state (Fig. 4.20). This effect persists well beyond the dilute limit, regardless of the alloy composition. This result suggests that the magnetic disorder (in the PM state) tends to reduce the chemical-interaction (therefore chemical-composition) effects. Such a reduction of chemical-interaction effect due to the magnetic disorder was indeed evidenced in some dilute bcc Fe systems as shown above. The different diffusion proper-

ties of ordered and disordered magnetic states indicate that the magnetic ground state is not a proper descriptor of diffusion in the PM concentrated alloys.

Diffusion in bcc Fe-Mn

Using the same methodology, we have also determined the tracer diffusion coefficients in rather dilute bcc Fe-Mn alloys, up to 2 at.% Mn, and closely compared the obtained results with the tracer diffusion experimental data by S. Divinski *et al.* [98]. Both simulations and experiments considered temperatures below and above the Curie point, ranging from 700 K to 1200 K. The main goal of this study is to investigate the correlation between the alloy composition and the magnetic-transition impact on atomic diffusion. In particular, as already shown above, the Curie transition has a very weak effect on Mn-solute diffusion in the extremely dilute limit. It is then interesting to know if this behavior persists with an increasing Mn content.

First, Fig. 4.21 gives both experimental and simulation results for temperatures of 1120 K and 838 K. We see a very reasonable quantitative agreement, attesting the validity of the modelling approach.

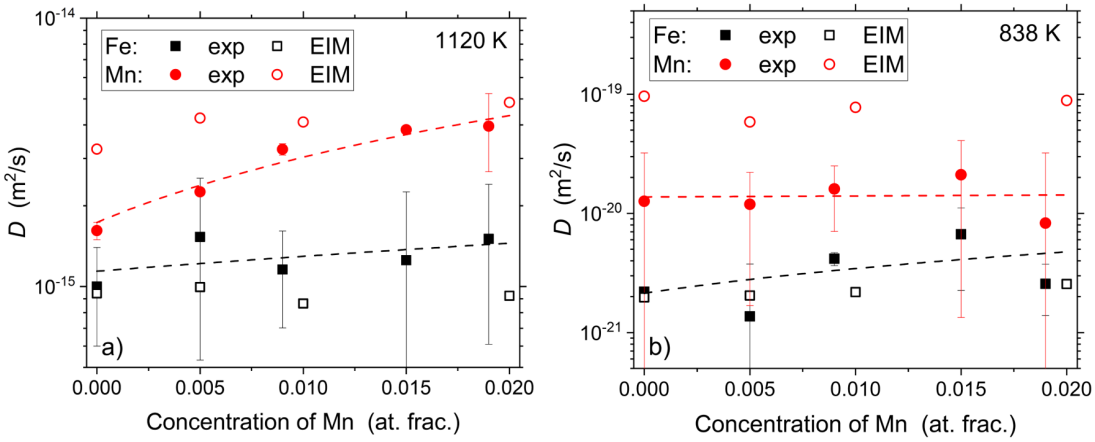

Figure 4.21: Mn (red symbols) and Fe (black symbols) diffusion in bcc Fe-Mn alloys at 1023 K (a) and 838 K (b). The experimental data (filled symbols) are compared with the EIM + kMC predictions (open symbols). The dashed lines represent the experimentally established trends.

Then, as clearly visible in Fig. 4.22, the simulation results show a stronger composition dependency of the Mn than the Fe diffusion coefficients. This behavior is also consistent with the 1120 K experimental data (Fig. 4.21).

As in the case of Fe-Ni, our simulation results allow us to gain insight into the distinct behavior of the various constituents of the tracer diffusion coefficients, that is, the equilibrium vacancy concentration, the migration free energy, the correlation factor and the solute-vacancy binding energy. Details are described in

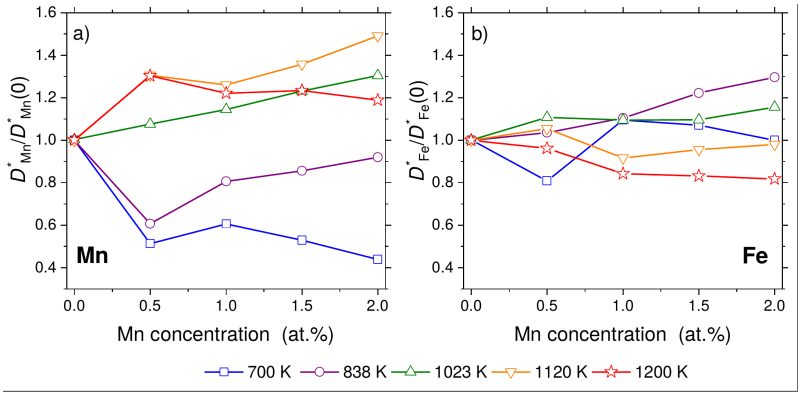

Figure 4.22: EIM + kMC results on relative tracer diffusion coefficients with regard to the extremely dilute value of (a) Mn and (b) Fe as functions of the Mn concentration, for various temperatures.

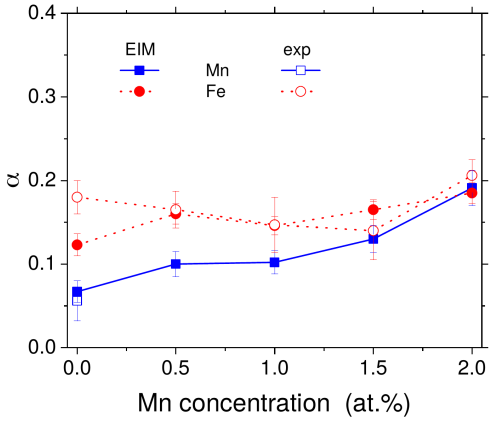

Figure 4.23: The α parameter as defined in the Ruch model (Eq. 4.9) [81] from experimental (empty symbols) and EIM (solid symbols) results, for Mn (blue) and Fe (red) tracers diffusion.

Ref. [98]. For instance, above the Curie temperature (*e.g.* 1120 K), we find a larger Mn-vacancy binding energy with increasing Mn concentration, which is the main reason of the increased Mn diffusion coefficients with respect to the infinitely diluted limit (Fig. 4.22). On the other side, below the Curie temperature (*e.g.*838 K), we note a decrease of the correlation factor and an increase of the solute migration barrier with a larger Mn content, making the overall reduced Mn diffusion coefficients compared to the infinitely diluted case (Fig. 4.22).

Similar to previous findings on the diffusion properties in extremely dilute α-Fe systems and in Fe-Ni alloys, the present simulation results also suggest that, in the PM state, magnetic disorder significantly reduces the chemical effects. This is more visible in the properties related to Mn diffusion, in the weaker concentration dependency of the Mn jump frequency and of its correlation factor in the PM state

than in the FM state, as well as a smaller Mn–vacancy binding in the PM state [98].

Finally, concerning the composition dependence of the magnetic-transition impact, we plot the α parameter in Fig. 4.23. This parameter is defined in Eq. 4.9:

$$\alpha = \frac{Q^{\mathrm{FM}} - Q^{\mathrm{PM}}}{Q^{\mathrm{PM}}}, \tag{4.9}$$

It comes from the Ruch model [81] providing a quantitative idea of the relative change of the diffusion activation energy (slope in the Arrhenius plot) between the perfectly FM and PM states (respectively Q^{FM} and Q^{PM}). As can be see in Fig. 4.23, there is a significant increase of the α parameter for Mn diffusion with increasing Mn concentration, while this one remains practically unchanged for Fe diffusion. For instance, in Fe–2.0at.% Mn, this α parameter attains similar values for both Mn and Fe, while α for Mn diffusion is significantly smaller than that for Fe in the extremely dilute limit (see Secs. 4.5.1 and 4.5.2).

4.6 Magnetism versus microstructure

In view of the validity of the present modelling approach on prediction of the diffusion properties in Fe alloys, we expect it to be also capable to predict kinetics of processes driven by atomic diffusion, for example phase ordering and precipitation, and interfacial segregation. In particular, this methodology could allow us to gain insights into the interplay between the microstructure evolution and the change of local and global magnetism in the magnetic metallic alloys.

As an example of such interplay, H. Yamamoto [190] raised, based on experimental measurement, differences in magnetic behavior of quenched and 773 K-annealed Fe-Cr random alloys, initially prepared from Fe and Cr powders at 1372 K. The Cr concentrations considered range from 20 to 46 wt.%.

We have applied a combination of EIM and MC and kMC simulations to elucidate this microstructure-magnetism correlation in Fe-Cr alloys [191]. For this first attempt, we applied a previously-implemented interaction and diffusion model (without spin variables) [31], coupled with kMC, to describe the microstructure evolution along the simulated annealing. Then, we transferred snapshots of the resulting chemical configurations to the MCE (also used in Sec/ 4.2) [115] based MC for the determination of magnetic properties. In this way, we obtained both chemical and the corresponding magnetic configurations as a function of time. The reason of this two-step simulation is because the development of the "kinetic" version of our magnetic EIM for Fe-Cr is still ongoing. We went beyond the scope of the Yamamoto's work by considering not only Fe-rich but also Cr-rich alloys.

We have performed simulated annealing of initially random alloys at 773 K for times of the order of 10^6 s. This thermal annealing substantially changes the alloys microstructure. As expected from our predicted Fe-Cr phase diagram, solute atoms quickly form clusters in the both systems (Fe-32 at.% Cr and Cr-25

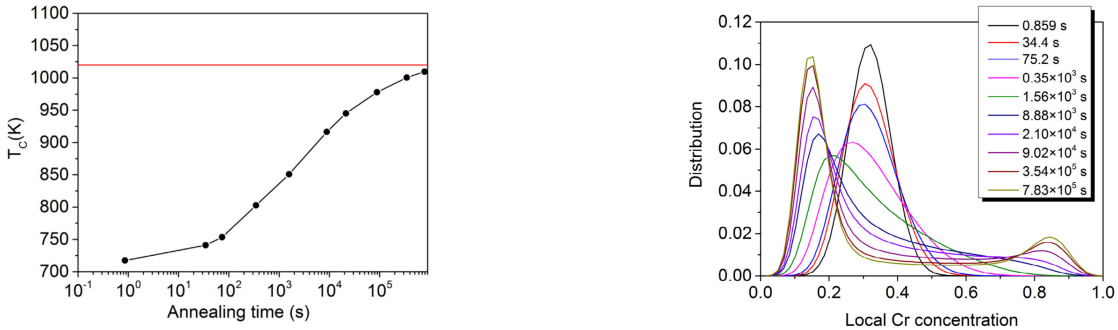

(a) (b)

Figure 4.24: Time evolution during the 773 K annealing of the overall Curie temperature (a), and the distribution of local Cr concentration up to fifth-neighbor shell of each atom (b), in the Fe-32 at.% Cr alloy. The emergence of two peaks in (b) indicates a phase separation.

at.% Fe). The clusters sizes increase with time according to power law [191].

For the Fe-32 at. % Cr alloy, the global magnetization and Curie temperature increase with increasing annealing time and cluster/precipitate size (Fig. 4.24a). It is not surprising that at large simulation times, the Curie temperature approaches the value for Fe-15 at. % Cr solid solution (1020 K based on this MCE), which corresponds to the chemical composition and configuration of the Fe-rich phase in the completely phase-separated alloy at 773 K. Indeed, as shown in Fig. 4.24b, at long simulation times, the emerged Fe-rich phase already contains around 15% Cr. The Cr-rich phase formed has a very small contribution to the global Curie temperature due to its much smaller volume fraction. Our results provide explanation for the magnetization difference between quenched and annealed samples by Yamamoto [190]. At that time, the origin of his observation was unclear, but now we can state that this difference stems from formation and growth of α'-precipitates and decrease of Cr content in the Fe-rich matrix (from 32% to 15%) with annealing time.

For the Cr-25 at.% Fe alloy, precipitation also results in an increase of the overall Curie temperature (Fig. 4.25a), although at the end of the simulation time (arounf 10^6 s), the global Curie temperature (800 K) remains below the expected value in the Fe-rich precipitates (1020 K). Two factors contribute to this result: (i) vacancy mediated atomic-diffusion (and therefore microstructure evolution) is slower in Cr-rich alloys compared to Fe-rich ones, and (ii) Fe-rich minority precipitates in Cr-25 at. % Fe is affected by Cr-rich surroundings that suppress ferromagnetism[191] (Fig. 4.25b).

By determining the correlation between the precipitation and the evolution of magnetism, the simulation results also suggest a way to monitor the precipitation stage (for example the characteristic size of precipitates [191]) via the overal Curie

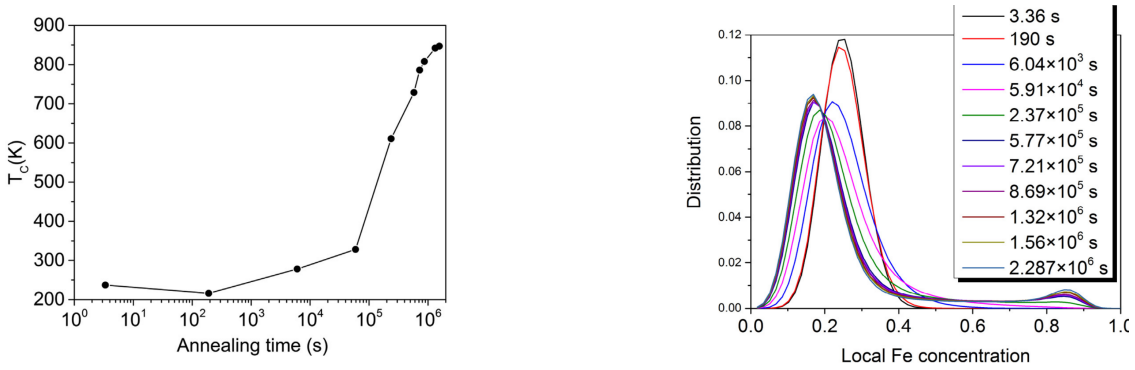

(a) (b)

Figure 4.25: Time evolution during the 773 K annealing of the overall Curie temperature (a), and the distribution of local Fe concentration up to fifth-neighbor shell of each atom (b), in the Cr-25 at.% Fe alloy. The emergence of two peaks in (b) indicates a phase separation.

temperature of the system. But obviously, in the case of a two-phase system, the experimentally measured magnetization and Curie point are not homogeneous properties in the entire sample. Atomiistic simulations are therefore useful for a detailed interpretation of their values and their origin.

4.7 Associated collaborations and publications

A significant part of results shown in this Chapter comes from the Ph.D thesis work of R. Soulairol, of A. Schneider, and of K. Li. I also appreciate fruitful collaborations with M.Y. Lavrentiev, S. Dudarev and C. Barreteau on the studies of Sec. 4.2. In addition, the work on the finite temperature magnetic effects is directly connected to our frenco-german ANR MAGIKID project, which promoted various stimulating collaborations with german colleagues, especially with S. Divinski, T. Hickel, R. Drautz, and with french colleagues: H. Amara and V. Pierron-Bohnes *et al.*. A postdoc (V.T. Tran) was also hired thanks to this project. I am also very thankful to F. Soisson for the support and collaboration concerning the Monte Carlo simulations.

Please find below a list of most relevant publications related to the content of this Chapter: P4.1 to P4.4 for Sec. 4.2, P4.5, P4.6 and P4.8 for Sec. 4.3, P4.7 and P4.8 for Sec. 4.4.1, P4.9 to P4.11 for Sec. 4.5, and P4.12 for Sec. 4.6.

- **P4.1: Structure and magnetism of bulk Fe and Cr: from plane waves to LCAO methods**

  R Soulairol, CC Fu, C Barreteaun, J. Phys. Condens. Matter **22**, 29550 (2010), doi:10.1088/0953-8984/22/29/295502.

Abstract: Magnetic, structural and energetic properties of bulk Fe and Cr were studied using first-principles calculations within density functional theory (DFT). We aimed to identify the dependence of these properties on key approximations of DFT, namely the exchange–correlation functional, the pseudopotential and the basis set. We found a smaller effect of pseudopotentials (PPs) on Fe than on Cr. For instance, the local magnetism of Cr was shown to be particularly sensitive to the potentials representing the core electrons, i.e. projector augmented wave and Vanderbilt ultrasoft PPs predict similar results, whereas standard norm-conserving PPs tend to overestimate the local magnetic moments of Cr in bcc Cr and in dilute bcc FeCr alloys. This drawback is suggested to be closely correlated to the overestimation of Cr solution energy in the latter system. On the other hand, we point out that DFT methods with very reduced localized basis sets (LCAO: linear combination of atomic orbitals) give satisfactory results compared with more robust plane-wave approaches. A minimal-basis representation of '3d' electrons comes to be sufficient to describe non-trivial magnetic phases including spin spirals in both fcc Fe and bcc Cr, as well as the experimental magnetic ground state of bcc Cr showing a spin density wave (SDW) state. In addition, a magnetic 'spd' tight binding model within the Stoner formalism was proposed and validated for Fe and Cr. The respective Stoner parameters were obtained by fitting to DFT data. This efficient semiempirical approach was shown to be accurate enough for studying various collinear and non-collinear phases of bulk Fe and Cr. It also enabled a detailed investigation of different polarization states of SDW in bcc Cr, where the longitudinal state was suggested to be the ground state, consistent with existing experimental data.

- **P4.2: Magnetic and energetic properties of low-index Cr surfaces and Fe/Cr interfaces: A first-principles study**

  R Soulairol, CC Fu, C. Barreteau Phys. Rev. B **84**, 155402 (2011),

  https://doi.org/10.1103/PhysRevB.84.155402.

  Abstract: Density functional theory calculations are performed to investigate the impact of magnetism on the energetics of low-index Cr surfaces and Fe/Cr interfaces, that is, Cr(100), Cr(110), Fe/Cr(100), and Fe/Cr(110). We have also determined the stability of various Cr magnetic structures, particularly the spin-density waves, in the presence of these surfaces and interfaces. We show that the most stable structure of the spin-density wave is mainly dictated by the subtle balance between bulk and surface/interface influences, and strongly dependent on the surface/interface orientation. Regarding the Cr surfaces, we confirm the role of magnetism to lower the surface energy of Cr(100) with respect to Cr(110). Among all the possible orientations of the wave vector, only the out-of-plane wave is found to be

stable near Cr(100) surfaces with the high-moment sites located at the surface layer. At variance, the in-plane wave is shown to be the most stable one, consistent with experimental data for very thin Cr(110) films. Concerning the Fe/Cr interfaces, magnetic frustrations are identified to be responsible for a higher formation energy of Fe/Cr(110) compared to that of Fe/Cr(100). This unusual anisotropy of interface energies is clearly different from the corresponding interfaces between Cr and a nonmagnetic element, Cu. Two ways are suggested to relax partially the magnetic frustrations at the (110) interface and to lower its formation energy. Noncollinear magnetic configurations can be developed where local moments of Fe and Cr atoms are perpendicular to each other. Also, in order to preserve phase coherence, in-plane spin-density waves show a very stable magnetic structure with the nodes at the interface layer. The presence of low-moment sites at Fe/Cr(110) offer another way to relax the magnetic frustrations and lower the interfacial energy.

- **P4.3: Low-and high-temperature magnetism of Cr and Fe nanoclusters in iron-chromium alloys**

  CC Fu, MY Lavrentiev, R Soulairol, SL Dudarev, D Nguyen-Manhn Phys. Rev. B **91**, 094430 (2015),

  https://doi.org/10.1103/PhysRevB.91.094430.

  Abstract: Low-energy magnetic states and finite-temperature properties of Cr nanoclusters in bulk bcc Fe and Fe nanoclusters in bulk Cr are investigated using density functional theory (DFT) and the Heisenberg-Landau Hamiltonian based magnetic cluster expansion (MCE). We show, by means of noncollinear magnetic DFT calculations, that magnetic frustration caused by competing ferromagnetic and antiferromagnetic interactions either strongly reduces local magnetic moments while keeping collinearity or generates noncollinear magnetic structures. Small Cr clusters generally exhibit collinear ground states. Noncollinear magnetic configurations form in the vicinity of small Fe clusters if antiferromagnetic Fe-Cr coupling dominates over ferromagnetic Fe-Fe interactions. MCE predictions broadly agree with DFT data on the low-energy magnetic structures, and extend the DFT analysis to larger systems. Nonvanishing cluster magnetization caused by the dominance of Fe-Cr over Cr-Cr antiferromagnetic coupling is found in Cr nanoclusters using both DFT and MCE. Temperature dependence of magnetic properties of Cr clusters is strongly influenced by the surrounding iron atoms. A Cr nanocluster remains magnetic until fairly high temperatures, close to the Curie temperature of pure Fe in the large cluster size limit. Cr-Cr magnetic moment correlations are retained at high temperatures due to the coupling of interfacial Cr atoms with the Fe environment. Variation of magnetization of Fe-Cr alloys as a function of temperature and Cr clusters

size predicted by MCE is assessed against the available experimental data.

- **P4.4: Local environment dependence of Mn magnetism in bcc iron-manganese alloys: A first-principles study**

  A Schneider, CC Fu, C Barreteau, Phys. Rev. B **98**, 094426 (2018),

  https://doi.org/10.1103/PhysRevB.98.094426.

  Abstract: Magnetic behavior of a 3d solute in a ferromagnetic lattice can be very sensitive to local environment, which is the case of manganese in bcc Fe. Body-centered cubic iron-manganese alloys are studied by means of density functional theory in order to elucidate properties of the lowest-energy magnetic states. Multiple magnetic minima are determined even for the simplest case of an isolated Mn and a Mn dimer in bcc iron. The magnetoenergetic landscape is analyzed within and beyond the collinear magnetic approximation. A direct correlation is identified between the local electronic charge and the local magnetic moment of a Mn solute, being either isolated or forming a small cluster. In particular, the presence of a vacancy near the Mn atom, inducing a local charge decrease, tends to favor the antiferromagnetic Fe-Mn interaction while the presence of an interstitial impurity with a strong electronic hybridization with Mn can favor a ferromagnetic Fe-Mn interaction. Energetic and magnetic properties of Fe-Mn alloys are systematically investigated for a large range of Mn concentrations. An unmixing tendency is clearly noted. A detailed magnetic analysis suggests the Mn-Mn magnetic interactions to be generally dominant over the Fe-Mn interactions, both exhibiting an antiferromagnetic tendency. The average magnetic moment of the Mn atoms in locally random alloys tends to be antiparallel (parallel) to lattice Fe moments for Mn concentrations smaller (larger) than approximately 6 at. %. The transition concentration is shown to be lowered if considering Mn clustering which is energetically favorable. The unsolved discrepancies between experimental and theoretical predictions on the critical concentration for the Mn magnetic behavior change in Fe-Mn solid solution are discussed in the light of the obtained results.

- **P4.5: Ab initio based models for temperature-dependent magnetochemical interplay in bcc Fe-Mn alloys**

  A Schneider, CC Fu, O Waseda, C Barreteau, T Hickel, Phys. Rev. B **103** , 024421 (2021),

  https://doi.org/10.1103/PhysRevB.103.024421

  Abstract: Body-centered cubic (bcc) Fe-Mn systems are known to exhibit a complex and atypical magnetic behavior from both experiments and 0 K electronic-structure calculations, which is due to the half-filled 3d band of Mn. We propose effective interaction models for these alloys, which contain both atomic-spin and chemical variables. They were parameterized

on a set of key density functional theory (DFT) data, with the inclusion of noncollinear magnetic configurations being indispensable. Two distinct approaches, namely a knowledge-driven and a machine-learning approach have been employed for the fitting. Employing these models in atomic Monte Carlo simulations enables the prediction of magnetic and thermodynamic properties of the Fe-Mn alloys, and their coupling, as functions of temperature. This includes the decrease of Curie temperature with increasing Mn concentration, the temperature evolution of the mixing enthalpy, and its correlation with the alloy magnetization. Also, going beyond the defect-free systems, we determined the binding free energy between a vacancy and a Mn atom, which is a key parameter controlling the atomic transport in Fe-Mn alloys.

- **P4.6: Ground-state properties and lattice-vibration effects of disordered Fe-Ni systems for phase stability predictions**

  K Li, CC Fu, Phys. Rev. Materials **4**, 023606 (2020).

  https://doi.org/10.1103/PhysRevMaterials.4.023606.

  Abstract: By means of density functional theory, we perform a focused study of both body-centered-cubic (bcc) and face-centered-cubic (fcc) Fe-Ni random solid solutions, represented by special quasirandom structures. The whole concentration range and various magnetic configurations are considered. Excellent agreement on the concentration dependence of magnetization is found between our results and experimental data, except in the Invar region. Some locally antiferromagnetic fcc structures are proposed to approach experimental values of magnetization. Vibrational entropies of ordered and disordered systems are calculated for various concentrations, showing an overall good agreement with available experimental data. The vibrational entropy systematically contributes to stabilize disordered rather than ordered structures and is not negligible compared to the configurational entropy. Free energy of mixing is estimated by including the vibrational and ideal configurational entropies. From them, low- and intermediate-temperature Fe-Ni phase diagrams are constructed, showing a better agreement with experimental data than the one from a recent thermodynamic assessment for some phase boundaries below 700 K. The determined order-disorder transition temperatures for the L10 and L12 phases are in good agreement with the experimental values, suggesting an important contribution of vibrational entropy.

- **P4.7: Effects of magnetic excitations and transitions on vacancy formation: cases of fcc Fe and Ni compared to bcc Fe**

  K Li, CC Fu, A Schneider Phys. Rev. B **104** , 104406 (2021),

  https://doi.org/10.1103/PhysRevB.104.104406.

Abstract: Vacancy is one of the most frequent defects in metals. We study the impacts of magnetism on vacancy formation properties in fcc Ni, and in bcc and fcc Fe, via density functional theory (DFT) and effective interaction models combined with Monte Carlo simulations. Overall, the predicted vacancy formation energies and equilibrium vacancy concentrations are in good agreement with experimental data, available only at the high-temperature paramagnetic regime. Effects of magnetic transitions on vacancy formation energies are found to be more important in bcc Fe than in fcc Fe and Ni. The distinct behavior is correlated to the relative roles of longitudinal and transversal spin excitations. At variance with the bcc-Fe case, we note a clear effect of longitudinal spin excitations on the magnetic free energy of vacancy formation in fcc Fe and Ni, leading to its steady variation above the respective magnetic transition temperature. Below the Néel point, such effect in fcc Fe is comparable but opposite to the one of the transversal excitations. Regarding fcc Ni, although neglecting the longitudinal spin excitations induces an overestimation of the Curie temperature by 220 K, no additional effect is visible below the Curie point. The distinct effects on the three systems are closely linked to DFT predictions of the dependence of vacancy formation energy on the variation of local magnetic-moment magnitudes and orientations.

- **P4.8: Magnetochemical effects on phase stability and vacancy formation in fcc Fe-Ni alloys**

  K Li, CC Fu, M Nastar, F Soisson, MY Lavrentiev, Phys. Rev. B **106**, 024106 (2022),

  https://doi.org/10.1103/PhysRevB.106.024106.

  Abstract: We investigate phase stability and vacancy formation in fcc Fe-Ni alloys over a broad composition-temperature range, via a density functional theory parametrized effective interaction model, which includes explicitly spin and chemical variables. On-lattice Monte Carlo simulations based on this model are used to predict the temperature evolution of the magnetochemical phase. The experimental composition-dependent Curie and chemical order-disorder transition temperatures are successfully predicted. We point out a significant effect of chemical and magnetic orders on the magnetic and chemical transitions, respectively. The resulting phase diagram shows a magnetically driven phase separation around 10–40% Ni and 570–700 K, between ferromagnetic and paramagnetic solid solutions, in agreement with experimental observations. We compute vacancy formation magnetic free energy as a function of temperature and alloy composition. We identify opposite magnetic and chemical disordering effects on vacancy formation in the alloys with 50% and 75% Ni. We find that thermal magnetic effects on vacancy formation are much larger in concentrated

Fe-Ni alloys than in fcc Fe and Ni due to a stronger magnetic interaction.

- **P4.9: Atomic Diffusion in -iron across the Curie Point: An Efficient and Transferable Ab-Initio–Based Modeling Approach**

  A Schneider, CC Fu, F Soisson, C Barreteau, Phys. Rev. Lett. 124 , 215901 (2020),

  https://doi.org/10.1103/PhysRevLett.124.215901.

  Abstract: An accurate prediction of atomic diffusion in Fe alloys is challenging due to thermal magnetic excitations and magnetic transitions. We propose an efficient approach to address these properties via a Monte Carlo simulation, using ab initio–based effective interaction models. The temperature evolution of self- and Cu diffusion coefficients in α-iron are successfully predicted, particularly the diffusion acceleration around the Curie point, which requires a quantum treatment of spins. We point out a dominance of magnetic disorder over chemical effects on diffusion in the very dilute systems.

- **P4.10: Impact of magnetic transition on Mn diffusion in α-iron: Correlative state-of-the-art theoretical and experimental study**

  O Hegde, V Kulitckii, A Schneider, F Soisson, T Hickel, J Neugebauer, G. Wilde, S. Divinski, CC Fu, Phys. Rev. B **104**, 184107 (2021),

  https://doi.org/10.1103/PhysRevB.104.184107.

  Abstract: An accurate prediction of atomic diffusion in Fe alloys is challenging due to thermal magnetic excitations and magnetic transitions. We investigate the diffusion of Mn in bcc Fe using an effective interaction model and first-principles based spin-space averaged relaxations in magnetically disordered systems. The theoretical results are compared with the dedicated radiotracer measurements of 54Mn diffusion in a wide temperature range of 773 to 1173 K, performed by combining the precision grinding (higher temperatures) and ion-beam sputtering (low temperatures) sectioning techniques. The temperature evolution of Mn diffusion coefficients in bcc iron in theory and experiment agree very well and consistently reveal a reduced acceleration of Mn solute diffusion around the Curie point. By analyzing the temperature dependencies of the ratio of Mn diffusion coefficients to self-diffusion coefficients we observe a dominance of magnetic disorder over chemical effects on high-temperature diffusion. Therefore, the missing acceleration mainly reflects an anomalous behavior of the Mn solute in the magnetically ordered low-temperature state of the Fe host, as compared to other transition metals.

- **P4.11: Predicting atomic diffusion in concentrated magnetic alloys: The case of paramagnetic Fe-Ni**

K Li, CC Fu, M Nastar, F Soisson, Physical Review B **107**, 094103 (2023).

https://doi.org/10.1103/PhysRevB.107.094103.

Abstract: Predicting atomic diffusion in concentrated magnetic systems is challenging due to thermal magnetic effects and complex magnetochemical interplay. We propose an efficient approach via kinetic Monte Carlo using ab initio parametrized models. We demonstrate its accuracy in the case of Fe-Ni alloys, where we successfully predict and explain the weak composition dependence of diffusion coefficients due to a compensation of distinct contributions of their constituents. The diffusion-behavior difference between the paramagnetic and the magnetic ground states is elucidated, evidencing the role of magnetic disorder.

- **P4.12: Correlation between microstructure and magnetic properties during phase separation in concentrated Fe-Cr alloys**

  MY Lavrentiev, CC Fu, F Soisson, J. Mag. and Mag. Mater. **506**, 166763 (2020),

  https://doi.org/10.1016/j.jmmm.2020.166763.

  Abstract: We report a theoretical study of microstructure, magnetic properties, and their relationship in relatively concentrated Fe-Cr alloys in both Fe- and Cr-rich regions. Annealing of initially random systems at 500 °C for times of the order of 106 s substantially changes their microstructure. In both systems, solute atoms form clusters with their sizes increasing with time according to power law, with exponent being close to 0.2. For the Fe-32 at. % Cr alloy, magnetization and the Curie temperature increase with increasing annealing time and cluster size. At large simulation times, the Curie temperature approaches its value for Fe-15 at. % Cr, the concentration of completely phase-separated iron-rich alloy. For the Cr-25 at. % Fe alloy, precipitation also results in an increase of magnetization and the Curie temperature, although characteristic times are about one order of magnitude greater.

Chapter 5

Conclusions and Perspectives

With this report, I intent to summarize some of our most relevant results concerning diffusion and clustering of structural point defects and solutes in various Fe systems, via DFT calculations and DFT informed upper-scale simulations.

Chapter 2 describes the predicted diffusion mechanisms and activation energies of the elementary structural defects (vacancies, **SIAs!** (**SIAs!**) and their small clusters) in α-Fe. It is also shown how these DFT results contribute to an accurate interpretation of data from *e.g.* electrical resistivity measurements and magnetic after effect experiments in irradiated pure and C or N doped Fe. The DFT predictions also enabled to solve discrepancies between various experimental conclusions.

Chapter 3 is focused on diffusion and clustering with vacancies of interstitial and substitutional solutes in α-Fe. We consider the common interstitial solutes (C, N and O), yttrium (representing oversized solutes), and two gas elements (He and H) of interest under high-energy neutron irradiation.

The relative affinity of the interstitial C, N and O solutes with vacancies, and the lowest-energy configurations of the solute-vacancy clusters are strongly dictated by the electronic charge distribution around the solutes. Various impacts of the high stability of vacancy-X (X = C, N, O) clusters against dissociation are determined. For instance, the total vacancy concentration and the effective diffusivity of vacancies are significantly increased and decreased, respectively, in the presence of a tiny amount of the solutes. At variance with the common belief, O and N atoms can play a stronger role than C solutes in some cases. Also, different from the widely accepted scenario, once the interstitial solutes are trapped by vacancies, they do not necessarily become less mobile. This is indeed the case of solute diffusion via the V_3X clusters, which are equally or more mobile than the single X solutes.

Among the substitutional solutes, we pay a particular attention to the case of oversized elements. Their vacancy-mediated diffusion cannot be described by the standard mechanism. Instead, we propose it to diffuse via macrojumps. These atoms generally diffuse faster than the host atoms in bcc and fcc lattices,

which is the case of yttrium in iron. But, opposite to the standard substitutional solutes, their tracer diffusion coefficients do not increase with increasing vacancy concentration.

It is also found that the He-Fe repulsion is the main driving force dictating He behavior in bcc Fe, such as the He-He and He-vacancy clustering. The stability of a cluster/bubble containing He, against emission of He or point defects, is governed by its local pressure (He-to-vacancy ratio). With an energetic preference to form H-Fe than H-H bonds, the clustering behavior of H atoms in Fe is clearly different from the one of He. At variance with standard substitutional solutes, The dominant He migration mechanism is highly dependent of vacancy and SIA concentrations in the system. Accounting for a rather small set of DFT data, a rate theory based modelling was able to successfully reproduce the experimental rate of He desorption from irradiated Fe during isothermal annealling. There, the inclusion of interstitial C impurities in our model revealed to be indispensable. Finally. following the He segregation to Fe GBs, we confirm the He effect to reduce GB cohesion. We predict this effect to be stronger with He atoms being isolated than forming clusters/bubbles at GBs. Even in the former situation, a very large amount of He (around 5000 appm) would be required to induce a complete GB decohesion. Although not directly comparable, these findings are fully compatible with available experimental evidence.

In Chapter 4, I focus on the magnetic degree of freedom, which plays a key role in properties of Fe alloys. To this end, we performed some DFT calculations beyond the collinear-magnetism approximation, and some others constraining local magnetic moments. In order to account for finite temperature magnetic excitations and transitions, we have developed and applied spin-atomic on-lattice MC and kMC approaches, using DFT parametrized EIMs.

First, the presence of low-temperature magnetic frustration in bcc Fe-Cr is shown to modify the energetic hierarchy of various low-index Fe/Cr interfaces, and to affect properties of Fe and Cr nano-clusters. Two ways are identified to partially resolve the magnetic frustration: developing either non-collinear structures or a distribution of small moment sites (*e.g.* SDWs). Our results also revealed a strong sensitivity of Mn magnetism in FM bcc Fe, depending on the local chemical enviroment and the electronic density around the Mn solute. It can be deduced from our DFT studies that, in bcc Fe-cr systems, the Fe-Cr AF interaction tendency dominates over the Cr-Cr anti-ferromagnetism in the underlying FM Fe lattice, while the situation is reversed in the bcc Fe-Mn system, with the AF Fe-Mn interaction generally weaker than the Mn-Mn magnetic interaction. These overall "rules" are useful to determine the lowest-energy magnetic configurations.

When including both spin and atomic variables and their coupling in our DFT informed simulations, we were able to accurately predict magnetic and chemical phase diagrams in a broad range of alloy compositions, as shown for bcc Fe-Co and Fe-Cr, and fcc Fe-Ni alloys. In addition, these simulations enabled a split-

ting of effects of chemical and magnetic excitations and of lattice vibration on the phase transitions. These separate contributions are not obvious to obtain via experiments..

Moreover, we predicted temperature evolution of tracer diffusion coefficients of atoms in Fe alloys for various alloy compositions. The results at high temperatures are in very good agreement with experimental data, including the "kink" around the magnetic transition. These studies allow, on one hand, to complete the missing experimental diffusion data at intermediate and low temperatures, and on the other hand, to gain insights into the distinct behavior of each of the components of the diffusion coefficients (equilibrium vacancy concentration, vacancy-atom binding, correlation factor, and jump frequencies). Thanks to the knowledge on the individual contributions, this approach is able to predict quite easily diffusion properties in equilibrium and various non-equilibrium conditions. Concerning the impact of magnetic disorder, it can be concluded from all our studies that the magnetic disorder, occurring in the PM state, significantly reduces chemical-interaction effects in the Fe alloys, reflected by *e.g.* a weaker local environment dependence of vacancy jump frequencies and therefore an increase of correlation factors, and a reduction of compositional dependence of the diffusion properties, Finally, It is worth noting that the present approach is particularly important for the determination of defects formation and diffusion properties in austenitic Fe alloys (*e.g.* Fe-Ni, Ni-Cr and Fe-Ni-Cr), which are often in a PM state at temperatures of technological interest.

Related to the studies shown in this HDR report, some immediate perspectives consist in an application of this EIM-MC approach to the formation and diffusion of SIAs in the austenitic Fe alloys. These properties, especially in the PM state, is practically unknown and extremely important for the understanding of kinetic processes under irradiation. Also, we will include the finite-temperature magnetic effects in our study of carbides in Fe alloys. We expect it to have a significant impact on the theoretical predictions, since Curie temperature of the carbides are generally much lower than that of the bcc Fe matrix.

From a methodological point of view, our current EIMs take into account explicitly the chemical and the magnetic variables, while the lattice vibration effects are only implicitly included through the model parameters, and the thermal expansion is neglected. A relatively short-term perspective is to extend our modelling approach to account for temperature dependent lattice vibration and expansion, as well as their coupling with magnetic and chemical variables. As a first step, this could be achieved via new EIMs parametrized on the temperature dependent data from off-lattice semi-empirical magnetic potentials or Tight Binding models.

References

[1]M. Y. Lavrentiev, R. Soulairol, C.-C. Fu, D. Nguyen-Manh **and** S. L. Dudarev, "Noncollinear magnetism at interfaces in iron-chromium alloys: the ground states and finite-temperature configurations", Phys. Rev. B **84**, 144203 (2011).

[2]A. Schneider, C.-C. Fu, F. Soisson **and** C. Barreteau, "Atomic diffusion in α-iron across the curie point: an efficient and transferable ab initio–based modeling approach", Phys. Rev. Lett. **124**, 215901 (2020).

[3]C. Barouh, T. Schuler, C.-C. Fu **and** M. Nastar, "Interaction between vacancies and interstitial solutes (c, n, and o) in $\alpha-$Fe: from electronic structure to thermodynamics", Phys. Rev. B **90**, 054112 (2014).

[4]J. Soler, E Artacho, J. Gale, A Garcia, J Junquera, P Ordejón **and** D Sanchez-Portal, J. Phase Equilibria **14**, 2745 (2002).

[5]J. Marian, B. D. Wirth, A. Caro, B. Sadigh, G. R. Odette, J. M. Perlado **and** T. Diaz de la Rubia, "Dynamics of self-interstitial cluster migration in pure α-fe and fe-cu alloys", Phys. Rev. B **65**, 144102 (2002).

[6]C. Domain **and** C. S. Becquart, "Ab initio calculations of defects in fe and dilute fe-cu alloys", Phys. Rev. B **65**, 024103 (2001).

[7]S. Takaki, J. Fuss, H. Kuglers, U. Dedek **and** H. Schultz, "The resistivity recovery of high purity and carbon doped iron following low temperature electron irradiation", Radiation Effects **79**, 87–122 (1983).

[8]R. A. Johnson, "Interstitials and vacancies in α iron", Phys. Rev. **134**, A1329–A1336 (1964).

[9]D. Nguyen-Manh, A. P. Horsfield **and** S. L. Dudarev, "Self-interstitial atom defects in bcc transition metals: group-specific trends", Phys. Rev. B **73**, 020101 (2006).

[10]C.-C. Fu, F. Willaime **and** P. Ordejón, "Stability and mobility of mono- and di-interstitials in α-fe", Phys. Rev. Lett. **92**, 175503 (2004).

[11]R Soulairol, C.-C. Fu **and** C Barreteau, "Structure and magnetism of bulk fe and cr: from plane waves to LCAO methods", Journal of Physics: Condensed Matter **22**, 295502 (2010).

[12]F. Willaime, C. Fu, M. Marinica **and** J. Dalla Torre, "Stability and mobility of self-interstitials and small interstitial clusters in -iron: ab initio and empirical potential calculations", Nuclear Instruments and Methods in Physics Research Section B: Beam Interactions with Materials and Atoms **228**, 92–99 (2005).

[13]D. A. Terentyev, T. P. C. Klaver, P. Olsson, M.-C. Marinica, F. Willaime, C. Domain **and** L. Malerba, "Self-trapped interstitial-type defects in iron", Phys. Rev. Lett. **100**, 145503 (2008).

[14]C.-C. Fu, J. D. Torre, F. Willaime, J. L. Bocquet **and** A. Barbu, "Multiscale modelling of defect kinetics in irradiated iron], url = https://doi.org/10.1038/nmat1286", Nature Mater. **4**, 68 (2005).

[15]Y. Abe, Y. Satoh **and** N. Hashimoto, "Vacancy migration in α-iron investigated using in situ high-voltage electron microscopy", Philosophical Magazine, 1–21 (2022).

[16]T Jourdan, C. C. Fu, L Joly, J. L. Bocquet, M. J. Caturla **and** F Willaime, "Direct simulation of resistivity recovery experiments in carbon-doped -iron", Physica Scripta **2011**, 014049 (2011).

[17]H. Blythe, H. Kronmüller, A. Seeger **and** F. Walz, "A review of the magnetic relaxation and its application to the study of atomic defects in -iron and its diluted alloys", physica status solidi (a) **181**, 233–345 (2000).

[18]A. Theodorou, M.-A. Syskaki, Z. Kotsina, M. Axiotis, G. Apostolopoulos **and** C.-C. Fu, "Interactions between irradiation defects and nitrogen in -fe: an integrated experimental and theoretical study", Acta Materialia **239**, 118227 (2022).

[19]A. L. Nikolaev **and** T. E. Kurennykh, "On the interaction between radiation-induced defects and foreign interstitial atoms in -iron", Journal of Nuclear Materials **414**, 374–381 (2011).

[20]C. C. Fu, E. Meslin, A. Barbu, F. Willaime **and** V. Oison, "Effect of c on vacancy migration in α-iron", **in**Theory, modeling and numerical simulation Vol. 139, Solid State Phenomena (**september** 2008), **pages** 157–164.

[21]T. Schuler, C. Barouh, M. Nastar **and** C.-C. Fu, "Equilibrium vacancy concentration driven by undetectable impurities", Phys. Rev. Lett. **115**, 015501 (2015).

[22]C. Barouh, T. Schuler, C.-C. Fu **and** T. Jourdan, "Predicting vacancy-mediated diffusion of interstitial solutes in α-fe", Phys. Rev. B **92**, 104102 (2015).

[23]E. Hayward **and** C.-C. Fu, "Interplay between hydrogen and vacancies in α-fe", Phys. Rev. B **87**, 174103 (2013).

[24]A. D. Leclaire **and** A. B. Lidiard, "LIII. Correlation effects in diffusion in crystals", Philos. Mag. **1**, 518–527 (1956).

[25]A. D. Le Claire, "Correlation effects in diffusion in solids", **in***Physical chemistry: an advance treatise* Vol. 10 (Academic Press (New York), 1970) Chap. 5.

[26]A. D. Le Claire, "Solute diffusion in dilute alloys", Journal of Nuclear Materials **69-96**, 70 (1978).

[27]Y. Adda **and** J. Philibert, *La diffusion dans les solides* (Institut national des sciences et techniques nucléaires, 1966).

[28]H. Mehrer, *Diffusion in solids* (Springer Berlin, Heidelberg, 2007).

[29]F. Soisson **and** C.-C. Fu, "Cu-precipitation kinetics in $\alpha-$Fe from atomistic simulations: vacancy-trapping effects and cu-cluster mobility", Phys. Rev. B **76**, 214102 (2007).

[30]H. Amara, C. C. Fu, F. Soisson **and** P. Maugis, "Aluminum and vacancies in α-iron: dissolution, diffusion, and clustering", Phys. Rev. B **81**, 174101 (2010).

[31]E. Martínez, O. Senninger, C.-C. Fu **and** F. Soisson, "Decomposition kinetics of fe-cr solid solutions during thermal aging", Phys. Rev. B **86**, 224109 (2012).

[32]O. Senninger, F. Soisson, E. Martínez, M. Nastar, C.-C. Fu **and** Y. Bréchet, "Modeling radiation induced segregation in iron–chromium alloys", Acta Materialia **103**, 1–11 (2016).

[33]O. Hegde, V. Kulitckii, A. Schneider, F. Soisson, T. Hickel, J. Neugebauer, G. Wilde, S. Divinski **and** C.-C. Fu, "Impact of magnetic transition on mn diffusion in α-iron: correlative state-of-the-art theoretical and experimental study", Phys. Rev. B **104**, 184107 (2021).

[34]O. Senninger, E. Martínez, F. Soisson, M. Nastar **and** Y. Bréchet, "Atomistic simulations of the decomposition kinetics in fe–cr alloys: influence of magnetism", Acta Materialia **73**, 97–106 (2014).

[35]D. J. Hepburn, D. Ferguson, S. Gardner **and** G. J. Ackland, "First-principles study of helium, carbon, and nitrogen in austenite, dilute austenitic iron alloys, and nickel", Phys. Rev. B **88**, 024115 (2013).

[36]A. Claisse **and** P. Olsson, "First-principles calculations of (y, ti, o) cluster formation in body centred cubic iron-chromium", Nuclear Instruments and Methods in Physics Research Section B: Beam Interactions with Materials and Atoms **303**, QC 20131203, 18–22 (2013).

[37]J.-L. Bocquet, C. Barouh **and** C.-C. Fu, "Migration mechanism for oversized solutes in cubic lattices: the case of yttrium in iron", Phys. Rev. B **95**, 214108 (2017).

[38]C.-C. Fu **and** F. Willaime, "Ab initio study of helium in $\alpha-$Fe: dissolution, migration, and clustering with vacancies", Phys. Rev. B **72**, 064117 (2005).

[39]C. Hin, B. D. Wirth **and** J. B. Neaton, "Formation of Y_2O_3 nanoclusters in nanostructured ferritic alloys during isothermal and anisothermal heat treatment: a kinetic monte carlo study", Phys. Rev. B **80**, 134118 (2009).

[40]E. Meslin, C.-C. Fu, A. Barbu, F. Gao **and** F. Willaime, "Theoretical study of atomic transport via interstitials in dilute Fe−P alloys", Phys. Rev. B **75**, 094303 (2007).

[41]T. Seletskaia, Y. Osetsky, R. E. Stoller **and** G. M. Stocks, Phys. Rev. Lett. **94**, 046403 (2005).

[42]C.-C. Fu **and** F. Willaime, "Interaction between helium and self-defects in -iron from first principles", Journal of Nuclear Materials **367-370**, 244–250 (2007).

[43]N. Juslin **and** K. Nordlund, "Pair potential for fe–he", Journal of Nuclear Materials **382**, Microstructural Processes in Irradiated Materials, 143–146 (2008).

[44]R. Vassen, H. Trinkaus **and** P. Jung, Phys. Rev. B **44**, 4206 (1991).

[45]H Trinkaus **and** B. Singh, "Helium accumulation in metals during irradiation – where do we stand?", Journal of Nuclear Materials **323**, Proceedings of the Second IEA Fusion Materials Agreement Workshop on Modeling and Experimental Validation, 229–242 (2003).

[46]C. J. Ortiz, M. J. Caturla, C. C. Fu **and** F. Willaime, "Influence of carbon on the kinetics of he migration and clustering in α-Fe from first principles", Phys. Rev. B **80**, 134109 (2009).

[47]C. C. Fu **and** F. Willaime, "First principles calculations in iron: structure and mobility of defect clusters and defect complexes for kinetic modelling", Comptes Rendus Physique **9**, 335–342 (2008).

[48]E. Hayward, R. Hayward **and** C.-C. Fu, "Predicting distinct regimes of hydrogen behavior at nano-cavities in metals", Journal of Nuclear Materials **476**, 36–44 (2016).

[49]Y. Hayashi **and** W. Shu, "Iron (ruthenium and osmium)-hydrogen systems", **in**Hydrogen in metal systems ii Vol. 73, Solid State Phenomena (**august** 2000), **pages** 65–114.

[50]L. Zhang, C.-C. Fu **and** G.-H. Lu, "Energetic landscape and diffusion of he in α-fe grain boundaries from first principles", Phys. Rev. B **87**, 134107 (2013).

[51]L. Zhang, C.-C. Fu, E. Hayward **and** G.-H. Lu, "Properties of he clustering in -fe grain boundaries", Journal of Nuclear Materials **459**, 247–258 (2015).

[52]J. R. Rice **and** J.-S. Wang, "Embrittlement of interfaces by solute segregation", Materials Science and Engineering: A **107**, Poceedings of the Symposium on Interfacial Phenomena in Composites: Processing Characterization and Mechanical Properties, 23–40 (1989).

[53]P. Jung, J. Henry, J. Chen **and** J.-C. Brachet, "Effect of implanted helium on tensile properties and hardness of 9% cr martensitic stainless steels", Journal of Nuclear Materials **318**, Fifth International Workshop on Spallation Materials Technology, 241–248 (2003).

[54]K. Miyahara, Y. Sakamoto, S. Hamada, H. Kayano **and** Y. Hosoi, "Microstructure and mechanical properties of alpha-particle irradiated cr-mn and the other stainless steels", Journal of Nuclear Materials **179-181**, 652–655 (1991).

[55]J Henry, M.-H Mathon **and** P Jung, "Microstructural analysis of 9containing 0.5 at.% helium", Journal of Nuclear Materials **318**, Fifth International Workshop on Spallation Materials Technology, 249–259 (2003).

[56]G. Kresse **and** J. Hafner, "Ab initio molecular dynamics for liquid metals", Phys. Rev. B **47**, 558–561 (1993).

[57]G. Kresse **and** J. Furthmüller, "Efficient iterative schemes for ab initio total-energy calculations using a plane-wave basis set", Phys. Rev. B **54**, 11169–11186 (1996).

[58]G. Kresse **and** J. Furthmüller, "Efficiency of ab-initio total energy calculations for metals and semiconductors using a plane-wave basis set", Comput. Mater. Sci. **6**, 15–50 (1996).

[59]P. Giannozzi, S. Baroni, N. Bonini, M. Calandra, R. Car, C. Cavazzoni, D. Ceresoli, G. L. Chiarotti, M. Cococcioni, I. Dabo, A. Dal Corso, S. de Gironcoli, S. Fabris, G. Fratesi, R. Gebauer, U. Gerstmann, C. Gougoussis, A. Kokalj, M. Lazzeri, L. Martin-Samos, N. Marzari, F. Mauri, R. Mazzarello, S. Paolini, A. Pasquarello, L. Paulatto, C. Sbraccia, S. Scandolo, G. Sclauzero, A. P. Seitsonen, A. Smogunov, P. Umari **and** R. M. Wentzcovitch, "Quantum espresso: a modular and open-source software project for quantum simulations of materials", Journal of Physics: Condensed Matter **21**, 395502 (19pp) (2009).

[60]I. Abrikosov, A. Ponomareva, P. Steneteg, S. Barannikova **and** B. Alling, "Recent progress in simulations of the paramagnetic state of magnetic materials", Curr. Opin. Solid State Mater. Sci. **20**, 85–106 (2016).

[61]S. V. Okatov, A. R. Kuznetsov, Y. N. Gornostyrev, V. N. Urtsev **and** M. I. Katsnelson, "Effect of magnetic state on the γ-α transition in iron: First-principles calculations of the Bain transformation path", Phys. Rev. B **79**, 094111 (2009).

[62]P. Olsson, I. A. Abrikosov, L. Vitos **and** J. Wallenius, "Ab initio formation energies of fe–cr alloys", J. Nucl. Mater. **321**, 84–90 (2003).

[63]L. Delczeg, B. Johansson **and** L. Vitos, "Ab initio description of monovacancies in paramagnetic austenitic Fe-Cr-Ni alloys", Phys. Rev. B **85**, 174101 (2012).

[64]V. I. Razumovskiy, A. Reyes-Huamantinco, P. Puschnig **and** A. V. Ruban, "Effect of thermal lattice expansion on the stacking fault energies of fcc Fe and Fe75Mn25 alloy", Phys. Rev. B **93**, 054111 (2016).

[65]D. Gambino **and** B. Alling, "Lattice relaxations in disordered fe-based materials in the paramagnetic state from first principles", Physical Review B **98**, 064105 (2018).

[66] A. V. Ruban **and** V. I. Razumovskiy, "Spin-wave method for the total energy of paramagnetic state", Phys. Rev. B **85**, 174407 (2012).

[67] H. Wen, P.-W. Ma **and** C. Woo, "Spin-lattice dynamics study of vacancy formation and migration in ferromagnetic BCC iron", J. Nucl. Mater. **440**, 428–434 (2013).

[68] H. Wen **and** C. Woo, "Self diffusion anomaly in ferromagnetic metals: a density-functional-theory investigation of magnetically ordered and disordered fe and co", J. Nucl. Mater. **470**, 102 (2016).

[69] P.-W. Ma **and** S. L. Dudarev, "Longitudinal magnetic fluctuations in Langevin spin dynamics", Phys. Rev. B **86**, 054416 (2012).

[70] P.-W. Ma **and** S. L. Dudarev, "Atomistic Spin-Lattice Dynamics", **in***Handb. mater. model.* (Springer International Publishing, Cham, 2020), **pages** 1017–1035.

[71] M. Y. Lavrentiev, J. S. Wróbel, D. Nguyen-Manh **and** S. L. Dudarev, "Magnetic and thermodynamic properties of face-centered cubic Fe–Ni alloys", Phys. Chem. Chem. Phys. **16**, 16049 (2014).

[72] M. Y. Lavrentiev, J. S. Wróbel, D. Nguyen-Manh, S. L. Dudarev **and** M. G. Ganchenkova, "Magnetic cluster expansion model for random and ordered magnetic face-centered cubic Fe-Ni-Cr alloys", J. Appl. Phys. **120**, 043902 (2016).

[73] V.-T. Tran, C.-C. Fu **and** A. Schneider, "Effective interaction model for coupled magnetism and phase stability in bcc fe-co systems", Computational Materials Science **183**, 109906 (2020).

[74] M. Trochet, F. Soisson, C.-C. Fu **and** M. Lavrentiev, "Influence of magnetic excitation and vibrational entropy on the phase diagram of $Fe_{1-x}Cr_x$ alloys", Computational Materials Science **199**, 110698 (2021).

[75] A. Schneider, C.-C. Fu, O. Waseda, C. Barreteau **and** T. Hickel, "Ab initio based models for temperature-dependent magnetochemical interplay in bcc fe-mn alloys", Phys. Rev. B **103**, 024421 (2021).

[76] K. Li, C.-C. Fu, M. Nastar, F. Soisson **and** M. Y. Lavrentiev, "Magnetochemical effects on phase stability and vacancy formation in fcc fe-ni alloys", Phys. Rev. B **106**, 024106 (2022).

[77] S. Huang, D. L. Worthington, M. Asta, V. Ozolins, G. Gosh **and** P. K. Liaw, Acta Mater. **58**, 1982 (2010).

[78] H. Ding, V. I. Razumovskiy **and** M. Asta, Acta Mater. **70**, 130 (2014).

[79] N. Sandberg, Z. Chang, L. Messina, P. Olsson **and** P. Korzhavyi, Phys. Rev. B **92**, 184102 (2015).

[80] O. Hegde, M. Grabowski, X. Zhang, O. Waseda, T. Hickel, C. Freysoldt **and** J. Neugebauer, "Atomic relaxation around defects in magnetically disordered materials computed by atomic spin constraints within an efficient lagrange formalism", Physical Review B **102**, 144101 (2020).

[81]L Ruch, D. Sain, H. Yeh **and** L. Girifalco, "Analysis of Diffusion in Ferromagnets", Journal of Physics and Chemistry of Solids **37**, 649–653 (1976).

[82]H. Guan, S. Huang, J. Ding, F. Tian, Q. Xu **and** J. Zhao, "Chemical environment and magnetic moment effects on point defect formations in CoCrNi-based concentrated solid-solution alloys", Acta Mater. **187**, 122–134 (2020).

[83]X. Zhang **and** M. H. F. Sluiter, "Ab initio prediction of vacancy properties in concentrated alloys: The case of fcc Cu-Ni", Phys. Rev. B **91**, 174107 (2015).

[84]C. Li, J. Yin, K. Odbadrakh, B. C. Sales, S. J. Zinkle, G. M. Stocks **and** B. D. Wirth, "First principle study of magnetism and vacancy energetics in a near equimolar NiFeMnCr high entropy alloy", J. Appl. Phys. **125**, 155103 (2019).

[85]J. B. Piochaud, T. P. C. Klaver, G. Adjanor, P. Olsson, C. Domain **and** C. S. Becquart, "First-principles study of point defects in an fcc Fe-10Ni-20Cr model alloy", Phys. Rev. B **89**, 024101 (2014).

[86]J. Wróbel, D. Nguyen-Manh, S. Dudarev **and** K. Kurzydłowski, "Point defect properties of ternary fcc Fe-Cr-Ni alloys", Nucl. Instruments Methods Phys. Res. Sect. B Beam Interact. with Mater. Atoms **393**, 126–129 (2017).

[87]A. Manzoor, Y. Zhang **and** D. S. Aidhy, "Factors affecting the vacancy formation energy in Fe70Ni10Cr20 random concentrated alloy", Comput. Mater. Sci. **198**, 110669 (2021).

[88]S. Zhao, G. M. Stocks **and** Y. Zhang, "Defect energetics of concentrated solid-solution alloys from ab initio calculations: Ni0.5Co0.5, Ni0.5Fe0.5, Ni0.8Fe0.2 and Ni0.8Cr0.2", Phys. Chem. Chem. Phys. **18**, 24043–24056 (2016).

[89]J. Mayer, C. Elsässer **and** M. Fähnle, "Concentrations of Atomic Defects in B2-FexAl1x. An Ab-Initio Study", Phys. Status Solidi **191**, 283–298 (1995).

[90]M. Hagen **and** M. Finnis, "Point defects and chemical potentials in ordered alloys", Philos. Mag. A Phys. Condens. Matter, Struct. Defects Mech. Prop. **77**, 447–464 (1998).

[91]Y. Mishin **and** C. Herzig, "Diffusion in the Ti–Al system", Acta Mater. **48**, 589–623 (2000).

[92]C. Woodward, M. Asta, G. Kresse **and** J. Hafner, "Density of constitutional and thermal point defects in L12 Al3Sc", Phys. Rev. B **63**, 094103 (2001).

[93]M. de Koning, C. R. Miranda **and** A. Antonelli, "Atomistic prediction of equilibrium vacancy concentrations in Ni3Al", Phys. Rev. B **66**, 104110 (2002).

[94]J. Rogal, S. V. Divinski, M. W. Finnis, A. Glensk, J. Neugebauer, J. H. Perepezko, S. Schuwalow, M. H. F. Sluiter **and** B. Sundman, "Perspectives on point defect thermodynamics", Phys. status solidi **251**, 97–129 (2014).

[95]A. V. Ruban **and** M. Dehghani, "Atomic configuration and properties of austenitic steels at finite temperature: Effect of longitudinal spin fluctuations", Phys. Rev. B **94**, 104111 (2016).

[96]D. Morgan **and** Y. Zhang, "Comment on "Thermal vacancies in random alloys in the single-site mean-field approximation"", Phys. Rev. B **101**, 136101 (2020).

[97]Y. Zhang, A. Manzoor, C. Jiang, D. Aidhy **and** D. Schwen, "A statistical approach for atomistic calculations of vacancy formation energy and chemical potentials in concentrated solid-solution alloys", Comput. Mater. Sci. **190**, 110308 (2021).

[98]V. Kulitckii, A. Schneider, O. Lukianova, G. Wilge, C.-C. Fu **and** S. Divinski, "Atomic diffusion in bcc Fe–Mn alloys: Theoretical analysis and experimental measurements across the Curie temperature ", Acta Materialia **251**, 118883 (2023).

[99]R. Drautz **and** M. Fähnle, "Spin-cluster expansion: parametrization of the general adiabatic magnetic energy surface with ab initio accuracy", Phys. Rev. B **69**, 104404 (2004).

[100]R. Drautz **and** M. Fähnle, "Parametrization of the magnetic energy at the atomic level", Phys. Rev. B **72**, 212405 (2005).

[101]V. Pierron-Bohnes, P. Cadeville **and** F. Gauthier, J. Phys. F: Met. Phys. **82**, 184430 (1983).

[102]M. Y. Lavrentiev, D. Nguyen-Manh **and** S. L. Dudarev, Phys. Rev. B **81**, 184202 (2010).

[103]J. B. J Chapman, P.-. W. Ma **and** S. L. Dudarev, Phys. Rev. B **99**, 184413 (2019).

[104]M. Levesque, E. Martínez, C.-C. Fu, M. Nastar **and** F. Soisson, "Simple concentration-dependent pair interaction model for large-scale simulations of fe-cr alloys", Phys. Rev. B **84**, 184205 (2011).

[105]Y. Wang, K. Li, F. Soisson **and** C. S. Becquart, "Combining DFT and CALPHAD for the development of on-lattice interaction models: The case of Fe-Ni system", Phys. Rev. Mater. **4**, 113801 (2020).

[106]A. V. Ruban, S. Khmelevskyi, P. Mohn **and** B. Johansson, "Temperature-induced longitudinal spin fluctuations in fe and ni", Phys. Rev. B **75**, 054402 (2007).

[107]L. Bergqvist **and** A. Bergman, "Realistic finite temperature simulations of magnetic systems using quantum statistics", Phys. Rev. Mater. **2**, 013802 (2018).

[108]K. Li, C.-C. Fu, M. Nastar **and** F. Soisson, "Predicting atomic diffusion in concentrated magnetic alloys: The case of paramagnetic Fe–Ni", Phys. Rev. B **107**, 094103 (2023).

[109]B. Widom, "Some Topics in the Theory of Fluids", J. Chem. Phys. **39**, 2808–2812 (1963).

[110]A. Einstein, Adv. Phys. **17**, 549 (1905).

[111]A. Einstein, Adv. Phys. **19**, 371 (1906).

[112]M. Von Smoluchowski, Adv. Phys. **21**, 756 (1906).

[113]R Soulairol, C.-C. Fu **and** C Barreteau, "Magnetic and energetic properties of low-index cr surfaces and fe/cr interfaces: a first-principles study", Phys. Rev. B **84**, 155402 (2011).

[114]C.-C. Fu, M. Y. Lavrentiev, R. Soulairol, S. L. Dudarev **and** D. Nguyen-Manh, "Low- and high-temperature magnetism of cr and fe nanoclusters in iron-chromium alloys", Phys. Rev. B **91**, 094430 (2015).

[115]M. Lavrentiev, S. Dudarev **and** D. Nguyen-Manh, "Magnetic cluster expansion simulations of fecr alloys", Journal of Nuclear Materials **386-388**, Fusion Reactor Materials, 22–25 (2009).

[116]H Fritzsche, J Hauschild, A Hoser, S Bonn **and** J Klenke, Europhys. Lett. **49**, 507–513 (2000).

[117]H Fritzsche, S Bonn, J Hauschild, J Klenke, K Prokes **and** G. McIntyre, Phys. Rev. B **65**, 144408 (2002).

[118]R Soulairol, C.-C. Fu **and** C Barreteau, "Structure and magnetism of bulk fe and cr: from plane waves to lcao methods", J. Phys.: Condens. Matter **22**, 295502 (2010).

[119]P. Olsson, T. P. C. Klaver **and** C. Domain, Phys. Rev. B **81**, 054102 (2010).

[120]V. I. Anisimov, V. P. Antropov, A. I. Liechtenstein, V. A. Gubanov **and** A. V. Postnikov, Phys. Rev. B **37**, 5598 (1988).

[121]A. Schneider, C.-C. Fu **and** C. Barreteau, "Local environment dependence of mn magnetism in bcc iron-manganese alloys: a first-principles study", Phys. Rev. B **98**, 094426 (2018).

[122]A. V. Ruban **and** V. I. Razumovskiy, "First-principles based thermodynamic model of phase equilibria in bcc fe-cr alloys", Phys. Rev. B **86**, 174111 (2012).

[123]T. P. C. Klaver, R. Drautz **and** M. W. Finnis, "Magnetism and thermodynamics of defect-free fe-cr alloys", Phys. Rev. B **74**, 094435 (2006).

[124]S. Lintzen, J. von Appen, B. Hallstedt **and** R. Dronskowski, "The fe–mn enthalpy phase diagram from first principles", Journal of Alloys and Compounds **577**, 370–375 (2013).

[125]A. Diaz-Ortiz, R. Drautz, M. Fähnle **and** H. Dosch, "First-principles study of the interplay between magnetism and phase equilibria in fe–co alloys", Journal of Magnetism and Magnetic Materials **272-276**, Proceedings of the International Conference on Magnetism (ICM 2003), 780–782 (2004).

[126]A. Díaz-Ortiz, R. Drautz, M. Fähnle, H. Dosch **and** J. M. Sanchez, "Structure and magnetism in bcc-based iron-cobalt alloys", Phys. Rev. B **73**, 224208 (2006).

[127]J. Wang, X.-G. Lu, N. Zhu **and** W. Zheng, "Thermodynamic and diffusion kinetic studies of the fe-co system", Calphad **58**, 82–100 (2017).

[128]A. Zunger, S.-. H. Wei, L. G. Ferreira **and** J. E. Bernard, "Special quasirandom structures", Phys. Rev. Lett. **65**, 353 (1990).

[129]A. T. Paxton **and** M. W. Finnis, "Magnetic tight binding and the iron-chromium enthalpy anomaly", Phys. Rev. B **77**, 024428 (2008).

[130]H. Yamauchi, H. Watanabe, Y. Suzuki **and** H. Saito, J. Phys. Soc. Jpn. **36**, 971 (1974).

[131]V.-T. Tran, C.-C. Fu **and** K. Li, "Predicting magnetization of ferromagnetic binary fe alloys from chemical short range order", Computational Materials Science **172**, 109344 (2020).

[132]W. Xiong, P. Hedström, M. Selleby, J. Odqvist, M. Thuvander **and** Q. Chen, "An improved thermodynamic modeling of the fe–cr system down to zero kelvin coupled with key experiments", Calphad **35**, 355–366 (2011).

[133]P. A. Korzhavyi, A. V. Ruban, J. Odqvist, J.-O. Nilsson **and** B. Johansson, "Electronic structure and effective chemical and magnetic exchange interactions in bcc fe-cr alloys", Phys. Rev. B **79**, 054202 (2009).

[134]S. Bigdeli **and** M. Selleby, Calphad **64**, 185 (2019).

[135]C. Paduani, E. Galvao da Silva, G. A. Perez-Alcazar **and** M. McElfresh, J. Appl. Phys. **70**, 7524 (1991).

[136]S. Arajs, Phys. Stat. Sol. **11**, 121 (1965).

[137]C. Li, F. Sommer **and** E. J. Mittemeijer, Mater. Sci. Engin. **A325**, 307 (2002).

[138]C. Sadron, Ann. Phys. Paris **17**, 371 (1932).

[139]V. A. Shabashov, K. A. Kozlov, V. V. Sagaradze, A. L. Nikolaev, K. A. Lyashkov, V. A. Semyonkin **and** V. I. Voronin, "Short-range order clustering in bcc fe–mn alloys induced by severe plastic deformation", Phil. Mag. **98**, 560–576 (2018).

[140]I. Jacobs, H. Patchen **and** N. Johnson, "Raising the curie point in the iron-cobalt- (aluminum) system", J. Appl. Phys. **69**, 5924 (1991).

[141]M. Hansen, *Constitution of binary alloys* (McGraw-Hill New York, 1958).

[142]R. Forrer, J. Phys. le Radium **1**, 49 (1930).

[143]T. Massalski **and** H. Kamoto, *Binary alloy phase diagrams* (ASM International, 1900).

[144]K. Li **and** C.-C. Fu, "Ground-state properties and lattice-vibration effects of disordered Fe-Ni systems for phase stability predictions", Phys. Rev. Mater. **4**, 023606 (2020).

[145]I. Ohnuma, S. Shimenouchi, T. Omori, K. Ishida **and** R. Kainuma, "Experimental determination and thermodynamic evaluation of low-temperature phase equilibria in the Fe–Ni binary system", Calphad Comput. Coupling Phase Diagrams Thermochem. **67**, 101677 (2019).

[146]M. Peschard, "Contribution à l'étude des Ferro-nickels", Rev. Métallurgie **22**, 490–514 (1925).

[147]J. Crangle **and** G. C. Hallam, "The Magnetization of Face-Centred Cubic and Body-Centred Cubic Iron + Nickel Alloys", Proc. R. Soc. A Math. Phys. Eng. Sci. **272**, 119–132 (1963).

[148]H. Asano, "Magnetism of γ Fe-Ni Invar Alloys with Low Nickel Concentration", J. Phys. Soc. Japan **27**, 542–553 (1969).

[149]S. Komura, T. Takeda **and** Y. Endoh, "Evidence for the correlation of the magnetic inhomogeneous structure with the fluctuation of chemical composition in Fe-Ni Invar alloys", J. Magn. Magn. Mater. **50**, 69–73 (1985).

[150]T. Takeda, S. Komura, T. Miyazaki, Y. Endoh **and** S. Itoh, "Small-angle scattering of polarized neutrons from an Fe65Ni35 Invar alloy", J. Magn. Magn. Mater. **70**, 431–433 (1987).

[151]J. Paulevé, D. Dautreppe, J. Laugier **and** L. Néel, "Une nouvelle transition ordre-désordre dans Fe-Ni (50-50)", J. Phys. le Radium **23**, 841–843 (1962).

[152]T. G. Kollie **and** C. R. Brooks, "The heat capacity of Ni3Fe: experimental data from 300 to 1670 K", Phys. Status Solidi **19**, 545–554 (1973).

[153]J. W. Drijver, F. Van Der Woude **and** S Radelaar, "Order-disorder transition in Ni3 Fe studied by Mössbauer spectroscopy", Phys. Rev. Lett. **34**, 1026–1029 (1975).

[154]J. Van deen **and** F. Van Der Woude, "Phase diagram of the order-disorder transition in Ni3Fe", Acta Metall. **29**, 1255–1262 (1981).

[155]K. Li, C.-C. Fu **and** A. Schneider, "Effects of magnetic excitations and transitions on vacancy formation: cases of fcc fe and ni compared to bcc fe", Phys. Rev. B **104**, 104406 (2021).

[156]L. De Schepper, D. Segers, L. Dorikens-Vanpraet, M. Dorikens, G. Knuyt, L. M. Stals **and** P. Moser, "Positron annihilation on pure and carbon-doped α-iron in thermal equilibrium", Phys. Rev. B **27**, 5257–5269 (1983).

[157]O. I. Gorbatov, A. Hosseinzadeh Delandar, Y. N. Gornostyrev, A. V. Ruban **and** P. A. Korzhavyi, J. Nucl. Mater. **475**, 140 (2016).

[158]H.-E. Schaefer, K. Maier, M. Weller, D. Herlach, A. Seeger **and** J. Diehl, "Vacancy formation in iron investigated by positron annihilation in thermal equilibrium", Scr. Metall. **11**, 803–809 (1977).

[159]C. W. Schulte, J. L. Campbell **and** J. A. Jackman, "Temperature dependence of positron annihilation in iron and vanadium", Appl. Phys. **16**, 29–34 (1978).

[160]S. M. Kim **and** W. J. Buyers, "Vacancy formation energy in iron by positron annihilation", J. Phys. F Met. Phys. **8**, L103–L108 (1978).

[161]H. Matter, J. Winter **and** W. Triftshäuser, "Phase Tansformations and Vacancy Formation Energies of Transition Metals by Positron Annihilation", Appl. Phys. **20**, 135–140 (1979).

[162]W. Wycisk **and** M. Feller-Kniepmeier, "Quenching experiments in high purity Ni", J. Nucl. Mater. **69-70**, 616–619 (1978).

[163]L. C. Smedskjaer, M. J. Fluss, D. G. Legnini, M. K. Chason **and** R. W. Siegel, "The vacancy formation enthalpy in Ni determined by positron annihilation", J. Phys. F Met. Phys. **11**, 2221–2230 (1981).

[164]J. Wolff, M. Franz, J. E. Kluin **and** D. Schmid, "Vacancy formation in nickel and α-nickel-carbon alloy", Acta Mater. **45**, 4759–4764 (1997).

[165]H.-P. Scholz, "Messungen der absoluten leerstellenkonzentration in nickel und geordneten intermetallischen nickel-legierungen mit einem differentialdilatometer (Measurements of the absolute vacancy concentration in nickel and ordered intermetallic nickel alloys with a differential dilatometer)", phdthesis (University of Göttingen, 2001).

[166]T. Troev, C. Angelov **and** I. Mincov, "Positron annihilation measurements of quenched-in defects in Ni", Phys. Lett. A **138**, 65–68 (1989).

[167]W. Chambron **and** A. Caplain, "Etude des lacunes en tres faible concentration dans l'alliage fer-nickel a 70% de nickel par la methode de l'anisotropie magnetique", Acta Metall. **22**, 357–366 (1974).

[168]A. Caplain **and** W. Chambron, "Energies de formation et de migration des lacunes dans les alliages fer-nickel de structure C.F.C. par la methode de l'anisotropie magnetique induite", Acta Metall. **25**, 1001–1011 (1977).

[169]L. Girifalco, "Vacancy Concentration + Diffusion in Order-disorder Alloys", Journal of Physics and Chemistry of Solids **25**, 323–& (1964).

[170]D. Graham **and** D. H. Tomlin, "Self-diffusion in iron", Philos. Mag. **8**, 1581 (1963).

[171]C. M. Walter **and** N. L. Peterson, "Isotope effect in self-diffusion in iron", Phys. Rev. **178**, 922–929 (1969).

[172]F. Buffington, K Hirano **and** M Cohen, "Self Diffusion in Iron", Acta Metallurgica **9**, 434–439 (1961).

[173]D. W. James **and** G. M. Leak, "Self-diffusion and diffusion of cobalt in alpha and delta-iron", Philos. Mag. **14**, 701 (1966).

[174]G Hettich, H Mehrer **and** K Maier, "Self-diffusion In Ferromagnetic Alpha-iron", Scripta Metallurgica **11**, 795–802 (1977).

[175]J. Geise **and** C Herzig, "Impurity diffusion of vanadium and self-diffusion in iron", Z. Metallkde. **78**, 291 (1987).

[176]Y. Iijima, K. Kimura **and** K. Hirano, "Self-diffusion and isotope effect in alpha-iron", Acta Metall. **36**, 2811–2820 (1988).

[177]M. Luebbehusen **and** H. Mehrer, "Self-diffusion in -iron: the influence of dislocations and the effect of the magnetic phase transition", Acta Metall. Mater. **36**, 2811 (1988).

[178]G. R. Speich, J. A. Gula **and** R. M. Fisher, *The electron microprobe* (Wiley, New York, 1966).

[179]S. J. Rothman, N. L. Peterson, C. M. Walter **and** L. J. Nowicki, "The diffusion of copper in iron", Journal of Applied Physics **39**, 5041–5044 (1968).

[180]V. A. Lazarev **and** V. M. Golikov, Fiz. Metal. Metalloved **29**, 598 (1970).

[181]G Salje **and** M Fellerkniepmeier, "Diffusion and Solubility of Copper in Iron", Journal of Applied Physics **48**, 1833–1839 (1977).

[182]C. H. Woo, H. Wen, A. A. Semenov, S. L. Dudarev **and** P.-W. Ma, "Quantum heat bath for spin-lattice dynamics", Phys. Rev. B **91**, 104306 (2015).

[183]M Lübbenhusen **and** H Mehrer, "Self-diffusion in Alpha-iron - The Influence of Dislocations and the Effect of the Magnetic Phase-transition", Acta Metallurgica et Materialia **38**, 283–292 (1990).

[184]J. Kirkaldy, P. Smith **and** R. Sharma, "Diffusion of Manganese in Paramagnetic Bcc Iron", Metallurgical Transactions **4**, 624–625 (1973).

[185]R. Borg **and** C. Birchenall, "Self-diffusion in alpha-iron", Transactions of The American Institute of Mining and Metallurgical Engineers **218**, 980–984 (1960).

[186]L. Messina, M. Nastar, N. Sandberg **and** P. Olsson, "Systematic electronic-structure investigation of substitutional impurity diffusion and flux coupling in bcc iron", Phys. Rev. B **93**, 184302 (2016).

[187]B. Million, J. Růžičková, J. Velíšek **and** J. Vřešťál, "Diffusion processes in the FeNi system", Mater. Sci. Eng. **50**, 43–52 (1981).

[188]J. M. Cowley, "An Approximate Theory of Order in Alloys", Phys. Rev. **77**, 669–675 (1950).

[189]J. M. Cowley, "Short-Range Order and Long-Range Order Parameters", Phys. Rev. **138**, A1384–A1389 (1965).

[190]H. Yamamoto, "A study on the nature of aging of fe-cr alloys by means of the mössbauer effect", Japanese Journal of Applied Physics **3**, 745 (1964).

[191]M. Y. Lavrentiev, C.-C. Fu **and** F. Soisson, "Correlation between microstructure and magnetic properties during phase separation in concentrated fe-cr alloys", Journal of Magnetism and Magnetic Materials **506**, 166763 (2020).

Appendix A

Curriculum Vitae

Personal information:

First name : Chu-Chun
Last name : Fu
Gender: feminine
Nationality: french, argentinian
Personal address : 70, avenue Aristide Briand, 92120 Montrouge, France
Afiliation: Université Paris-Saclay, CEA, Service de recherche en Corrosion et Comportement des Matériaux, SRMP, F-91191 Gif sur Yvette, France
Current position : senior researcher at CEA Saclay, France
E-mail : chuchun.fu@cea.fr
Phone : +33 1 69 08 29 32

Education:

- **Jan.1997-May 2001*** Doctoral thesis in Physics, University of Buenos Aires, Argentina

  Thesis topic: Molecular Dynamics study of the diffusio of Si and the deposit of C on the Si(001) surfaces. (http://hdl.handle.net/20.500.12110/tesis_n3341_Fu)

  Thesis director: Dr. Mariana Weissmann

  **In Argentina, the typical duration of thesis in Physics is 4 – 5 years)*

- **Mar.1988-Dec.1994** Bachelor + Master degree in Physics, University of Buenos Aires, Argentina

Employment

- **Since Jan. 2005** Permanent researcher at SRMP (Section de Recherches de Métallurgie Physique) CEA-Saclay, France

- Nov.2002-Dec.2004 Post-doctoral fellow at SRMP, CEA-Saclay, France
- Jun.2001-Oct.2002 Associate researcher at CINAM, CNRS, Marseille, France

Language:
Excellent in Chinese and Spanish, fluent in English and French

Research topics

During my Ph.D thesis and the first postdoctoral stay at CINAM, my research was devoted to properties of some semiconductor systems such as amorphous silicon-carbide (SiC), Si surfaces, C fullerenes and nanotubes.

After I joined SRMP, my research work concerns properties of defects in transition-metal systems of interest for nuclear-energy industry. The aim is to provide fundamental knowledge of electronic structures and atomic-scale mechanisms at the origin of macroscopic behaviour of the considered materials. The defects considered include the elementary radiation damage (vacancies and self-interstitial atoms), impurities and alloying elements, and extended defects such as surfaces, interfaces and grain boundaries. A strong focus is placed on iron based alloys, with a particular attention on the magneto-chemical correlation.

Methodology:

- First principles methods within the density functional theory (DFT) is the main approach, where new implementations are made in existing codes (Quantum Espresso, Vasp, Siesta) for the studies of our interest (e.g. constrained structural relaxation algorithms for computing energy barriers and features for non-collinear magnetism and constrained local magnetism…). Also, pseudopotentials and localized pseudo-atomic basis sets have been developed for various transition metals.
- Semi-empirical tight binding and effective-interaction models (resp. TB and EIM) are developed using the DFT data, in order to perform simulations with larger systems and at longer time-scales. A specificity of our EIMs is to include both chemical and spin variables, to capture the effects of magneto-chemical interplay on thermodynamic and kinetic properties of magnetic alloys, via spin-atomic Monte Carlo simulations.
- In order to explore complex energetic landscapes for determining *e.g.* optimal diffusion paths, a combination of DFT calculations and empirical-potential molecular dynamics is applied.
- Mesoscopic Rate Theory and Monte Carlo models are parameterized on DFT data, and applied for real-time simulation of various experiments.

Supervision of doctoral and post-doctoral works

Supervision or co-supervision of **11 doctoral students** since 2004
Supervision of **7 postdocs** since 2008
Supervision of **10 master-level and 1 doctoral-level internship fellows** since 2004

Doctoral thesis:

- **Guillaume Verité** : (co-supervision: 30 %)
  Oct. 2004 – Sep. 2007
  Topic: Structure, Stability and Mobility of point defects in hcp Zr : an ab initio study **(2 papers published)**
  Awarded by : Université Pierre et Marie Curie, Ecole doctorale de Physique de la région parisienne
  Co-supervised with François Willaime (SRMP, CEA Saclay)
  Thesis director : Denis Gratias (CNRS)
  Working place : SRMP, CEA Saclay, France

- **Maximilien Levesque**: (co-supervision: 30 %)
  Oct. 2007 – Oct. 2010
  Topic: Unmixing and surface segregation in Fe-Cr alloys : from electronic structures to thermodynamic models **(3 papers published)**
  Awarded by : Université Paris-Sud 11, Orsay, specialité Physique du Solide
  Co-supervised with Frederic Soisson and Maylise Nastar (SRMP, CEA Saclay)
  Thesis director: Michèle Gupta (Univ. Paris XI)
  Working place : SRMP, CEA Saclay, France

- **Romain Soulairol** (supervision : > 95%)
  Sep. 2008 – Sep. 2011
  Topic: Theoretical study of the correlation between magnetism and properties of defects in iron, chromium, and their alloys **(7 papers published)**
  Awarded by : Université Pierre et Marie Curie - Paris VI. Ecole doctorale de physique et chimie des matériaux
  Thesis director : Cyrille Barreteau (CEA Saclay)
  Working place : SRMP, CEA Saclay, France

- **Caroline Barouh** (supervision : > 95 %)
  Oct. 2012 – Oct. 2015
  Topic: Multi-scale modelling of interactions between vacancies and alloying elements in ferritic steels **(4 papers published)**

Awarded by : Université d'Orléans : école doctorale énergie, matériaux, science de la terre et de l'univers
Thesis director: Marie-France Barthe (CNRS-CEMHTI)
Working place : SRMP, CEA Saclay, France

- **Elric Barbé** (co-supervision : 50 %)
  Oct. 2015 – Oct. 2018
  Topic: Multi-scale simulation of the mechanical behavior of metal-carbide interfaces from electronic structures **(1 paper published)**
  Doctoral school: Université Pierre et Marie Curie - Paris VI. Ecole doctorale de sciences mécaniques, acoustiques, électronique, et robotique de Paris.
  Co-supervised with Maxime Sauzay (CEA Saclay)
  Thesis director: Maxime Sauzay (CEA Saclay)
  Working place : SRMP, CEA Saclay, France

- **Anton Schneider** (supervision : > 95 %)
  Oct. 2016 – Oct. 2019
  Topic: Theoretical study of the interplay between magnetism and defects in Fe based alloys **(7 published papers)**
  Doctoral school: Université Pierre et Marie Curie - Paris VI. Ecole doctorale de physique et chimie des matériaux
  Thesis director : Cyrille Barreteau (CEA Saclay)
  Working place : SRMP, CEA Saclay, France

- **Océane Buggenhoudt** (supervision : >85%)
  Oct. 2018 – Oct. 2021
  Topic: Modelling and simulation of carbides in -Fe alloys from first principles: alloying elements, diffusion and nucleation **(1 published paper + 1 to be submitted)**
  Doctoral school: Université Paris Saclay. Ecole doctorale PHENICS
  Thesis director : Jean-Luc Béchade (CEA Saclay)
  Working place : SRMP, CEA Saclay, France

- **Kangming Li** (supervision : >90%)
  Oct. 2018 – Oct. 2021
  Topic: Magnetochemical coupling effects on thermodynamics, point-defect formation and diffusion in Fe-Ni alloys: a theoretical study **(5 published papers + 1 in preparation)**
  Doctoral school: Université Paris Saclay. Ecole doctorale n○ 564: Physique en Île-de-France

Thesis director : Maylise Nastar (CEA Saclay)
Working place : SRMP, CEA Saclay, France

- **Hilal Bozkurt** (supervision : > 90%)
  Jan. 2022 – Jan. 2025
  Topic: Modelling finite-temperature magnetic effects in iron-based alloys
  Doctoral school: Université Paris Saclau. Ecole doctorale d'Onde et Matière,
  Thesis director : Cyrille Barreteau (CEA Saclay)
  Working place : SRMP, CEA Saclay, France

- **Thomas Mainguy** (supervision : > 90%)
  Oct. 2022 – Oct. 2025
  Topic: Modelling the coupling between chemistry, magnetism and defects in austenitic alloys
  Doctoral school: Université Université Paris Saclay. Ecole doctorale n○ 564: Physique en Île-de-France
  Thesis director : Maylise Nastar (CEA Saclay)
  Working place : SRMP, CEA Saclay, France

- **Thomas Mainguy** (supervision : > 85%)
  Apr. 2023 – Apr. 2026
  Topic: Carbides in ferritic steels: thermodynamics, precipitation and impact on mechanical properties.
  Doctoral school: Université Université Paris Saclay. Ecole doctorale n○ 564: Physique en Île-de-France
  Thesis director : Jean-Luc Béchade (CEA Saclay)
  Working place : SRMP, CEA Saclay, France

Post-docs:

- **Hakim Amara** (1 year: 2008-2009)
  Topic: Synergistic effect of C and Al in bcc iron : an *ab initio* study

- **Eduardo Machado (**2 years: 2008-2009)
  Topic: implementation for improvements in the DFT code 'SIESTA for metallic magnetic systems'

- **Enrique Martinez** (1 year : 2008-2009)
  Topic: Cr effects in the behavior of He in iron from ab initio studies

- **Rajaraman Ramalingam** (1 year: 2009)
  Topic: Properties of Y, Ti and O in -iron : simulation and comparison with PAS (positron anihilation spectroscopy) experimental data

- **Tristana Sondon** (1 year : 2010-2011)
  Topic: Implementation of the PAW (projector augmented wave) potential in the DFT-SIESTA code

- **Erin Hayward** (21 months : 2012 – 2014)
  Topic: Synergistic effect of He-H in bcc metals from atomistic studies

- **Van Truong Tran** (24 months 2018 – 2019)
  Topic: Modelling of co-influence between magnetism and defects in binary Fe-Co alloys.

Diverse professional activities and responsibilities

- Over **25 invited talks** since 2005 (e.g. **MRS** Materials Research Society international annual Fall meeting (Boston, USA), **ICCP** (International conference in computational physics), **ICFRM** (International conference on Fusion Reactor Materials**,** ,**DIMAT** (International conference on Diffusion in Materials), **COSIRES** (Computer Simulation of Radiation Effects in Solids) , **TMS**, **THERMEC** etc.)
- **Teaching**
  - **Diffusion school** (Ecole sur la diffusion dans les solides, **1st edition** : Marseille, France, **2015** ; **2nd edition** : online, **2021**)
  - **MATGEN-IV** (international school on Materials on Generation IV Nuclear systems (Corsica, France 2007)
  - **Undergraduated practical courses (300 hours)** of 'Electrocity and Magnetism' at Department of Physics of University of Buenos Aires, Argentina (1998-1999)

- **Jury member of 6 Ph.D thesis** defences: 3 in France (thesis awarded by UPMC, Université d'Orleans, and Université Aix-Marseille, respectively), 1 in Spain (Univ. Politécnica de Madrid), 1 in Swenden (KTH), and 1 in Greece (Demokritos).
- **Organization of symposia at international conferences:**
  - a serie of **5 symposia** in **MRS** Fall Meeting (Boston, USA) on Nuclear Materials Research, in 2008, 2010, 2012 and 2016
  - a symposium in the international conference '**Condensed Matter in Paris**' in August 2014, Paris, France
  - a symposium (Microstructural processes in Irradiated Materials) at international **TMS** conference 2017 (San Diego 2017)
- **Board member** of the Condensed Matter Division of the French Physics Society: **SFP** (2011-2014)
- **Editorial board member** of an international journal : **Computational Materials Science** (Elsevier)
- "Structural Materials" working group member of the **European Psi-K network** (since 2023**).**
- **Referee for international journals**: over 100 articles reviewed since 2004 for Physical Review Letter, Physical Review B, Acta Materialia, Journal of Applied Physics, Journal of Physics Condensed Matter, Journal of Nuclear Materials, Computational Materials Science, etc.
- **Referee of European projects: "**Eurofusion enabling research projects", and of projects for requesting CPU resources on high performance computer (HPC) Marconi-Fusion in Italy (since 2016)
- **Referee of proposals** to apply for french CPU resources via DARI-GENCI (from 2018 to 2022)
- **Coordinator** (french side) of the french-chinese (ANR-NSFC) **HSynThEx project** (3 years: 2011-2013), and of the french-german (ANR-DFG) **MAGIKID** project (3 years: 2017 – 2020)
- **Principal investigator** (PI) participating various European projects (since 2006)
- **International collaborations** with various researchers in Germany, UK, Spain, USA, Finland, China and Greece. Resulting in common publications and/or ANR international-collaboration projects.

Publications:

88 publications since 1999. They include 1 Nature Materials, 3 Physical Review Letters, 34 Physical Review B, 3 Physical Review Materials, 5 Acta Materialia, 14 Journal of Nuclear Materials, and 4 Surface Science…**Number of citations=5021, h-index=35**

List of Publications

60 peer-reviewed articles, where 8 of them (in blue) are related to my doctoral thesis:

Kulitckii, V., Schneider, A., Lukianova, O., Wilde, G.,, **Fu, C-C**., Divinski, S.
Atomic diffusion in bcc Fe–Mn alloys: Theoretical analysis and experimental measurements across the Curie temperature
(2023) Acta Materialia **251**, 118883,

Bienvenu, B., **Fu, C-C**., Clouet, E.
Interplay between magnetic excitations and plasticity in body-centered cubic chromium
(2023) Physical Review B **107**, 134105.

Fedorov, M., Wróbel, J.S., London, A.J., Kurzydłowski, K.J., **Fu, C.-C**., Tadić, T., Dudarev, S.L., Nguyen-Manh, D.
Precipitation of Cr-rich clusters in Fe-Cr alloys: Effects of irradiation from first principles modeling and experimental observations
(2023) Journal of Nuclear Materials **587**, 154715.

Li, K., **Fu, C.-C**., Nastar, M ., Soisson, F.
Predicting atomic diffusion in concentrated magnetic alloys: The case of paramagnetic Fe-Ni
(2023) Physical Review B **10**7, 094103.

Li, K., **Fu, C.-C**., Nastar, M ., Soisson, F., Lavrentiev, M. Y.
Magnetochemical effects on phase stability and vacancy formation in fcc Fe-Ni alloys
(2022) Physical Review B **106**, 024106.

Theodorou, A., Syskaki, M.-A., Kotsina, Z., Axiotis M., Apostolopoulos, G., **Fu, C.-C.**
Interactions between irradiation defects and nitrogen in -Fe:an integrated experimental and theoretical study,
(2022) Acta Materialia **239**, 118227.

Front, A., Förster, G., Tran, V.T., **Fu, C.-C**., Barreteau, C., Ducastelle, F., Amara, H.

Simulation of thermodynamic properties of magnetic transition metals from an efficient tight-binding model: The case of cobalt and beyond,
(2022) Physical Review B, **155**, 144101.

Schneider, A., **Fu, C.-C**., Waseda, O., Barreteau, C., Hickel, T.,
Ab-initio based models for temperature-dependent magneto-chemical interplay in bcc Fe-Mn alloys
(2021) Physical Review B, **103**, 024421.

Buggenhoudt, O., Schuler, T., **Fu, C.-C**., Bechade, J.-L.
Predicting carbon diusion in cementite from first principles,
(2021) Physical Review Materials, **5**, 063401.

Trochet, M., Soisson, F., **Fu, C.-C**., Lavrentiev, M.Y.,
Influence of magnetic excitation and vibrational entropy on the phase diagram of Fe1xCrx alloys
(2021) Computational Materials Science **199**, 110698.

Cardias Alves de Almeida, R., Barreteau, C., Thibaudeau, P., **Fu, C.-C.**
Spin dynamics from a constrained magnetic Tight-Binding model
(2021) Physical Review B **103**, 235436

Li, K., **Fu, C.-C**., Schneider. A.
Effects of magnetic excitations and transitions on vacancy formation: cases of fcc Fe and Ni compared to bcc Fe
(2021) Physical Review B, **104**, 104406

Hegde, O., Kulitckii, V., Schneider, A., Soisson, F.,,Hickel, T.,Neugebauer, J., Wilde, G., Divinski, S., **Fu, C.-C.**
The impact of magnetic transition on Mn diffusion in α-iron:Correlative state-of-the-art theoretical and experimental study
(2021) Physical Review B **104**, 184107.

Schneider, A., **Fu, C.-C**., Soisson, F., Barreteau, C.
Atomic diffusion across the Curie point: an efficient and transferable ab Initio–based modeling approach
(2020) Physical Review Letters **124**, 215901.

Lavrentiev, M.Y., **Fu, C.-C.,** Soisson, F.
Correlation between microstructure and magnetic properties during phase separation in concentrated Fe-Cr alloys,
(2020) Journal of Magnetism and Magnetic Materials **506**, 166763.

Bienvenu,B., Fu, C.-C., Clouet, E.
Impact of magnetism on screw dislocations in body-centered cubic chromium
(2020) Acta Materialia **200**, 570.

Tran, V.-T., **Fu, C.-C.,** Li, K.
Predicting magnetization of ferromagnetic binary Fe alloys from chemical short range order,
(2020) Computational Materials Science **172**, 109344.

Tran, V.-T., **Fu, C.-C**., Schneider, A.
Effective interaction model for coupled magnetism and phase stability in bcc Fe-Co systemes
(2020) Computational Materials Science **183**, 109906._

Li, K., **Fu, C.-C.**
Ground-state properties and lattice-vibration effects of disordered Fe-Ni systems for phase stability predictions,
(2020) Physical Review Materials **4,** 023606.

Herschberg, R., **Fu, C.-C.**,, Nastar, M., Soisson, F.
Atomistic modelling of the diffusion of C in Fe-Cr alloys
(2019) Acta Materialia **165**, 638.

Schneider, A., **Fu, C.-C.,** Barreteau, C.
Local environment dependence of Mn magnetism in bcc iron-manganese alloys: a first-principles study
(2018) Physical Review B, **98**, 094426.

Barbé, E., **Fu, C.-C**., Sauzay, M.
Fracture of coherent interfaces between an fcc metal matrix and the Cr23C6 carbide precipitate from first principles
(2018) Physical Review Materials, **2**, 023605.

Bocquet, J.-L., Barouh, C., **Fu, C.-C.**
Migration mechanism for oversized solutes in cubic lattices : the case of yttrium in iron
(2017) Physical Review B, **95** 214108.

Soulairol, R., Barreteau, C., **Fu, C.-C**.
Interplay between magnetism and energetics in Fe-Cr alloys from a predictive noncollinear magnetic tight-binding model
(2016) Physical Review B, **94**, art. no. 024427

Hayward, E., Hayward, R., **Fu, C.-C**.

Predicting distinct regimes of hydrogen behavior at nano-cavities in metals
(2016) Journal of Nuclear Materials, **476**, pp. 36-44

Kuopanportti, P., Hayward, E., **Fu, C.-C**., Kuronen, A., Nordlund, K.
Interatomic Fe-H potential for irradiation and embrittlement simulations
(2016) Computational Materials Science, **111**, pp. 525-531.

Senninger, O., Soisson, F., Martínez, E., Nastar, M., **Fu, C.-C**., Bréchet, Y.
Modeling radiation induced segregation in iron–chromium alloys
(2016) Acta Materialia, **103**, pp. 1-11

Barouh, C., Schuler, T., **Fu, C.-C.**, Jourdan, T.
Predicting vacancy-mediated diffusion of interstitial solutes in α -Fe
(2015) Physical Review B, **92**, art. no. 104102

Schuler, T., Barouh, C., Nastar, M., **Fu, C.-C**.
Equilibrium Vacancy Concentration Driven by Undetectable Impurities
(2015) Physical Review Letters, **115**, art. no. 015501, .

Fu, C.-C., Lavrentiev, M.Y., Soulairol, R., Dudarev, S.L., Nguyen-Manh, D.
Low- and high-temperature magnetism of Cr and Fe nanoclusters in iron-chromium alloys
(2015) Physical Review B, **91**, art. no. 094430

Zhang, L., **Fu, C.-C**., Hayward, E., Lu, G.-H.
Properties of He clustering in -Fe grain boundaries
(2015) Journal of Nuclear Materials, **459**, pp. 247-258

Barouh, C., Schuler, T., **Fu, C.-C**., Nastar, M.
Interaction between vacancies and interstitial solutes (C, N, and O) in α- Fe: From electronic structure to thermodynamics
(2014) Physical Review B, **90**, art. no. 054112

Hayward, E., **Fu, C.-C**.
Interplay between hydrogen and vacancies in α-Fe
(2013) Physical Review B, **87**, art. no. 174103

Vérité, G., Domain, C., **Fu, C.-C**., Gasca, P., Legris, A., Willaime, F.
Self-interstitial defects in hexagonal close packed metals revisited: Evidence for low-symmetry configurations in Ti, Zr, and Hf
(2013) Physical Review B, **87**, art. no. 134108

Zhang, L., **Fu, C.-C**., Lu, G.-H.

Energetic landscape and diffusion of He in α-Fe grain boundaries from first principles
(2013) Physical Review B, **87**, art. no. 134107

Martínez, E., Senninger, O., **Fu, C.-C**., Soisson, F.
Decomposition kinetics of Fe-Cr solid solutions during thermal aging
(2012) Physical Review B, **86**, art. no. 224109

Levesque, M., Martínez, E., **Fu, C.-C**., Nastar, M., Soisson, F.
Simple concentration-dependent pair interaction model for large-scale simulations of Fe-Cr alloys
(2011) Physical Review B, **84**, art. no. 184205

Lavrentiev, M.Y., Soulairol, R., **Fu, C.-C**., Nguyen-Manh, D., Dudarev, S.L.
Noncollinear magnetism at interfaces in iron-chromium alloys: The ground states and finite-temperature configurations
(2011) Physical Review B, **84**, art. no. 144203

Soulairol, R., **Fu, C.-C**., Barreteau, C.
Magnetic and energetic properties of low-index Cr surfaces and Fe/Cr interfaces: A first-principles study
(2011) Physical Review B, **84** , art. no. 155402

Martínez, E., **Fu, C.-C.**
Cr interactions with He and vacancies in dilute Fe-Cr alloys from first principles
(2011) Physical Review B, **84** , art. no. 014203

Soulairol, R., **Fu, C.-C**., Barreteau, C.
Vacancy and substitutional impurities in the spin-density wave state of Cr from first principles
(2011) Physical Review B, **83**, art. no. 214103

Ortiz, C.J., Caturla, M.J., **Fu, C.C**., Willaime, F.
Erratum: Influence of carbon on the kinetics of He migration and clustering in α-Fe from first principles (Physical Review B (2009) 80 (134109))
(2011) Physical Review B, **83**, art. no. 139905

Soulairol, R., **Fu, C.-C**., Barreteau, C.
Structure and magnetism of bulk Fe and Cr: From plane waves to LCAO methods
(2010) Journal of Physics Condensed Matter, **22** (29), art. no. 295502

Amara, H., **Fu, C.C**., Soisson, F., Maugis, P.
Aluminum and vacancies in -iron: Dissolution, diffusion, and clustering
(2010) Physical Review B, **81**, art. no. 174101

Ortiz, C.J., Caturla, M.J., **Fu, C.C**., Willaime, F.
Influence of carbon on the kinetics of He migration and clustering in α-Fe from first principles
(2009) Physical Review B, **80**, art. no. 134109

Meslin, E., Barbu, A., Boulanger, L., Radiguet, B., Pareige, P., Arakawa, K., **Fu, C.C**.
Cluster-dynamics modelling of defects in -iron under cascade damage conditions
(2008) Journal of Nuclear Materials, **382** (2-3), pp. 190-196

Soisson, F., **Fu, C.-C.**
Cu-precipitation kinetics in α-Fe from atomistic simulations: Vacancy-trapping effects and Cu-cluster mobility
(2007) Physical Review B, **76**, art. no. 214102

Ortiz, C.J., Caturla, M.J., **Fu, C.C**., Willaime, F.
He diffusion in irradiated α-Fe: An ab-initio-based rate theory model
(2007) Physical Review B, **75**, art. no. 100102

Meslin, E., **Fu, C.-C**., Barbu, A., Gao, F., Willaime, F.
Theoretical study of atomic transport via interstitials in dilute Fe-P alloys
(2007) Physical Review B, **75**, art. no. 094303

Weissmann, M., García, G., Kiwi, M., Ramírez, R., **Fu, C.-C.**
Theoretical study of iron-filled carbon nanotubes
(2006) Physical Review B, **73**, art. no. 125435
Fu, C.-C., Willaime, F.
Ab initio study of helium in α-Fe: Dissolution, migration, and clustering with vacancies
(2005) Physical Review B , **72**, art. no.064117

Fu, C.-C., Torre, J.D., Willaime, F., Bocquet, J.-L., Barbu, A.
Multiscale modelling of defect kinetics in irradiated iron
(2005) Nature Materials, **4** (1), pp. 68-74

Fu, C.-C., Métois, J.-J., Astier, J.P., Saúl, A., Weissmann, M.
Catalytic effect of carbon in shaping Si(1 1 1) surfaces
(2004) Surface Science, **563** (1-3), pp. 48-56

Fu, C.-C., Willaime, F., Ordejón, P.
Stability and mobility of mono- and Di-interstitials in α-Fe
(2004) Physical Review Letters, **92**, pp. 175503-1

Fu, C.-C., Saúl, A.

Theoretical study of the role of surface defects on the dimer dynamics on Si(0 0 1)
(2003) Surface Science, **527** (1-3), pp. 113-123

Fu, C.-C., Fava, J., Weht, R., Weissmann, M.
Molecular dynamics study of the fragmentation of silicon-doped fullerenes
(2002) Physical Review B, **66**, art. no. 045405, pp. 454051-454058

Fu, C.-C., Weissmann, M., Saúl, A.
Molecular dynamics study of dimer flipping on perfect and defective Si(001) surfaces
(2001) Surface Science, **494** (2), pp. 119-130

Fu, C.-C., Weissmann, M., Saul, A.
Diffusion pathways for Si ad-dimers on Si(0 0 1): A high temperature molecular dynamics study
(2001) Surface Science, **481** (1-3), pp. 97-104

Fu, C.-C., Weissmann, M., Machado, M., Ordejón, P.
Ab initio study of silicon-multisubstituted neutral and charged fullerenes
(2001) Physical Review B, **63** (8), art. no. 085411, pp. 854111-854119

Fu, C.-C., Weissmann, M.
Tight-binding molecular-dynamics study of amorphous carbon deposits over silicon surfaces
(1999) Physical Review B, **60** pp. 2762-2770

19 peer-reviewed conference papers :

Ventelon, L., Willaime, F., **Fu, C.-C**., Heran, M., Ginoux, I.
Ab initio investigation of radiation defects in tungsten: Structure of self-interstitials and specificity of di-vacancies compared to other bcc transition metals
(2012) Journal of Nuclear Materials, **425** (1-3), pp. 16-21

Jourdan, T., **Fu, C.C**., Joly, L., Bocquet, J.L., Caturla, M.J., Willaime, F.
Direct simulation of resistivity recovery experiments in carbon-doped α-iron
(2011) Physica Scripta T, **T145**, art. no. 014049

Soulairol, R., **Fu, C.-C**., Barreteau, C.
Magnetism and defects in Fe, Cr and their alloy [Magnétisme et défauts dans le Fe, le Cr et leur alliage]
(2011) Revue de Metallurgie. Cahiers D'Informations Techniques, **108** (1), pp. 27-31

Levesque, M., Martinez, E., Soisson, F., **Fu, C.C**., Nastar, M.
Iron-chromium alloys and surfaces: From ab initio calculations to segregation isotherms [L'alliage fer-chrome et ses surfaces: des calculs ab initio aux isothermes de ségrégation]
(2011) Revue de Metallurgie. Cahiers D'Informations Techniques, **108** (1), pp. 21-25

Martinez, E., **Fu, C.C**., Levesque, M., Nastar, M., Soisson, F.
Simulations of decomposition kinetics of Fe-Cr solid solutions during thermal aging
(2011) Solid State Phenomena, **172-174**, pp. 1016-1021

Ortiz, C.J., Caturla, M.J., **Fu, C.C**., Willaime, F.
Impurity effects on He diffusion in α-Fe
(2009) Journal of Nuclear Materials, **386-388** (C), pp. 33-35

Gao, N., **Fu, C.-**C., Samaras, M., Schäublin, R., Victoria, M., Hoffelner, W.
Multiscale modelling of bi-crystal grain boundaries in bcc iron
(2009) Journal of Nuclear Materials, **385** (2), pp. 262-267

Samaras, M., Hoffelner, W., **Fu, C.C**., Guttmann, M., Stoller, R.E.
Materials modeling - A key for the design of advanced high temperature reactor components
(2008) Societe Francaise d'Energie Nucleaire - International Congress on Advances in Nuclear Power Plants - ICAPP 2007, "The Nuclear Renaissance at Work", 2, pp. 1188-1197

Fu, C.-C., Meslin, E., Barbu, A., Willaime, F., Oison, V.
Effect of C on vacancy migration in α-iron
(2008) Solid State Phenomena, **139**, pp. 157-164

Soisson, F., **Fu, C.-C.**
Atomistic simulations of copper precipitation and radiation induced segregation in α-iron
(2008) Solid State Phenomena, **139**, pp. 107-112

Fu, C.-C., Willaime, F.
Interaction between helium and self-defects in α-iron from first principles
(2007) Journal of Nuclear Materials, **367-370** A (SPEC. ISS.), pp. 244-250

Soisson, F., **Fu, C.-C**.
Energetic landscapes and diffusion properties in FeCu alloys
(2007) Solid State Phenomena, **129**, pp. 31-39

Vérité, G., Willaime, F., **Fu, C.C**.

Anisotropy of the vacancy migration in Ti, Zr and Hf hexagonal close-packed metals from first principles
(2007) Solid State Phenomena, **129**, pp. 75-81

Ortiz, C.J., Caturla, M.J., **Fu, C.C**., Willaime, F.
Role of trapping impurities on He desorption and clustering in irradiated α-Fe
(2006) Materials Research Society Symposium Proceedings, **978**, pp. 55-66

Willaime, F., **Fu, C.C**.
First principles calculations of helium solution energies in BCC transition metals
(2006) Materials Research Society Symposium Proceedings, **981**, pp. 1-6

Dalla Torre, J., **Fu, C.-C**., Willaime, F., Barbu, A., Bocquet, J.-L.
Resistivity recovery simulations of electron-irradiated iron: Kinetic Monte Carlo versus cluster dynamics
(2006) Journal of Nuclear Materials, **352** (1-3), pp. 42-49

Ortiz, C.J., Caturla, M.J., **Fu, C.C**., Willaime, F.
Modeling nucleation and growth of defects in irradiated Fe in the presence of He using rate theory and kinetic Monte Carlo methods
(2005) Materials Research Society Symposium Proceedings, **908**, pp. 55-60

Willaime, F., **Fu, C.C**., Marinica, M.C., Dalla Torre, J.
Stability and mobility of self-interstitials and small interstitial clusters in α-iron: Ab initio and empirical potential calculations
(2005) Nuclear Instruments and Methods in Physics Research, Section B: Beam Interactions with Materials and Atoms, **228** (1-4 SPEC. ISS.), pp. 92-99

Fu, C.-C., Weissmann, M., Saúl, A.
Finite temperature simulation of ad-dimer diffusion between dimer row and trough on Si(001)
(2001) Applied Surface Science, **175-176**, pp. 36-42

9 review articles:

Malerba, L., Caturla, M.J., Gaganidze, E., Kaden, C., Konstantinović, M.J., Olsson, P., Robertson, C., Rodney, D., Ruiz-Moreno,A.M., Serrano, M., Aktaa, J., Anento, N., Austin, S., Bakaev, A., Balbuena, J.P.,Bergner, F.,Boioli, F., Boleininger, M., Bonny, G., Castin, N., Chapman, J.B.J., Chekhonin, P., Clozel, M., Devincre, B., Dupuy, L., Diego, G., Dudarev, S.L., **Fu, C.,-C**.*,, et al.*
Multiscale modelling for fusion and fission materials: The M4F project
(2021) Nuclear materials and energy **29**, 101051.

Linsmeier, C., **Fu, C.-C**., Kaprolat, A., Nielsen, S.F., Mergia, K., Schäublin, R., Lindau, R., Bolt, H., Buffière, J.-Y., Caturla, M.J., Décamps, B., Ferrero, C., Greuner, H., Hébert, C., Höschen, T., Hofmann, M., Hugenschmidt, C., Jourdan, T., Köppen, M., Płociński, T., Riesch, J., Scheel, M., Schillinger, B., Vollmer, A., Weitkamp, T., Yao, W., You, J.-H., Zivelonghi, A.
Advanced materials characterization and modeling using synchrotron, neutron, TEM, and novel micro-mechanical techniques - A European effort to accelerate fusion materials development
(2013) Journal of Nuclear Materials, **442**, pp. S834-S845

Rieth, M., Boutard, J.L., Dudarev, S.L., Ahlgren, T., Antusch, S., Baluc, N., Barthe, M.-F., Becquart, C.S., Ciupinski, L., Correia, J.B., Domain, C., Fikar, J., Fortuna, E., **Fu, C.-C**., Gaganidze, E., Galán, T.L., García-Rosales, C., Gludovatz, B., Greuner, H., Heinola, K., Holstein, N., Juslin, N., Koch, F., Krauss, W., Kurzydlowski, K.J., Linke, J., Linsmeier, C., Luzginova, N., Maier, H., Martínez, M.S., Missiaen, J.M., Muhammed, M., Muñoz, A., Muzyk, M., Nordlund, K., Nguyen-Manh, D., Norajitra, P., Opschoor, J., Pintsuk, G., Pippan, R., Ritz, G., Romaner, L., Rupp, D., Schäublin, R., Schlosser, J., Uytdenhouwen, I., Van Der Laan, J.G., Veleva, L., Ventelon, L., Wahlberg, S., Willaime, F., Wurster, S., Yar, M.A.
Review on the EFDA programme on tungsten materials technology and science
(2011) Journal of Nuclear Materials, **417** (1-3), pp. 463-467

Malerba, L., Ackland, G.J., Becquart, C.S., Bonny, G., Domain, C., Dudarev, S.L., **Fu, C.-C**., Hepburn, D., Marinica, M.C., Olsson, P., Pasianot, R.C., Raulot, J.M., Soisson, F., Terentyev, D., Vincent, E., Willaime, F.
Ab initio calculations and interatomic potentials for iron and iron alloys: Achievements within the Perfect Project
(2010) Journal of Nuclear Materials, **406** (1), pp. 7-18

Becquart, C.S., Barbu, A., Bocquet, J.L., Caturla, M.J., Domain, C., **Fu, C.-C**., Golubov, S.I., Hou, M., Malerba, L., Ortiz, C.J., Souidi, A., Stoller, R.E.
Modeling the long-term evolution of the primary damage in ferritic alloys using coarse-grained methods
(2010) Journal of Nuclear Materials, **406** (1), pp. 39-54

Dudarev, S.L., Boutard, J.-L., Lässer, R., Caturla, M.J., Derlet, P.M., Fivel, M., **Fu, C.-C**., Lavrentiev, M.Y., Malerba, L., Mrovec, M., Nguyen-Manh, D., Nordlund, K., Perlado, M., Schäublin, R., Van Swygenhoven, H., Terentyev, D., Wallenius, J., Weygand, D., Willaime, F.
The EU programme for modelling radiation effects in fusion reactor materials: An overview of recent advances and future goals
(2009) Journal of Nuclear Materials, **386-388** (C), pp. 1-7

Fu, C.C., Willaime, F.
First principles calculations in iron: structure and mobility of defect clusters and defect complexes for kinetic modelling
(2008) Comptes Rendus Physique, **9** (3-4), pp. 335-342

Caturla, M.J., Ortiz, C.J., **Fu, C.C**.
Helium and point defect accumulation: (ii) kinetic modelling
(2008) Comptes Rendus Physique, **9** (3-4), pp. 401-408

Victoria, M., Dudarev, S., Boutard, J.L., Diegele, E., Lässer, R., Almazouzi, A., Caturla, M.J., **Fu, C.C.**, Källne, J., Malerba, L., Nordlund, K., Perlado, M., Rieth, M., Samaras, M., Schaeublin, R., Singh, B.N., Willaime, F.
Modelling irradiation effects in fusion materials
(2007) Fusion Engineering and Design, **82** (15-24), pp. 2413-2421